Hadronic D and D_s meson decays

Anders Ryd*

Laboratory of Elementary-Particle Physics, Cornell University, Ithaca, New York 14853, USA

Alexey A. Petrov†

Department of Physics and Astronomy, Wayne State University, Detroit, Michigan 48201, USA and Michigan Center for Theoretical Physics, University of Michigan, Ann Arbor, Michigan 48109, USA

(published 23 January 2012)

A comprehensive review of hadronic decays of D and D_s mesons is provided. Current theoretical and experimental challenges and successes in understanding of hadronic transitions of those mesons are discussed. A brief overview of the theoretical and experimental tools is given before discussing the absolute branching fractions for D and D_s mesons. Cabibbo-suppressed and rare hadronic decays are discussed and compared with theory before discussing hadronic multibody decays.

DOI: 10.1103/RevModPhys.84.65 PACS numbers: 14.40.Lb

CONTENTS

I. INTRODUCTION

The discovery of charmed meson states in 1974 signaled a new era in particle physics. The arrival of the first heavy quark

*Anders.Ryd@cornell.edu
†apetrov@wayne.edu

solidified the evidence that the standard model (SM) provided a correct low-energy description of particle physics. Three decades later, the charm quark still plays an important role in studies of strong and weak interactions. It also serves as an important tool for exploring physics beyond the standard model, indirectly probing energy scales well above several TeV, which will be directly probed by the Large Hadron Collider (LHC). In some cases, charm transitions provide possibilities for almost background-free studies of low-energy signals of new physics. For example, signals of CP violation in the charm system predicted within the standard model are small, so any observation of CP violation in the current round of experiments would rather unambiguously signal the presence of new physics. Charm is also rather unique in that it is the only up-type quark that can have flavor oscillations.

A distinctive feature of all charmed hadrons is that their masses $\mathcal{O}(2\text{ GeV})$ place them in the middle of the region where nonperturbative hadronic physics is operative. While this fact does not markedly affect the theoretical description of leptonic and semileptonic decays of charmed hadrons, it poses challenges in the analyses of their hadronic transitions. There is a great deal of optimism, however, that abundant experimental data would provide some hints on the structure of charm hadronic decays, so those problems will eventually be overcome.

The data on charm transitions originate from several different types of experiments. Experiments at e^+e^- machines operating at the $\psi(3770)$ and $\psi(4140)$ resonances, such as CLEO-c and BES III, have several important advantages. First, the final state is extremely simple, being essentially just a $D\bar{D}$ pair. Second, the cross section for charm production is relatively high, $\sigma(D^0\bar{D}^0) = 3.66 \pm 0.03 \pm 0.06$ nb and $\sigma(D^+D^-) = 2.91 \pm 0.03 \pm 0.05$ nb at the $\psi(3770)$. In conjunction with low multiplicity of the final state, this allows for measurements of absolute branching fractions for several reference modes. We refer to these as reference modes as they are used to normalize other decay channels. Finally, in those experiments, the $D\bar{D}$ pairs are produced in a quantum-coherent state, which allows for unique probes of the structure of decay amplitudes and phases, as well as novel measurements of mixing and CP violation.

The B factory e^+e^- experiments *BABAR* and Belle, operating at the $\Upsilon(4S)$ center-of-mass energy, produce significant amounts of charm data. In fact, at the resonance center-of-mass energy, $\sigma(b\bar{b}) \sim 1.1$ nb, while $\sigma(c\bar{c}) \sim 1.3$ nb. The large integrated luminosities of these experiments produced large samples of reconstructed charm. The higher operating energy makes the production of charmed baryons possible.

Experiments at hadron machines, such as CDF and D0 at the Fermilab Tevatron, and fixed target facilities are plagued by even higher backgrounds. However, a much higher production cross section, combined with a relatively long lifetime of charmed hadrons, provides a possibility to trigger on charm decay events with displaced vertices. This technique allowed for hadron machines to be major players in charm physics. New results from the LHC experiments LHCb, ATLAS, and CMS will continue to supply us with new data.

This paper provides a comprehensive review of hadronic decays of D and D_s mesons. In this review we adopt the averages performed by the Particle Data Group (Amsler *et al.*, 2008). We will do our own averaging only if there are newer measurements that are not included in the review by the Particle Data Group.

This review is organized as follows. Section II contains a discussion of the discovery of open charm, followed in Sec. III by a discussion of the experimental techniques used for studying charm decays. This includes a discussion of the main experiments that have contributed to our understanding of D decays and the production mechanisms employed in these studies. Final-state radiation (FSR) is discussed in this section as it is an important effect in many of the precision measurements discussed in this review. Section IV provides a theoretical description of hadronic D decays. This includes a discussion of $SU(3)_F$ flavor symmetry, the flavor-flow-diagram approach, and factorization. These are common tools used to analyze and interpret hadronic D decay data. Sections V and VI discuss the determination of the absolute branching fractions for D and D_s decays. Rare and suppressed modes are discussed in Sec. VII. Section VIII deals with the issue of final-state interactions and baryonic D decays. Multibody decays and Dalitz-plot studies are discussed in Sec. IX. This review concludes in Sec. X with a summary and outlook.

II. DISCOVERY OF OPEN CHARM

The arrival of the quark model in 1964 (Gell-Mann, 1964; Zweig, 1964) simplified the description of elementary particles. The idea that all observed particles are made of the three quarks, u, d, and s, was gaining acceptance. By the early 1970s, the proton structure was probed and the quarks were found to be real particles. Further development of perturbative quantum chromodynamics and the concept of asymptotic freedom allowed consistent explanation of those experiments in terms of those three quark flavors. The possible existence of a fourth quark had been theoretically discussed in the 1960s (Björken and Glashow, 1964); however, it was not required.

Hints of the incompleteness of the current picture came after experimental observation of rare, electroweak, decays of kaons. The observed rate for $K_L^0 \to \mu^+\mu^-$ turned out to be smaller than predicted. Similarly, the K_S^0-K_L^0 mass difference did not agree with predictions based on having only the u, d, and s quarks. To solve those problems, Glashow, Iliopoulos, and Maiani (1970) (GIM) proposed an elegant mechanism, which involved adding the forth quark c. The resulting mechanism not only established the absence of the tree-level flavor-changing neutral currents in the standard model, but also provided for reduced rates for $K_L^0 \to \mu^+\mu^-$ decays by requiring cancellations with additional diagrams involving intermediate charm quarks. Using the observed rate for $K_L^0 \to \mu^+\mu^-$ and K_S^0-K_L^0 mass difference, it was estimated that the charm quark would have a mass in the range of 1 to 3 GeV (Gaillard and Lee, 1974; Gaillard, Lee, and Rosner, 1975). The existence of the new quark implied that it would form bound states with its own antiquark, as well as with the lighter quarks, which could be observed experimentally.

These bound states were experimentally discovered in November 1974 by two independent research groups at SLAC (Aubert *et al.*, 1974) and BNL (Augustin *et al.*, 1974). The mass of the observed J/ψ resonance of about

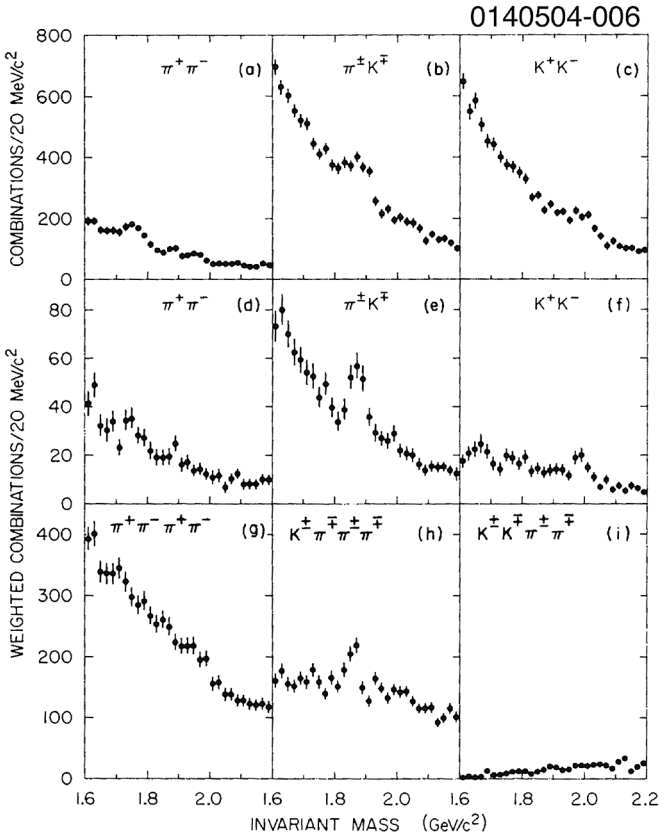

FIG. 1. The invariant mass distributions observed by the SLAC-LBL experiment for two and four hadrons in the final state. (a) $\pi^+\pi^-$ assigning pion mass to all tracks, (b) $K^\mp\pi^\pm$ assigning kaon and pion masses to all tracks, (c) K^+K^- assigning kaon mass to all tracks, (d) $\pi^+\pi^-$ weighted by $\pi\pi$ time-of-flight probability, (e) $K^\mp\pi^\pm$ weighted by $K\pi$ time of flight, (f) K^+K^- weighted by KK time of flight, (g) $\pi^+\pi^-\pi^+\pi^-$ weighted by 4π time-of-flight probability, (h) $K^\pm\pi^\mp\pi^+\pi^-$ weighted by $K3\pi$ time-of-flight probability, and (i) $K^\pm K^\mp\pi^+\pi^-$ weighted by $KK\pi\pi$ time-of-flight probability. From Goldhaber *et al.*, 1976.

3.1 GeV was in the range where a $c\bar{c}$ bound state was expected. In addition, the small width, of about 93 keV, was different from other high mass resonances observed. The interpretation of the J/ψ as a $c\bar{c}$ bound state was confirmed when "open-charm" states were discovered later, first the D^0 (Goldhaber *et al.*, 1976) and then the D^+ state (Peruzzi *et al.*, 1976). The first observation of the D^0 state was made in the final states $K^-\pi^+$ and $K^-\pi^+\pi^-\pi^+$. The observed invariant mass distributions are shown in Fig. 1.

Another source of information about open-charm mesons was neutrino scattering experiments, such as the Harvard-Pennsylvania-Wisconsin-Fermilab (HPWF) experiment (Benvenuti *et al.*, 1975a, 1975b). They reported observation of two opposite-sign muons in a reaction $\nu_\mu + N \to \mu^+\mu^- + X$, which was interpreted as evidence for production of a new heavy hadron with mass around 2 GeV/c^2. Those D mesons were produced in charged current interactions of neutrinos with d and s quarks. It is also interesting to note that there were hints of the existence of open-charm states in photoemulsion experiments even before the J/ψ had been discovered (Niu, Mikumo, and Maeda, 1971; Hoshino *et al.*, 1975).

After the observation of the D^0 and D^+ mesons it took a little longer to establish the D_s^+. There were several false sightings before the D_s^+, originally called the F meson, was observed by CLEO (Chen *et al.*, 1983). These observations established the charm quark as the fourth quark in the family of strongly interacting particles.

III. GENERAL REMARKS ON EXPERIMENTAL FACILITIES AND TECHNIQUES

Charm has been studied in a large number of different experiments. In e^+e^- collisions charm decays have been studied from threshold to the Z pole. There have also been a number of fixed target experiments, using either hadroproduction or photoproduction. The e^+e^- and fixed target experiments dominate the literature on charm meson decays. In addition, there are also studies using proton-antiproton collisions.

In this section we review some of the basic properties of the different types of production mechanisms and the experiments used to collect the data. First, e^+e^- experiments are discussed and then fixed target experiments. For e^+e^- experiments, where typically triggering is open and most of the produced events are recorded, we compare the luminosity and the produced number of $c\bar{c}$ events. A summary of e^+e^- experiments is given in Table I. For fixed target experiments a similar comparison is made in Table II for the number of exclusively reconstructed D mesons. At threshold the final-state charm mesons are produced without any additional hadrons. The CLEO-c experiment is described in more detail as it is the experiment operating near threshold with the largest data samples to date. At higher e^+e^- center-of-mass energy the charm hadrons are produced either in fragmentation of charm jets or in decays of heavier particles such as hadrons containing b quarks. A series of fixed target experiments has been performed to study charm and are discussed next. Fixed target experiments can be categorized as photoproduction or hadroproduction experiments based on the particle type incident on the target. Last, final-state radiation is discussed. The precision on many measurements of hadronic charm decays has reached the level where radiative corrections cannot be ignored.

A. Experiments using e^+e^- annihilation near threshold

At threshold D meson pairs are produced without any additional hadrons. This provides the experiments operating at threshold with a clean environment for studying charm decays. As will be discussed in Sec. III.A.3 the initial electron or positron may radiate low-energy photons, initial-state radiation (ISR), such that the total energy of the produced charm hadrons is less than the center-of-mass energy in the e^+e^- initial state.

Experiments that studied charm decays at threshold include the Mark I, II, and III experiments (Augustin *et al.*, 1975; Abrams *et al.*, 1979a; Bernstein *et al.*, 1984) at SPEAR; BES I, BES II, and BES III (Bai *et al.*, 1994, 2001; Collaboration, 2009) at BEPC, and CLEO-c (Kubota *et al.*, 1992; Peterson *et al.*, 2002; Artuso *et al.*, 2003) at CESR-c. The physics programs of CLEO-c and BES III are

TABLE I. Summary of charm samples produced in e^+e^- colliding beam experiments.

Experiment	Year	$\sqrt{s}$	$\int \mathcal{L}$	Produced charm
Mark III	1982–1988	3.77 GeV	9 pb^{-1}	28 000 $D^0\bar{D}^0$ 20 000 D^+D^-
		4.14 GeV	6.3 pb^{-1}	
BES I	1992–1993	4.03 GeV	22.3 pb^{-1}	
		4.14 GeV	1.8 pb^{-1}	
BES II	2001–2003	3.77 GeV	17.3 pb^{-1}	
CLEO-c	2003–2008	3.77 GeV	818 pb^{-1}	3.0×10^6 $D^0\bar{D}^0$ 2.4×10^6 D^+D^-
		4.17 GeV	589 pb^{-1}	0.58×10^6 $D_s^{\pm}D_s^{*\mp}$
BES III[a]	2009–	3.77 GeV	>900 pb^{-1}	
CLEO	1979–1988	10.5 GeV	314 pb^{-1}	0.41×10^6 $c\bar{c}$
CLEO II	1989–1994	10.5 GeV	4.7 fb^{-1}	6.1×10^6 $c\bar{c}$
CLEO II.V	1995–1999	10.5 GeV	9.1 fb^{-1}	12×10^6 $c\bar{c}$
CLEO III	2000–2003	10.5 GeV	15 fb^{-1}	19×10^6 $c\bar{c}$
ARGUS	1982–1992	10.5 GeV	514 pb^{-1}	0.67×10^6 $c\bar{c}$
BABAR	1999–2008	10.5 GeV	531 fb^{-1}	0.69×10^9 $c\bar{c}$
Belle[b]	1999–	10.5 GeV	1040 fb^{-1}	1.35×10^9 $c\bar{c}$
HRS	1982–1986	29 GeV	300 pb^{-1}	52 000 $c\bar{c}$
LEP	1989–1996	91 GeV	4.2×10^6 Z's Per experiment	220 000 $c\bar{c}$ Per experiment

[a]As of 1 August 2010.
[b]As of 30 June 2010.

described in detail by Briere *et al.* (2001) and Asner *et al.* (2008). For studies of D^0 and D^+ decays experiments have run at the $\psi(3770)$. The total hadronic cross section at the $\psi(3770)$ resonance was measured by CLEO-c (Besson *et al.*, 2006)

$$\sigma(e^+e^- \to \text{hadrons}) = 6.38 \pm 0.08^{+0.41}_{-0.30} \text{ nb}. \quad (1)$$

The cross sections for $D^0\bar{D}^0$ and D^+D^- production were measured by CLEO-c (Dobbs *et al.*, 2007)

$$\sigma(e^+e^- \to D^0\bar{D}^0) = 3.66 \pm 0.03 \pm 0.06 \text{ nb}, \quad (2)$$

$$\sigma(e^+e^- \to D^+D^-) = 2.91 \pm 0.03 \pm 0.05 \text{ nb}. \quad (3)$$

Adding these two measurements, CLEO-c obtains the total cross section for $D\bar{D}$ production at the $\psi(3770)$ to be $\sigma(e^+e^- \to D\bar{D}) = 6.57 \pm 0.04 \pm 0.10$ nb. This is larger than, but consistent with, the inclusive hadronic cross section discussed above. These results indicate that the majority of

TABLE II. The number of reconstructed charm mesons for different fixed target experiments.

Experiment	Year	Events recorded (10^6)	Reconstructed charm decays
Photoproduction:			
E691	1985	100	10 000
E687	1992	500	100 000
FOCUS (E831)	1996	7000	1.2×10^6
Hadroproduction:			
WA75	1984	2	350
NA32	1986	17	1300
WA82	1989	10	3000
E653	1988	10	1000
E769	1988	500	4000
E791	1992	20 000	200 000

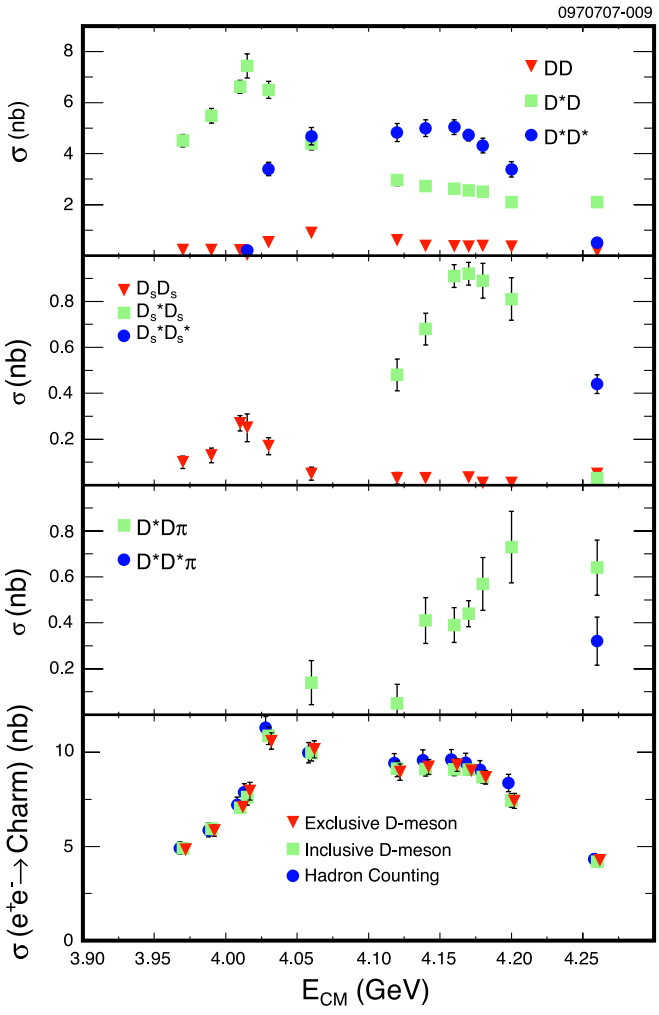

FIG. 2 (color online). The measured cross sections for different $D\bar{D}$ final states. From Cronin-Hennessy *et al.*, 2009.

the $\psi(3770)$ decays to $D\bar{D}$. CLEO-c (Adam *et al.*, 2005) and BES II (Bai *et al.*, 2005) observed some non-$D\bar{D}$ decays of the $\psi(3770)$. The largest of these decays is the radiative transition $\psi(3770) \to \gamma\chi_{c0}$ with a branching fraction of $(0.73 \pm 0.09)\%$. Summing the observed branching fractions for non-$D\bar{D}$ decays we obtain $(1.4 \pm 0.1)\%$, consistent with the cross-section measurements above. BES II (Ablikim *et al.*, 2006a, 2006b, 2007; 2008) performed indirect measurements of the cross section for $\psi(3770) \to$ non-$D\bar{D}^0$ final states as well as measurements of the $D\bar{D}$ cross sections. The PDG (Amsler *et al.*, 2008) averaged these measurements and found that $(14.7 \pm 3.2)\%$ of $\psi(3770)$ resonances decayed to non-$D\bar{D}$ final states. This result is inconsistent with the CLEO-c results at the 2σ level.

Different e^+e^- center-of-mass energies have been used for studies of D_s mesons. The cross sections for producing $D_{(s)}$ or $D^*_{(s)}$ mesons, as measured by CLEO-c (Cronin-Hennessy *et al.*, 2009), are shown in Fig. 2. BES collected data at 4.03 GeV. At this energy $D_s^+D_s^-$ mesons pairs are produced. CLEO-c, on the other hand, ran at a higher energy, about 4.17 GeV. At this energy pairs of $D_s^{\pm}D_s^{*\mp}$ mesons are produced. The D_s^* meson decays to either $D_s\gamma$ or $D_s\pi^0$, with branching fractions of $(94.2 \pm 0.7)\%$ and $(5.8 \pm 0.7)\%$, respectively (Aubert *et al.*, 2005d; Amsler *et al.*, 2008). The advantage of the higher energy is the larger cross section. CLEO-c reported (Cronin-Hennessy *et al.*, 2009) a cross section of 0.27 ± 0.03 nb at 4.03 GeV for $D_s^+D_s^-$ production and 0.92 ± 0.05 nb at 4.17 GeV for $D_s^{*\pm}D_s^{\mp}$ production. For most analyses the larger cross section outweighs the complication of the additional particles in the final state.

1. Quantum coherence

Threshold production of $D\bar{D}$ pairs can be explored to understand the phase structure of hadronic decay amplitudes of D^0 mesons. Here one can use the fact that neutral charm mesons D^0 and $\bar{D}^0$ mix. D^0-$\bar{D}^0$ mixing arises from electroweak or new physics $|\Delta C| = 2$ interactions that generate off-diagonal terms in the neutral D mass matrix [see, e.g. Artuso *et al.* (2008), and Bergmann *et al.* (2000) for more information]

$$\left[\mathbf{M} - i\frac{\mathbf{\Gamma}}{2}\right] \propto \begin{pmatrix} A & p^2 \\ q^2 & A \end{pmatrix}, \tag{4}$$

where A parametrizes masses and lifetimes of D^0 and $\bar{D}^0$ states and the complex parameters p^2 and q^2 parametrize contributions from $|\Delta C| = 2$ interactions. The nondiagonal structure of the mixing matrix of Eq. (4) leads to the (physical) mass eigenstates of a Hamiltonian of Eq. (4), D_1 and D_2 becoming superpositions of the flavor eigenstates D^0 and $\bar{D}^0$,

$$|D_{1,2}\rangle = p|D^0\rangle \pm q|\bar{D}^0\rangle, \tag{5}$$

where $|p|^2 + |q|^2 = 1$. A simplified assumption can be made that in the studies of strong phases described below CP violation may be neglected. This can be justified in the standard model by noting that CP-violating contributions are always suppressed by small values of the third-generation Cabibbo-Kobayashi-Maskawa (CKM) matrix elements (Artuso, Meadows, and Petrov, 2008). In such case $p = q$, and so mass eigenstates also become eigenstates of CP,

$$|D_\pm\rangle = \frac{1}{\sqrt{2}}[|D^0\rangle \pm |\bar{D}^0\rangle]. \tag{6}$$

It follows then that these CP eigenstates $|D_\pm\rangle$ do not evolve with time. Their mass and lifetime differences can be observed,

$$x = \frac{\Delta M_D}{\Gamma}, \qquad y = \frac{\Delta\Gamma_D}{2\Gamma}, \tag{7}$$

where $\Gamma = (\Gamma_+ + \Gamma_-)/2$ is the average lifetime of mass and CP eigenstates.

At threshold e^+e^- experiments, such as BES and CLEO-c, $D^0\bar{D}^0$ pairs are produced through resonances of specific charge conjugation. The $D^0\bar{D}^0$ will therefore be in an entangled state with the same quantum numbers as the parent resonance. In particular, since both mesons are pseudoscalars, charge conjugation reads $C = (-1)^L$, if the produced resonance has angular momentum L. This implies that the quantum mechanical state at the time of $D^0\bar{D}^0$ production is

$$\Psi = \frac{1}{\sqrt{2}}\{|D^0(\mathbf{k_1})\bar{D}^0(\mathbf{k_2})\rangle + C|D^0(\mathbf{k_2})\bar{D}^0(\mathbf{k_1})\rangle\}, \tag{8}$$

where $\mathbf{k_1}$ and $\mathbf{k_2}$ are the momenta of the mesons. Rewriting this in terms of the CP basis we arrive at

$$\begin{aligned}\Psi_{C=+1} &= \frac{1}{\sqrt{2}}\{|D_+(\mathbf{k_1})D_+(\mathbf{k_2})\rangle - |D_-(\mathbf{k_1})D_-(\mathbf{k_2})\rangle\},\\ \Psi_{C=-1} &= \frac{1}{\sqrt{2}}\{|D_-(\mathbf{k_1})D_+(\mathbf{k_2})\rangle + |D_+(\mathbf{k_1})D_-(\mathbf{k_2})\rangle\}.\end{aligned} \tag{9}$$

Thus in the $L =$ odd, $C = -1$ case, which applies to the experimentally important $\psi(3770)$ resonance, the CP eigenstates of the D mesons are anticorrelated, while if $L =$ even, $C = +1$ the eigenstates are correlated. This can happen when the $D^0\bar{D}^0$ pair is produced in the decays $\psi(4140) \to D\bar{D}\gamma$ of the more massive charmonium state $\psi(4140)$. In either case the CP conservation implies that correlation between the eigenstates is independent of when they decay. In this way, if $D(\mathbf{k_1})$ decays to the final state which is also a CP eigenstate, then the CP eigenvalue of the meson $D(\mathbf{k_2})$ is therefore *determined*: It is either the same as $D(\mathbf{k_1})$ for $C = +1$ or the opposite, as in the case of $C = -1$. The use of this eigenstate correlation as a tool to investigate CP violation was earlier suggested in K physics (Lipkin, 1968; Dunietz, Hauser, and Rosner, 1987; Bernabeu, Botella, and Roldan, 1988), and in B physics (Falk and Petrov, 2000; Atwood and Soni, 2002). In charm physics this method of *CP tagging* can be used to study relative strong phases of D^0 meson amplitudes. Such measurements are needed for studies of $D^0\bar{D}^0$ mixing.

To illustrate the method, the amplitude for the CP-tagged eigenstate decaying to, say, the $K\pi$ final state can be written as

$$\begin{aligned}\sqrt{2}\mathcal{A}(D_\pm \to K^-\pi^+) = \mathcal{A}(D^0 \to K^-\pi^+)\\ \pm \mathcal{A}(\bar{D}^0 \to K^-\pi^+),\end{aligned} \tag{10}$$

which follows from Eq. (6). This relation implies that

TABLE III. Correlated branching ratios for various processes. Correlated results are presented for $C = 1$ and normalized to the product of the uncorrelated branching fractions. CP violation is neglected.

Decay modes	Correlated branching fractions
$K^-\pi^+$ vs $K^-\pi^+$	R_m
$K^-\pi^+$ vs $K^+\pi^-$	$(1 + R_{\mathrm{ws},K\pi})^2 - 4r_{\delta,K\pi}(r_{\delta,K\pi} + y)$
$K^-\pi^+$ vs $S_\pm$	$1 + R_{\mathrm{ws},K\pi} \pm 2r_{\delta,K\pi} \pm y$
$K^-\pi^+$ vs $L^\pm$	$1 - \sqrt{R_{K\pi}}(y\cos\delta_{K\pi} + x\sin\delta_{K\pi})$
$S_\pm$ vs $S_\pm$	0
$S_\pm$ vs $S_\mp$	4
$S_\pm$ vs $L^\pm$	$1 \pm y$

$$1 \pm 2\cos\delta_{K\pi}\sqrt{R_{K\pi}} \equiv 1 \pm z_{K\pi}\sqrt{R_{K\pi}} = 2\frac{\mathcal{B}(D_\pm \to K^-\pi^+)}{\mathcal{B}(D^0 \to K^-\pi^+)}, \tag{11}$$

where R_f is the small ratio of the doubly Cabibbo-suppressed (DCS) decay rate to the Cabibbo-favored (CF) one (see Sec. IV), and δ_f is the strong phase difference between those amplitudes, $\mathcal{A}(\bar{D}^0 \to K^-\pi^+)/\mathcal{A}(D^0 \to K^-\pi^+) = -\sqrt{R_{K\pi}}e^{-i\delta_{K\pi}}$. Equation (11) can be used to extract $\delta_{K\pi}$ if the CP-tagged branching ratio is measured (Gronau, Grossman, and Rosner, 2001; Atwood and Petrov, 2005).

The method of quantum correlations can be used to study the multitude of parameters of D^0 decay and mixing (Atwood and Petrov, 2005; Asner *et al.*, 2006). In particular, correlated decays of D mesons into CP-mixed final states (such as $K^-\pi^+$), CP-specific final states $S_\pm$ (such as $S_+ = K^+K^-$ or $S_- = K_S\pi^0$), or a flavor specific semileptonic decay $L^\pm$ into a state containing $\ell^\pm$ can probe various combinations of mixing and decay parameters (see Table III). We defined the D^0-$\bar{D}^0$ mixing rate as $R_m = (x^2 + y^2)/2$ and the "wrong-sign" rate for the final state f as $R_{\mathrm{ws},f} = R_f + \sqrt{R_f}(y\cos\delta_f - x\sin\delta_f) + R_m$. Also, $r_{\delta,f} = \sqrt{R_f}\cos\delta_f \equiv \sqrt{R_f}z_f/2$. The quantum-correlated rates are clearly different from the singly tagged (ST) rates, i.e., when only one of the D^0 mesons is reconstructed. For example, the ST rate for the wrong-sign (e.g., $D^0 \to K^+\pi^-$) decay is given by $R_{\mathrm{ws},K\pi}$.

Besides the discussed studies of the phases of hadronic decay amplitudes, the results summarized in Table III can be used to extract D^0-$\bar{D}^0$ mixing parameters. The discussion of the current status of charm mixing goes beyond the scope of this review. For the most recent reviews, see Bianco *et al.* (2003), Artuso *et al.* (2008), and Gedalia and Perez (2010).

2. Experiments at threshold

The CLEO-c experiment plays a unique role here as it has a large data sample collected at threshold. The CLEO-c detector is an evolution of the CLEO III detector where the silicon-strip vertex detector was replaced with a low-mass inner six-layer drift chamber (Kubota *et al.*, 1992; Peterson *et al.*, 2002; Artuso *et al.*, 2003). The CLEO-c experiment is shown schematically in Fig. 3. The wires in the inner drift chamber are at a small stereo angle with respect to the drift chamber axis. This allows one to determine the z position of charged particles. The charged particle tracking system in

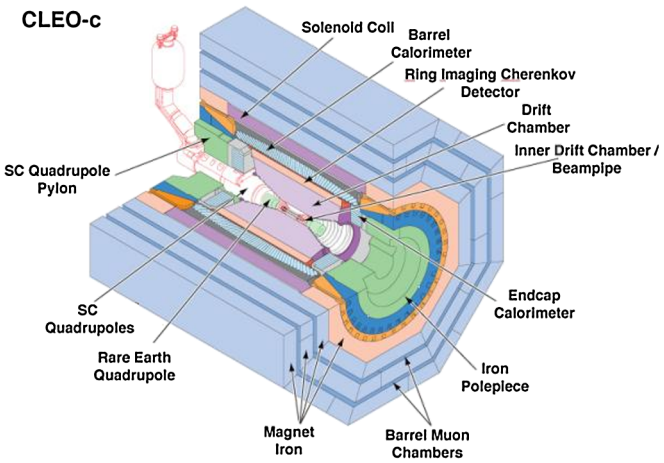

FIG. 3 (color online). The CLEO-c detector. The charged particle tracking system consists of an inner drift chamber near the interaction point and the main drift chamber for the momentum measurement. Radially outside the main drift chamber is the RICH detector for charged hadron identification followed by the CsI electromagnetic calorimeter. The instrumented flux return for muon detection is outside the superconducting solenoid coil.

CLEO-c also includes the 47-layer main drift chamber, operating in a 1.0 T magnetic field along the drift chamber axis. The CLEO-c tracking system provides a momentum resolution of about 0.6% for tracks with a momentum of 1 GeV that traverses all layers of the drift chamber. CLEO-c has excellent electromagnetic calorimetry from the approximately 7800 CsI(Tl) crystal calorimeter. For energies of 1 GeV the calorimeter has an energy resolution of about 2%. For energies of 100 MeV the resolution is about 5%. The excellent energy resolution and coverage allow CLEO-c to efficiently reconstruct π^0 and η mesons in the $\gamma\gamma$ final state. The π^0 mass resolution obtained is about 6 MeV. Charged hadrons are identified by a combination of specific ionization dE/dx in the drift chamber for particles with momenta below about 700 MeV. For higher momenta, where dE/dx is less powerful, CLEO-c uses the RICH detector to separate kaons from pions.

The BES III (Collaboration, 2009) detector constitutes a substantial upgrade of the earlier BES II detector. Among the new features are a 1 T magnetic field generated by a superconducting coil, a new drift chamber, and a CsI(Tl) doped electromagnetic calorimeter. The time-of-flight system provides π-K separation at 0.9 GeV with a 2σ separation. The operation with the BES III detector started in 2009 with a run which collected about 100×10^6 $\psi(2S)$ and 200×10^6 J/ψ events. In 2010 running at the $\psi(3770)$ started and as of August 2010 a sample of about 900 pb^{-1} was recorded.

3. Experimental features at threshold

At threshold D mesons are produced in pairs. A powerful analysis technique involves reconstructing one D meson exclusively. This allows experiments to infer the existence of another $\bar{D}$ meson in the event. This "tagging" or "double tag" technique was first used by MARK III (Baltrusaitis *et al.*, 1986; Adler *et al.*, 1988), but due to their relatively small sample of tags the technique was of limited use. With

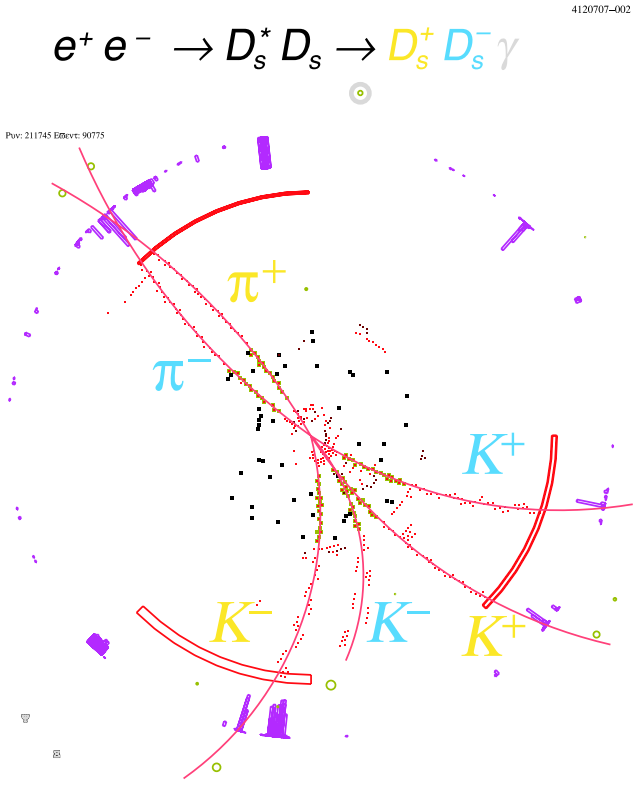

FIG. 4 (color online). Event display from CLEO-c showing a candidate $D_s^{*+}D_s^-$ event with $D_s^{*+} \to D_s^+\gamma$ and both $D_s^\pm$ candidates decaying to $K^+K^-\pi^\pm$. The charged particle trajectories, as determined from fits to the hits in the CLEO-c drift chambers, are shown as the curved lines.

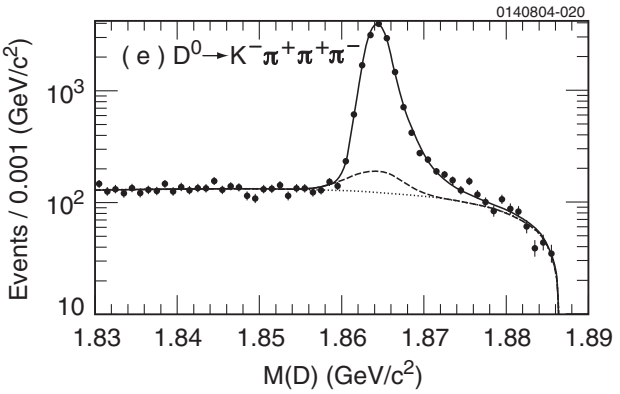

FIG. 5. The $M_{\rm BC}$ distribution. The dotted line shows the contribution from the ARGUS function that describes the combinatorial background. The solid and dashed lines show the contributions to the signal shape for two different detector resolution functions. The tail on the high side for the signal shape is due to initial-state radiation that lowers the energy of the produced D mesons.

much larger samples, and a more modern detector, the CLEO-c experiment has made great use of this tagging technique. The event environment at threshold is very clean. The $D\bar{D}$ signal is produced with no additional hadrons. An example from CLEO-c of a fully reconstructed $D_s^{*\pm}D_s^\mp$ is shown in Fig. 4.

Many analyses make use of fully reconstructed D candidates. The D candidates are built from charged kaons and pions, neutral pions, η, and K_S^0 mesons. CLEO-c typically requires that kaon and pion candidates are consistent with charged hadron particle identification based on energy loss in the drift chamber and Cherenkov radiation in the RICH detector. The K_S^0 candidates are reconstructed in the $\pi^+\pi^-$ final state. For the $\pi^+\pi^-$ pairs used to form K_S^0 candidates the usual track quality criteria are relaxed and no particle identification criteria are applied.

To extract the signal in fully reconstructed hadronic D decays it is typically required that the reconstructed D candidate energy is consistent with the beam energy, as each D in the final state will carry half of the center-of-mass energy. Specifically,

$$\Delta E \equiv E_{\rm cand} - E_{\rm beam}, \tag{12}$$

where

$$E_{\rm cand} = \sum_i \sqrt{\mathbf{p}_i^2 + m_i^2} \tag{13}$$

is the energy of the D candidate. For correctly reconstructed D candidates the ΔE distribution peaks at zero. The resolution on ΔE is mode dependent and the actual criteria applied vary between different analyses depending on the backgrounds and cleanliness of the signal that is desired.

After applying a mode dependent ΔE selection criteria the beam-constrained mass is formed

$$M_{\rm BC} \equiv \sqrt{E_{\rm beam}^2 - \left(\sum_i \mathbf{p}_i\right)^2}. \tag{14}$$

Here the candidate energy has been replaced by the beam energy which typically is much better known.

A typical plot of the $M_{\rm BC}$ distribution is shown in Fig. 5. The signal yield is determined by fitting the $M_{\rm BC}$ distribution to a background shape plus a signal shape. The background shape is due to combinatorial backgrounds either from other D decays or from continuum. The background is typically fit using an "ARGUS" function (Albrecht *et al.*, 1990)

$$a(M_{\rm BC}; m_0, \xi, \rho) = AM_{\rm BC}\left(1 - \frac{M_{\rm BC}^2}{m_0^2}\right)^\rho e^{\xi(1-M_{\rm BC}^2/m_0^2)}. \tag{15}$$

This function describes the phase-space distribution expected near the threshold at m_0 for $\rho = 1/2$ and $\xi = 0$. By allowing ρ and ξ to take on different values a more general function which can describe the data better is obtained.

For the signal shape several different parametrizations have been used. The most detailed description is that used, for example, by Dobbs *et al.* (2007). This form incorporates the effects of detector resolution, beam energy distribution, initial-state radiation, and the line shape of the $\psi(3770)$. The beam energy distribution, initial-state radiation, and the $\psi(3770)$ line shape control the energy of the produced D mesons. The effect of ISR is to produce the $\psi(3770)$ with an energy below the nominal e^+e^- center-of-mass energy. This produces a tail on the high side of the $M_{\rm BC}$ distribution as seen in Fig. 5. The detector resolution effects lead to a smearing of the measured momentum.

4. Systematic uncertainties

Many of the analyses discussed in this review are limited by systematic uncertainties. This applies, in particular, to the determination of the Cabibbo-favored D^0 and D^+ absolute branching fractions that are discussed in Sec. V. A substantial effort has been put into understanding the systematic uncertainties associated with track finding, K^0_S reconstruction, particle identification, and π^0 reconstruction. At the $\psi(3770)$ resonance many of these uncertainties can be evaluated using hadronic decays in an event environment similar to the channels studied. This gives confidence in the sometimes small systematic uncertainties obtained in these studies. The most detailed systematic studies carried out by CLEO-c are described by Dobbs *et al.* (2007). As the results of these studies are important for many results discussed in this review, some of these studies are discussed below.

Track finding has been studied in CLEO-c using a missing mass technique where all particles in an event are reconstructed except for one particle which they are interested in studying. As an example consider the use of the kaon in $D^0 \to K^-\pi^+$ to measure the kaon tracking efficiency. In this case the opposite $\bar{D}^0$ in the event is fully reconstructed in some channel and the π^+ from D^0 decay looked for. Given the $\bar{D}^0$ and π^+ candidates the missing mass in the event can be calculated as

$$M^2_{\rm miss} = (p_{\rm tot} - p_{\bar{D}} - p_{\rm other})^2, \tag{16}$$

where $p_{\bar{D}}$ is the four-momentum of the reconstructed $\bar{D}$, $p_{\rm other}$ is the four-momentum of the other particles that were combined with the tag $\bar{D}$, in this example the π^+, and $p_{\rm tot}$ is the four-momentum of the initial e^+e^- pair. In the missing mass squared calculation, the $\bar{D}$ momentum is rescaled to the momentum magnitude expected from the beam energy, but its direction is left unchanged. This constraint improves the $M^2_{\rm miss}$ resolution.

The missing mass candidates are separated into two samples: the sample where the missing particle was found and the remaining events where the missing particle was not found. An example is shown in Fig. 6. The case where the missing particle is found corresponds to a fully reconstructed $\psi(3770)$ event and is very clean. The events in this sample are fit to a signal shape using a sum of two Gaussians. A small background component is also included in the fit. For the sample where the missing particle is not found a clear peak

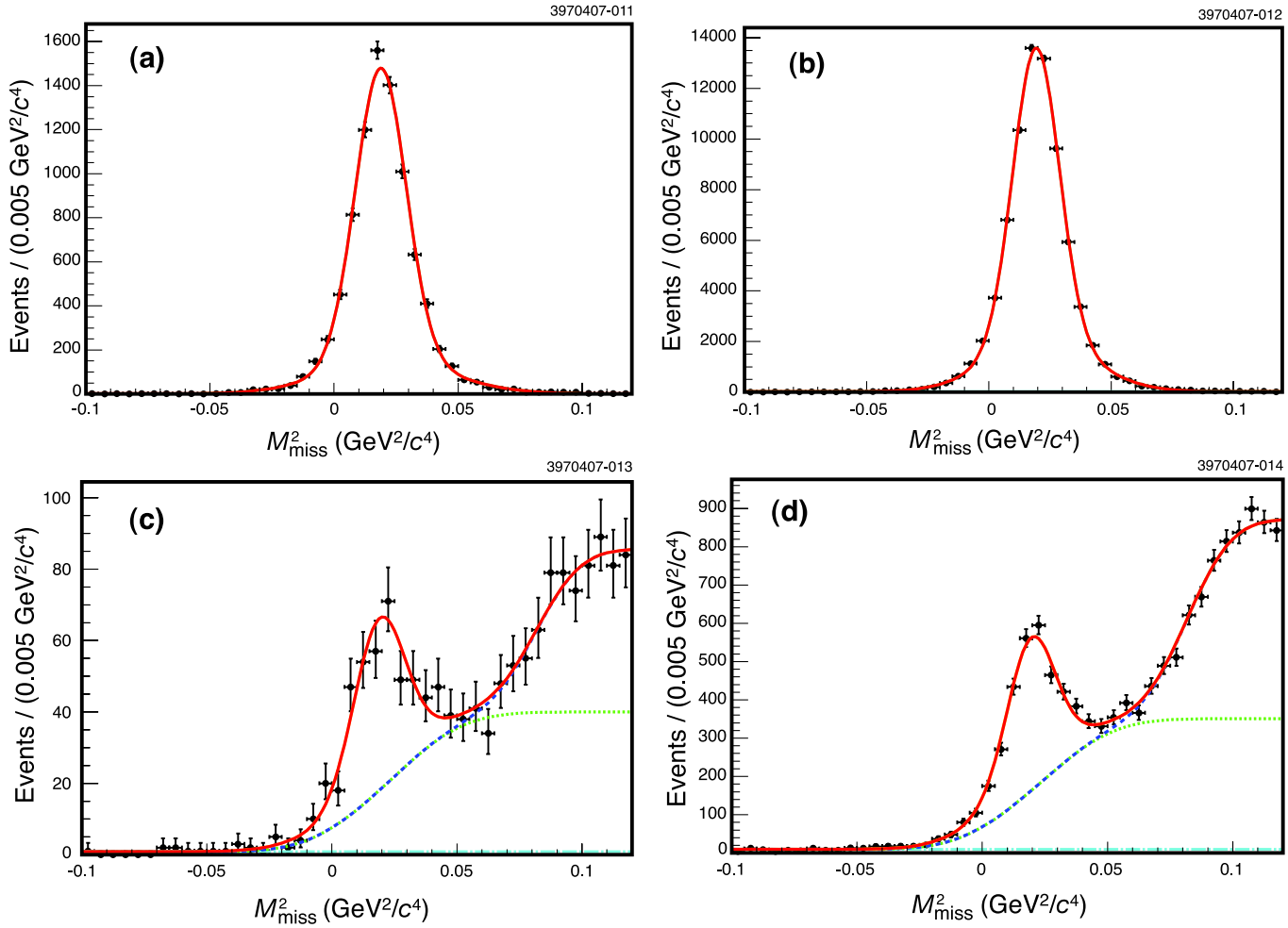

FIG. 6 (color online). Histograms of and fits to $M^2_{\rm miss}$ distributions from $D^+ \to K^-\pi^+\pi^+$ decays to determine the charged pion efficiency for $p_{\pi^+} > 0.2$ GeV. (a), (c) Events in data; (b), (d) events in Monte Carlo simulation. (a), (b) From decays in which the pion was found, while (c), (d) are from decays in which the pion was not found. The solid curves are fits to the data or Monte Carlo sample; the dashed curves in (c) and (d) are background contributions. From Dobbs *et al.*, 2007.

can be seen corresponding to the events where there was an inefficiency. In addition to this peak there are also substantial backgrounds. These backgrounds include semileptonic decays as well as higher multiplicity hadronic D decays. These backgrounds are parametrized using Monte Carlo simulated events.

As described in detail by Dobbs *et al.* (2007), CLEO-c measured the tracking efficiency for both kaons and pions in three momentum ranges ($0.2 < p < 0.5$ GeV, $0.5 < p < 0.7$ GeV, and $p > 0.7$ GeV). CLEO-c evaluated the tracking efficiency and found agreement between data and the Monte Carlo simulation and assigned a per track systematic uncertainty of $\pm 0.3\%$ for pions. For kaons an additional, uncorrelated with respect to the $\pm 0.3\%$, uncertainty of $\pm 0.6\%$ is added due to the evidence for a tracking efficiency difference between K^+ and K^-.

The $K^0_S \to \pi^+\pi^-$ reconstruction efficiency is studied in D^0 and $\bar{D}^0$ decays to $K^0_S\pi^+\pi^-$ decays using a technique similar to what was used for the tracking efficiencies. One tag D is fully reconstructed and two charged pions are required to be found. To factor out the track finding efficiency and also to reject $K^0_L\pi^+\pi^-$ and $K^0_S \to \pi^0\pi^0$ decays it is required that two additional tracks are found in the event. These tracks are required to satisfy loose consistency requirements coming from a K^0_S decay. The invariant masses of the two tracks are required to be in the range of 0.2 to 0.7 GeV. In addition, the difference between the missing momentum vector and the momentum vector of the sum of the two charged tracks is required to be less than 60 MeV. Events that satisfy these requirements are searched for a K^0_S candidate using the standard K^0_S vertex finder. Similar to the tracking studies the candidates are separated into two categories: where the K^0_S was found and where it was not found. Compared to the tracking systematics study described above the K^0_S study is more complicated because there are fake K^0_S candidates from wrong $\pi^+\pi^-$ tracks in either $K^0_S\pi^+\pi^-$ or $\pi^+\pi^-\pi^+\pi^-$ events. This gives rise to a "hole" in the events where the K^0_S candidate was not found because combinatorial background got promoted to signal. This is illustrated in Fig. 7. Using this technique CLEO-c assigns a systematic uncertainty of $\pm 1.8\%$ for the K^0_S finding efficiency.

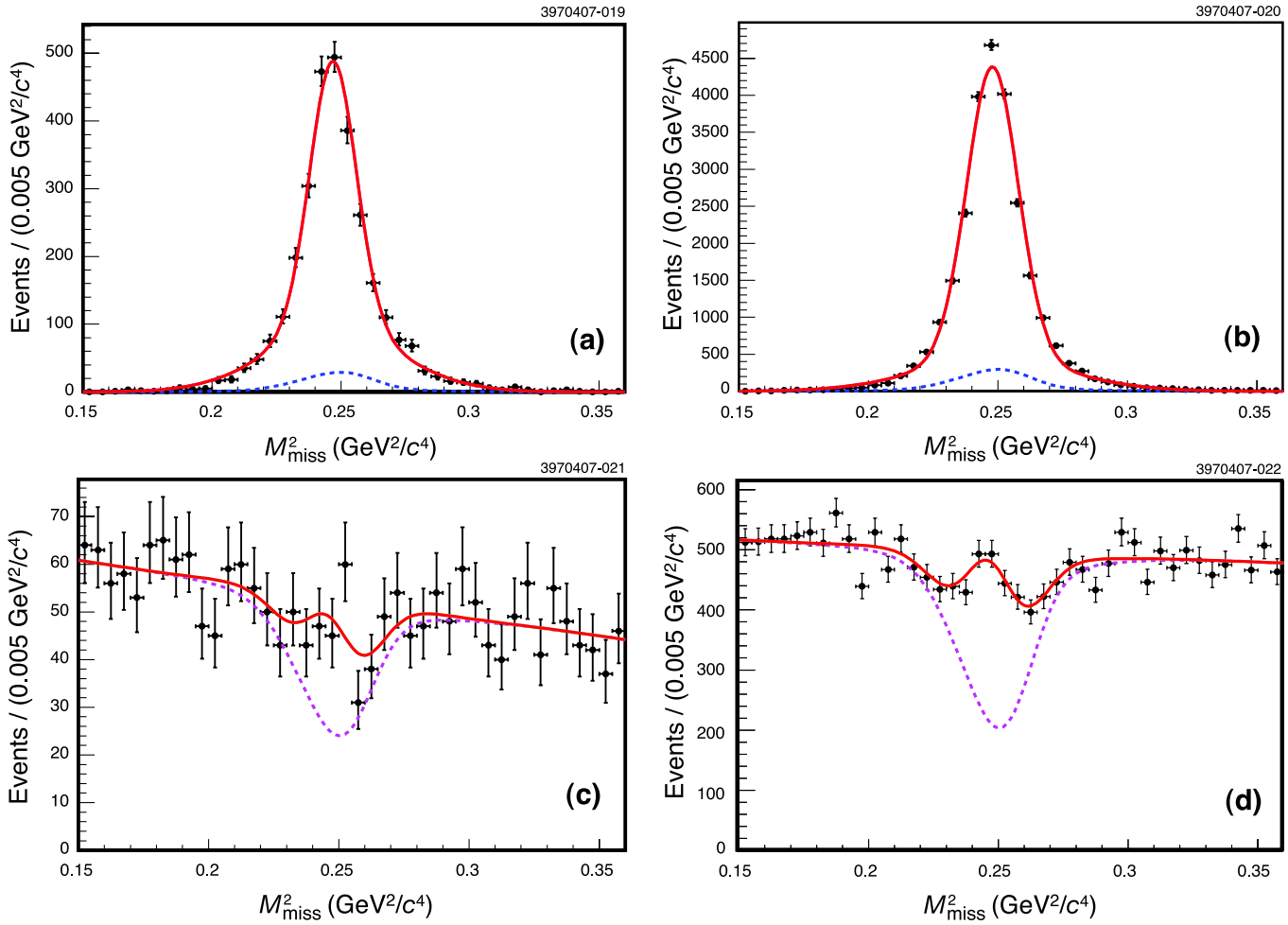

FIG. 7 (color online). Histograms of and fits to $M^2_{\rm miss}$ distributions to determine the K^0_S efficiency. (a), (c) Events in data; (b), (d) events in Monte Carlo simulation. (a), (b) From decays in which the K^0_S was found, while (c), (d) are from decays in which the K^0_S was not found. The background peak and deficit are determined by searching for K^0_S candidates in high and low sidebands of the K^0_S mass. (a), (b) Dashed curves are the contributions from fake K^0_S candidates. (c), (d)Dashed curve is the background, a linear function with a deficit due to events in which a fake K^0_S candidate was found, and the solid curve is the total fit function including the signal peak. The area between the curves is proportional to the number of K^0_S mesons not found. From Dobbs *et al.*, 2007.

The efficiency for $\pi^0 \to \gamma\gamma$ reconstruction has been studied using a missing mass technique in $\psi(2S) \to J/\psi\pi^0\pi^0$ events recorded at $E_{\text{c.m.}} = m_{\psi(2S)}$. CLEO-c assigns a $\pm 2.0\%$ uncertainty to the π^0 reconstruction efficiency.

B. $c\bar{c}$ production in e^+e^- above threshold

At energies above charm threshold, charm hadrons are produced in fragmentation of charm jets and are part of a jet, or are produced as secondary particles in decays of b hadrons. The largest charm samples are those produced at the B factories at e^+e^- center-of-mass energies near 10.58 GeV corresponding to the $\Upsilon(4S)$ resonance. The large cross section, about 1.3 nb, combined with the large integrated luminosities recorded by CLEO, *BABAR*, and Belle experiments produced large charm samples.

At even higher energy, the LEP operated near the Z resonance and produced over 4×10^6 Z bosons per experiment. The jet nature of the events here is more clear than at the $\Upsilon(4S)$.

Many studies of D^0 decays above charm threshold make use of a D^* tagging technique. In this technique a D^{*+} is reconstructed using the decay $D^{*+} \to D^0\pi^+$. Because of the small energy release in this decay, $M_{D^{*+}} - M_{D^0} - M_{\pi^+}$ is approximately 5.8 MeV; the reconstructed mass difference $M_{D^{*+}} - M_{D^0}$ provides a powerful tool to tag the presence of a D^0 and also determines the flavor at the time of production.

The CLEO, *BABAR*, and Belle experiments were designed to study B meson decays but they are also well suited for studying charm. These experiments all have excellent charged particle tracking capabilities and vertex detectors capable of detecting the separated vertices from the relatively long lived charm and beauty hadrons. All three experiments have CsI(Tl) electromagnetic calorimeters with excellent photon detection capabilities and electron identification using E/p. Detection of muons in all three experiments is done using an instrumented flux return. Also key for these experiments is the identification of charged hadrons, particularly K-π separation. The three experiments chose different technologies here. *BABAR* used a detector of internally reflected Cherenkov light (DIRC), CLEO-III used a ring imaging Cherenkov detector (RICH), and Belle used aerogel Cherenkov counters complemented by a time-of-flight system. All three different types of charged hadron particle identification detectors have worked well.

The *BABAR* and Belle experiments were built for an energy asymmetric collision to allow resolving the time evolution of the produced B mesons, as discussed by Harrison and Quinn (1998). The energy asymmetric collisions are reflected in the design of the detector; the interaction point is offset to optimize the acceptance due to the boost of the collision center of mass.

C. Fixed target experiments

Charm mesons are sufficiently light so that they can be produced efficiently in fixed target experiments. The main experimental challenge is to separate charm production from the large noncharm rate. The development of silicon based tracking detectors enabled experiments to effectively identify the long-lived charmed hadrons. The pioneering Fermilab photoproduction experiment E691 was the first experiment to produce large samples of reconstructed charm hadrons. In this experiment a beam of photons with an average energy around 180 GeV was incident on a beryllium target. The cross section for charm production was measured to be about 0.5 μb. This is about 0.5% of the 100 μb total hadronic cross section. The E791 experiment was a pioneering experiment for hadroproduction of charm: 200 000 hadronic charm decays were reconstructed. The most powerful tool for identifying the charm signal is to make use of the relatively long charm-hadron lifetimes, from 410.1 ± 1.5 fs for the D^0 to 1040 ± 7 fs for the D^+. Using silicon vertex detectors it is possible to separate the long-lived charm hadrons from the prompt backgrounds. A series of fixed target experiments for charm physics are summarized in Table II. The latest of these experiments at Fermilab, FOCUS or E831, reconstructed over 1.2×10^6 exclusive charm decays. The FOCUS spectrometer is shown in Fig. 8. The FOCUS experiment and experimental techniques are described by Link *et al.* (2002a, 2002d, 2004c). Measurements (Link *et al.*, 2002c, 2005a) from FOCUS dominate the world average for the lifetimes of charmed mesons.

D. Proton-antiproton experiments

The Fermilab Tevatron collider, colliding protons and antiprotons at a center-of-mass energy of 1.96 TeV, has produced a large number of charmed mesons. Each of the two experiments at the Tevatron, CDF and D0, has collect over 6 fb^{-1}. With a D^0 cross section of 13 μb^{-1} for $|\eta| < 1.0$ and $p_T > 5.5$ GeV this corresponds to over 10^{10} produced D^0 mesons. However, at a hadron collider the challenge is to trigger on these events. At CDF the use of a separated vertex trigger (Ashmanskas *et al.*, 2004) designed for B physics also allowed triggering on tracks from charmed hadrons. CDF has competitive results on a number of Cabibbo-suppressed (CS) charm meson branching fractions as discussed in Sec. VII.B.1.

E. Final-state radiation

The treatment of FSR is common to many analyses and is discussed here. In many earlier measurements the effects of final-state radiation were often omitted, but as the measurements have become increasingly more precise this has become an important effect that cannot be ignored. In the latest measurements of the branching fraction for $D^0 \to K^-\pi^+$ the size of the radiative correction is larger than the combined statistical and systematic uncertainties.

Any reaction involving charged particles also radiates photons (Bloch and Nordsieck, 1937). In fact, an arbitrarily large number of photons will be produced, although most of these are soft. In general, when we discuss a branching fraction for a process, as for example $\mathcal{B}(D^0 \to K^-\pi^+)$, this includes final states with additional (soft) photons. Experimentally, if photons are emitted with an energy that is smaller than the experimental resolution, these events are automatically included in the measurement. However, sometimes the photon energies are larger, and the energy carried

away by the photon will make the event fail the selection criteria. In order to account for this, and provide a measurement of a physically meaningful quantity, experiments simulate the effect of final-state radiation in their Monte Carlo simulations. This has been a common practice for semileptonic decays, in particular, with electrons in the final state, for quite some time. For hadronic final states this is not yet universally done. In D decays the first experiment that considered FSR corrections was CLEO (Akerib *et al.*, 1993). Today most measurements of hadronic D decays include FSR corrections.

For simulation of final-state radiation in hadronic decays the most commonly used tool is the PHOTOS package (Barberio and Was, 1994). In the measurement of the $D^0 \to K^-\pi^+$ branching fraction CLEO-c uses version 2.15 with interference enabled. The effect of interference, here referring to interference between photons radiated from different charged particles in the final state, is important. For the final state $D^0 \to K^-\pi^+$ the effect of including interference changes the fraction of events that radiate more than 30 MeV from 2.0% to 2.8%. Earlier versions of PHOTOS were able only to simulate the interference for decays to final state with a particle-antiparticle pair. PHOTOS has been compared with calculations to higher order in α and found to reproduce the amount of energy radiated well in semileptonic decays of B mesons and decays of τ leptons (Richter-Was, 1993). However, for hadronic final states there is an additional uncertainty introduced by the fact that the final-state particles, kaons and pions, are not pointlike. This uncertainty affects, in particular, higher energy photons that probe the structure of the final-state particles. Higher energy photons could also be radiated directly from the quarks; this effect is not included in the simulation. CLEO-c includes a 30% systematic uncertainty on the correction to the branching fraction due to including final-state radiation. Given the excellent agreement between exact calculations and next order calculations in α this systematic uncertainty is probably conservative.

For many earlier measurements it is not always clear what was done to correct for the FSR effects. If the effects due to FSR are not included in the analysis, it is hard to correct for it after the fact as the signal efficiency loss due to FSR depends on the selection criteria used and the experimental resolution.

IV. THEORETICAL DESCRIPTION OF D DECAYS

Hadronic decays of D mesons involve transitions of the initial-state D meson into several final-state mesons or baryons. Thus, they are described by an effective Hamiltonian containing four-quark operators. The theoretical description of hadronic decays of charmed mesons is significantly more complicated than leptonic or semileptonic ones, although relevant effective Hamiltonians look similar.

Charmed hadronic decays are usually classified by the degree of CKM matrix element suppression. Least suppressed, where the quark-level transitions are $c \to s u \bar{d}$ are labeled Cabibbo-favored decays and are governed by

$$\mathcal{H}_{\rm CF} = \frac{G_F}{\sqrt{2}} V_{ud} V_{cs}^* [C_1(\mu)\mathcal{O}_1 + C_2(\mu)\mathcal{O}_2] + \text{H.c.}, \tag{17}$$

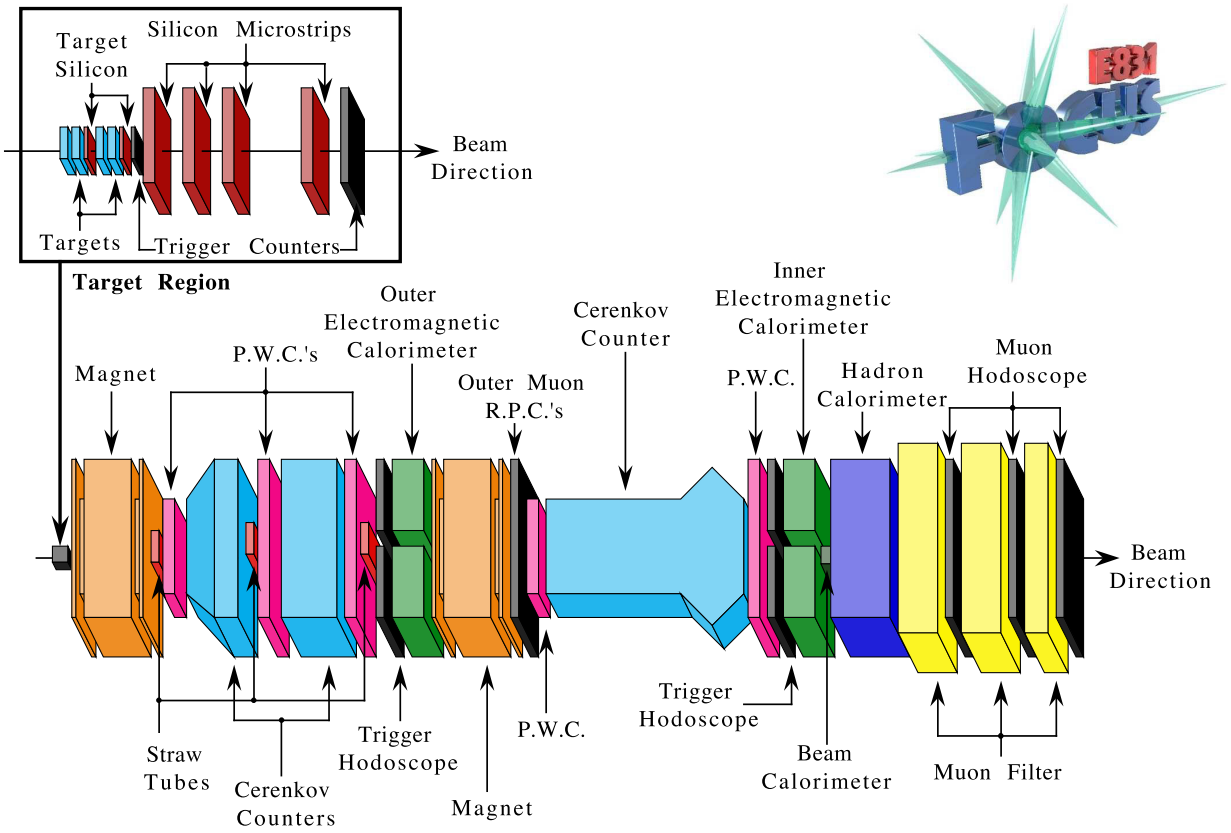

FIG. 8 (color online). The FOCUS (E831) spectrometer. Figure provided by the FOCUS Collaboration.

$$\mathcal{O}_1 = (\bar{s}_i \Gamma_\mu c_i)(\bar{u}_k \Gamma^\mu d_k), \tag{18}$$

$$\mathcal{O}_2 = (\bar{s}_i \Gamma_\mu c_k)(\bar{u}_k \Gamma^\mu d_i), \tag{19}$$

where $C_n(\mu)$ are the Wilson coefficients obtained by perturbative QCD running from M_W scale to the scale μ relevant for hadronic decay, and the Latin indices denote quark color. G_F is a Fermi constant, and $\Gamma_\mu = \gamma_\mu(1-\gamma_5)$.

The (CS or singly Cabibbo-suppressed (SCS) transitions are driven by $c \to du\bar{d}$ or $c \to su\bar{s}$ quark processes. Because of the presence of the quark-antiquark pair of the same flavor in the final state, the effective Hamiltonian takes a much more elaborate form,

$$\mathcal{H}_{\rm CS} = \frac{G_F}{\sqrt{2}} \sum_{q=s,d} V_{uq} V_{cq}^* [C_1(\mu)\mathcal{O}_1^q + C_2(\mu)\mathcal{O}_2^q] - \frac{G_F}{\sqrt{2}} V_{ub} V_{cb}^* \sum_{n=3}^{6} C_n(\mu)\mathcal{O} + \text{H.c.}, \tag{20}$$

$$\mathcal{O}_1 = (\bar{q}_i \Gamma_\mu c_i)(\bar{u}_k \Gamma^\mu q_k), \tag{21}$$

$$\mathcal{O}_2 = (\bar{q}_i \Gamma_\mu c_k)(\bar{u}_k \Gamma^\mu q_i), \tag{22}$$

where $q = d$, s, and $\mathcal{O}_{3-6}$ are the so-called "penguin" operators of the type $(\bar{u}c)_{V-A}\sum_q(\bar{q}q)_{V\pm A}$ [see, e.g., Buccella *et al.* (1995) and Buccella, Lusignoli, and Pugliese (1996)]. It is often easy to denote the degree of suppression by powers of the Wolfenstein parameter $\lambda = \sin\theta_C = V_{us} \simeq 0.22$, where θ_C is a Cabibbo angle.

The doubly Cabibbo-suppressed decay is the one in which $c \to du\bar{s}$ quark transition drives the decay. The effective Hamiltonian for DCS decay can be obtained from Eq. (17) by interchanging $s \leftrightarrow d$.

Calculations of hadronic decay rates governed by these transitions are quite complicated and model dependent. Most often, simplified assumptions, such as factorization (Buras, Gerard, and Ruckl, 1986; Bauer, Stech, and Wirbel, 1987), are used to estimate the needed branching ratios. Some dynamical approaches, such as QCD sum rules, have been used to justify those assumptions (Blok and Shifman, 1993). The main problem with reliable calculations of charmed meson decays is that they populate the energy range where nonperturbative quark dynamics is active. This leads to resonance effects that affect the phases of hadronic decay amplitudes (Falk, Nir, and Petrov, 1999), which makes predictions based on factorization quite unreliable.

It remains a difficult exercise in QCD to calculate nonfactorizable corrections to hadronic decay amplitudes. QCD sum rules provided the first systematic way to include those (Blok and Shifman, 1993), albeit in the SU(3) flavor-symmetry limit. A large N_c limit provided another interesting insight into this problem (Buras, Gerard, and Ruckl, 1986), however, calculation of (supposedly large) $1/N_c$ corrections is not possible at the moment. It was also shown (Gao, 2007) that application of the QCD factorization approach developed for B decays (Beneke *et al.*, 1999) does not provide a reliable method of calculation for charm hadronic transitions. The methods developed in those references represented fascinating exercises in using QCD-based approaches to calculate hadronic decay amplitudes. The discussion of those methods goes beyond the scope of this review, but we encourage the interested reader to examine those papers.

Instead of predicting an absolute decay rate, it is often useful to obtain relations among several decay rates. These relations are helpful when some decay rates in a relation are measured, and some are unknown. This allows for a relation to be used to predict the unknown transition rate(s). The relations can be built based on some symmetries, such as standard flavor SU(3) (Savage, 1991), or on an overcomplete set of universal quark-level amplitudes (Gronau *et al.*, 1994; Rosner, 1999). We discuss those methods below.

The partial width for a specific two-body decay of a charmed meson depends on both the invariant amplitude $\mathcal{A}$ and a phase-space factor. For a specific two-body decay into a PP final state,

$$\Gamma(D \to PP) = \frac{|\mathbf{p}|}{8\pi M_D^2} |\mathcal{A}(D \to PP)|^2, \tag{23}$$

where $|\mathbf{p}|$ is a center-of-mass three-momentum of each final-state particle. For a decay into a PV final state,

$$\Gamma(D \to PV) = \frac{|\mathbf{p}|^3}{8\pi M_D^2} |\mathcal{A}(D \to PV)|^2. \tag{24}$$

Note that in the case of the PP final state the final-state mesons are in the S wave, while in the case of the PV final state they are in a P wave. This is why $|\mathcal{A}(D \to PP)|$ has dimension of energy, while $|\mathcal{A}(D \to PV)|$ is dimensionless.

A. SU(3)$_F$ flavor symmetries

One popular approach that was adopted for studies of hadronic charm decays involves application of approximate flavor symmetries, such as flavor SU(3)$_F$. This approach is based on the fact that the QCD Lagrangian acquires that symmetry in the limit where masses of all light quarks are the same. The SU(3)$_F$ analysis of decay amplitudes cannot predict their absolute values. However, at least in the symmetry limit, this approach can relate transition amplitudes for different decays, which could prove quite useful for an experimental analysis. One potential difficulty with this approach is related to the fact that available experimental data show that flavor SU(3)$_F$ symmetry is broken in charm transitions, so symmetry-breaking corrections should be taken into account (Savage, 1991; Hinchliffe and Kaeding, 1996).

In the flavor-symmetry approach all particles are denoted by their SU(3)$_F$ representations. Charm quark transforms as singlet under flavor SU(3). The fundamental representation of SU(3)$_F$ is a triplet **3**, so the light quarks u, d, and s belong to this representation with $(1, 2, 3) = (u, d, s)$. The operator D_i that creates a $\bar{D}$ meson is of the form $\bar{c}u$, so it also transforms in the fundamental representation of SU(3). In the hadronic decay of a charm meson the final-state mesons are made of u, d, and s quarks, so they form either an octet **8** representation of SU(3)$_F$ (pseudoscalars $\pi^\pm$, π^0, $K^\pm$, K^0, $\bar{K}^0$, and η_8 and vectors $\rho^\pm$, ρ^0, $K^{*\pm}$, K^{*0}, $\bar{K}^{*0}$, and ω_8), e.g.,

$$P_i^k = \begin{pmatrix} \frac{1}{\sqrt{6}}\eta_8 + \frac{1}{\sqrt{2}}\pi^0 & \pi^+ & K^+ \\ \pi^- & \frac{1}{\sqrt{6}}\eta_8 - \frac{1}{\sqrt{2}}\pi^0 & K^0 \\ K^- & \bar{K}^0 & -\sqrt{\frac{2}{3}}\eta_8 \end{pmatrix}, \quad (25)$$

or an $SU(3)_F$ singlet (η_1 and ω_1). The physical states η, η', ϕ, and ω are linear combinations of $\eta_{1,8}$ and $\omega_{1,8}$ states, respectively.

The $\Delta C = -1$ part of the weak Hamiltonian has the flavor structure $(\bar{q}_i c)(\bar{q}_j q_k)$ [see Eq. (17)], so its matrix representation is written with a fundamental index and two antifundamentals H_k^{ij}. This operator is a sum of irreducible representations contained in the product $3 \times \bar{3} \times \bar{3} = \overline{15} + 6 + \bar{3} + \bar{3}$. In the limit in which the third generation is neglected, H_k^{ij} is traceless, so only the $\overline{15}$ (symmetric on i and j) and 6 (antisymmetric on i and j) representations appear. That is, the $\Delta C = -1$ part of $\mathcal{H}_w$ may be decomposed as $\frac{1}{2}(\mathcal{O}_{\overline{15}} + \mathcal{O}_6)$, where

$$\begin{aligned}\mathcal{O}_{\overline{15}} = {} & (\bar{s}c)(\bar{u}d) + (\bar{u}c)(\bar{s}d) + s_1(\bar{d}c)(\bar{u}d) \\ & + s_1(\bar{u}c)(\bar{d}d) - s_1(\bar{s}c)(\bar{u}s) - s_1(\bar{u}c)(\bar{s}s) \\ & - s_1^2(\bar{d}c)(\bar{u}s) - s_1^2(\bar{u}c)(\bar{d}s), \end{aligned} \quad (26)$$

$$\begin{aligned}\mathcal{O}_6 = {} & (\bar{s}c)(\bar{u}d) - (\bar{u}c)(\bar{s}d) + s_1(\bar{d}c)(\bar{u}d) - s_1(\bar{u}c)(\bar{d}d) \\ & - s_1(\bar{s}c)(\bar{u}s) + s_1(\bar{u}c)(\bar{s}s) - s_1^2(\bar{d}c)(\bar{u}s) \\ & + s_1^2(\bar{u}c)(\bar{d}s), \end{aligned} \quad (27)$$

and $s_1 = \sin\theta_C \approx 0.22$. The matrix representations $H(\overline{15})_k^{ij}$ and $H(6)_k^{ij}$ have nonzero elements

$$\begin{aligned} H(\overline{15})_k^{ij}&: H_2^{13} = H_2^{31} = 1, \qquad H_2^{12} = H_2^{21} = s_1, \\ & H_3^{13} = H_3^{31} = -s_1, \qquad H_3^{12} = H_3^{21} = -s_1^2, \\ H(6)_k^{ij}&: H_2^{13} = -H_2^{31} = 1, \qquad H_2^{12} = -H_2^{21} = s_1, \\ & H_3^{13} = -H_3^{31} = -s_1, \qquad H_3^{12} = -H_3^{21} = -s_1^2. \end{aligned} \quad (28)$$

In the $SU(3)_F$ limit the effective Hamiltonian for the hadronic decays to two pseudoscalars $D \to PP$ can be written as

$$\begin{aligned}\mathcal{H}_{\text{eff SU(3)}} = {} & a_{\overline{15}} D_i H(15)_k^{ij} P_j^l P_l^k + b_{\overline{15}} D_i P_l^i H(15)_k^{lj} P_j^k \\ & + c_6 D_i H(6)_k^{ij} P_j^l P_l^k. \end{aligned} \quad (29)$$

There are a number of amplitude relations that can be obtained from Eq. (29). In particular, it can be seen that it implies that $|A_{D^0 \to K^+K^-}| = |A_{D^0 \to \pi^+\pi^-}|$. In practice, the corresponding branching fractions differ by a factor of 3 (see Table XVI). Clearly, $SU(3)_F$ symmetry is broken in D decays.

A consistent approach should then include $SU(3)_F$-breaking corrections, which could consistently be included in the analysis. For example, one could assume that $SU(3)_F$ breaking is proportional to light-quark masses. In this case, it can be included in the analysis as a perturbation that transforms as $\mathbf{8} + \mathbf{1}$, as the quark mass operator belongs to the matrix representation $M_j^i = \text{diag}(m_u, m_d, m_s)$, which is an $\mathbf{8}$. Note that the $SU(3)_F$ breaking term that transforms as a triplet $\mathbf{3}$ also breaks isospin, so it is usually neglected in all analyses. A complete analysis with broken $SU(3)_F$ is possible (Savage, 1991; Hinchliffe and Kaeding, 1996), although it is not quite as useful due to a large number of unknown amplitudes.

In some cases one does not need to employ the full formalism of $SU(3)_F$, but rely only on its subgroups. An example of such a subgroup is isospin. Isospin relations among decay amplitudes are much more robust, as isospin breaking is believed to be quite small in charm decays. For example, the dipion modes $D^+ \to \pi^+\pi^0$, $D^0 \to \pi^+\pi^-$, and $D^0 \to \pi^0\pi^0$ are related by two isospin amplitudes A_0 and A_2 corresponding, respectively, to the S-wave dipion isospin $I = 0$ and $I = 2$ states produced

$$\begin{aligned} A^{+0} &= \sqrt{\frac{3}{2}}A_2, \qquad A^{+-} = \sqrt{\frac{2}{3}}A_0 + \sqrt{\frac{1}{3}}A_2, \\ A^{00} &= \sqrt{\frac{1}{3}}A_0 - \sqrt{\frac{2}{3}}A_2. \end{aligned} \quad (30)$$

Some conclusions about strong-interaction dynamics in D meson decays can be reached by extracting these amplitudes from experimental information. The phases of amplitudes in Eq. (30) give an indication of the size of strong interactions among decay products in those decays. Following the procedure outlined by Selen *et al.* (1993), CLEO obtained (Rubin *et al.*, 2006) $|A_2/A_0| = 0.420 \pm 0.014 \pm 0.016$ and $\arg(A_2/A_0) = (86.4 \pm 2.8 \pm 3.3)°$ from their results. As one can see, the phase is rather large. It is thus clear that final-state interactions play an important role in D decays.

Other subgroups of the $SU(3)_F$ also offer useful predictions. For example, the U spin, a symmetry of the Lagrangian with respect to $s \to d$ quark interchange, can be employed to obtain several useful relations. For example, for the decays of D^0 mesons into final states containing $M^0 = \pi^0$, η, and η', one obtains

$$\frac{\mathcal{A}(D^0 \to K^0 M^0)}{\mathcal{A}(D^0 \to \bar{K}^0 M^0)} = -\tan^2\theta_C. \quad (31)$$

Equation (31) derives from the following argument. The initial state D^0 contains c and $\bar{u}$ quarks, and so is a U-spin singlet. The CF transition $c \to sd\bar{d}$ and DCS transition $c \to du\bar{s}$ produce $U = 1$ finals states with opposite third component $U_3 = \pm 1$ in the decays of the D^0 meson. The final-state meson M^0 forms a linear combination of U-spin singlet and triplet states, while neutral kaons are $U = 1$, $U_3 = \pm 1$ states. Thus, the U-spin triplet part of M^0 cannot be produced, as it leads to the $U = 2$ final state. Thus, only the singlet part of M^0 can contribute to the transition, which leads to Eq. (31).

B. Flavor-flow (topological) diagram approach

Another useful approach to tackle hadronic decays of charmed mesons, equivalent to the $SU(3)_F$ amplitude method described above, is the flavor-flow [or topological SU(3)] approach, which involves an overcomplete set of quark diagrams (Gronau *et al.*, 1994; Rosner, 1999). The application of this method to D decays can even prove advantageous compared to the flavor SU(3) approach, as the number of unknown amplitudes grows rapidly if $SU(3)_F$ breaking is taken into account.

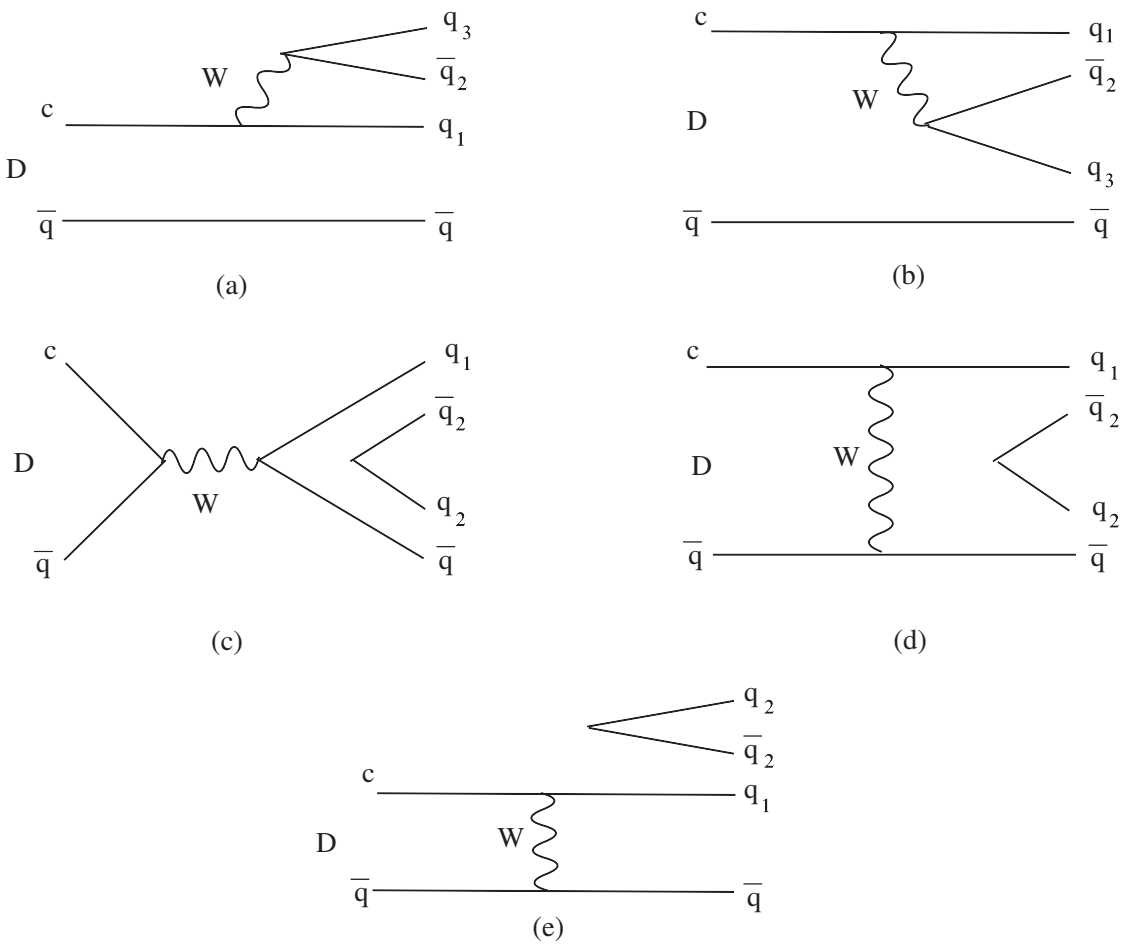

FIG. 9. Basic topological amplitudes for D meson decays. (a) Tree $T^{(\prime)}$; (b) color-suppressed $C^{(\prime)}$; (c) weak annihilation $A^{(\prime)}$;(d) weak exchange $E^{(\prime)}$; and (e) singlet weak exchange SE'. CSC amplitudes are usually denoted by primes.

In the topological flavor-flow approach each decay amplitude is parametrized according to the topology of Feynman diagrams (see Fig. 9): a color-favored tree amplitude (usually denoted by T), a color-suppressed tree amplitude (C), an exchange amplitude (E), and an annihilation amplitude (A). This set of amplitudes is sufficient for description of CF and DCS decays. For SCS decays other amplitudes must be added (Chiang, Luo, and Rosner, 2003).

In order to describe charm meson decays in terms of these amplitudes, it is convenient to decompose initial and final states according to their isospin structure. For instance, in the notation of Rosner (1999), the following phase conventions are used.

(1) Charmed mesons: $D^0 = -c\bar{u}$, $D^+ = c\bar{d}$, and $D_s = c\bar{s}$.
(2) Pseudoscalar mesons: $\pi^+ = u\bar{d}$, $\pi^0 = -(u\bar{u} - d\bar{d})/\sqrt{2}$, $\pi^- = -d\bar{u}$, $K^+ = u\bar{s}$, $K^0 = d\bar{s}$, $\bar{K}^0 = s\bar{d}$, $K^- = -s\bar{u}$, $\eta = (s\bar{s} - u\bar{u} - d\bar{d})/\sqrt{3}$, and $\eta' = (u\bar{u} + d\bar{d} - 2s\bar{s})/\sqrt{6}$.
(3) Vector mesons: $\rho^+ = u\bar{d}$, $\rho^0 = -(u\bar{u} - d\bar{d})/\sqrt{2}$, $\rho^- = -d\bar{u}$, $\omega^0 = (u\bar{u} + d\bar{d})/\sqrt{2}$, $K^{*+} = u\bar{s}$, $K^{*0} = d\bar{s}$, $\bar{K}^{*0} = s\bar{d}$, $K^{*-} = -s\bar{u}$, and $\phi = s\bar{s}$.

As with the SU(3)$_F$ approach, this method does not provide absolute predictions for the branching fractions in D meson decays. However, it provides relations among several decay amplitudes by matching the quark-level "flavor topology" graphs with the final states defined above. For example, a DCS transition $D^0 \to K^+\pi^-$ can proceed via a tree-level amplitude $T(c \to u\bar{s}d)$ and an exchange amplitude $E(c\bar{u} \to \bar{s}d)$. Matching those with the initial-state meson $D^0 = -c\bar{u}$ and final-state mesons $K^+ = u\bar{s}$ and $\pi^- = -d\bar{u}$, one obtains the following amplitude relation:

$$A(D^0 \to K^+\pi^-) = T + E \equiv \frac{G_F}{\sqrt{2}} V_{ud}V_{cs}^*(\mathcal{T} + \mathcal{E}), \quad (32)$$

where we use calligraphic notation for the amplitudes with $G_F/\sqrt{2}$ and CKM factors removed. Similarly, for other transitions one obtains

$$A(D^0 \to K^0\pi^0) = \frac{1}{\sqrt{2}}(C - E) = \frac{1}{\sqrt{2}}\frac{G_F}{\sqrt{2}} V_{us}V_{cd}^*(\mathcal{C}'' - \mathcal{E}''), \quad (33)$$

$$A(D^0 \to \bar{K}^0\pi^0) = \frac{1}{\sqrt{2}}(C - E) = \frac{1}{\sqrt{2}}\frac{G_F}{\sqrt{2}} V_{ud}V_{cs}^*(\mathcal{C} - \mathcal{E}), \quad (34)$$

$$A(D^+ \to K^0\pi^+) = C + A = \frac{G_F}{\sqrt{2}} V_{us}V_{cd}^*(\mathcal{C}'' + \mathcal{A}''), \quad (35)$$

$$A(D^+ \to \bar{K}^0\pi^+) = T + C = \frac{G_F}{\sqrt{2}} V_{ud}V_{cs}^*(\mathcal{T} + \mathcal{C}), \quad (36)$$

$$A(D^0 \to K^0\eta) = \frac{1}{\sqrt{3}}C = \frac{1}{\sqrt{3}}\frac{G_F}{\sqrt{2}} V_{us}V_{cd}^*\mathcal{C}'', \quad (37)$$

etc. Note that in Eq. (33) we denoted DCS amplitudes with double primes. Singly Cabibbo-suppressed amplitudes are conventionally denoted by a single prime. CF amplitudes can be related to SCS and DCS amplitudes by proper scaling with $\tan\theta_C$. We give particular examples below.

The employed phase convention makes it easy to build $SU(3)_F$-required sum rules. For example, for transitions $D^+ \to K^+\pi^0$, $D^+ \to K^+\eta$, and $D^+ \to K^+\eta'$, a sum rule

$$3\sqrt{2}A(K^+\pi^0) + 4\sqrt{3}A(K^+\eta) + \sqrt{6}A(K^+\eta') = 0 \quad (38)$$

can be written. With the flavor-flow parametrization,

$$A(D^+ \to \bar{K}^+\pi^0) = \frac{1}{\sqrt{2}}(T - A), \quad (39)$$

$$A(D^+ \to \bar{K}^+\eta) = -\frac{1}{\sqrt{3}}T, \quad (40)$$

$$A(D^+ \to \bar{K}^+\eta') = \frac{1}{\sqrt{6}}(T + 3A), \quad (41)$$

the above sum rule gives $3(T - A) - 4T + (T + 3A) = 0$.

Thus, provided that a sufficient number of decay modes is measured, one can predict both branching fractions and amplitude phases for a number of transitions. Still, no prediction for absolute branching ratios is possible in this approach.

C. Factorization ansatz

The simplest way to estimate an absolute decay rate of a charmed meson is to employ a factorization ansatz. This ansatz implies that the amplitude for the hadronic transition can be written as a product of known form factors. Schematically,

$$\mathcal{A}(D_q \to M_1M_2) = \langle M_1, M_2|\mathcal{H}|D_q\rangle \sim \langle M_1|(\bar{u}_k\Gamma^\mu q_k)|0\rangle \times \langle M_2|(\bar{q}_i\Gamma_\mu c_i)|D_q\rangle. \quad (42)$$

This is a clear simplification, as the first nonperturbative parameter $\langle M_1|(\bar{u}_k\Gamma^\mu q_k)|0\rangle$ can be written in terms of a meson decay constant f_{M_1},

$$\langle M_1|\bar{u}\gamma^\mu\gamma_5 q|0\rangle = if_{M_1}p_{M_1}^\mu, \quad (43)$$

which parametrizes the amplitude of probability for quarks to "find each other" in light mesons and be measured in leptonic decays of M_1,

$$\Gamma(M_1 \to \ell\nu) = \frac{G_F^2}{8\pi}f_{M_1}^2 m_\ell^2 m_{M_1}\left(1 - \frac{m_\ell^2}{m_{M_1}^2}\right)^2|V_{uq}|^2, \quad (44)$$

where m_{M_1} is the M_1 mass, m_ℓ is the mass of the final-state lepton, and $|V_{uq}|$ is the CKM matrix element associated with the $q \to u$ transition. The decay constants can also be computed in lattice gauge theories or using other nonperturbative approaches [see Artuso *et al.* (2008) for a recent review].

The second nonperturbative parameter $\langle M_2|(\bar{q}_i\Gamma_\mu c_i)|D_q\rangle$ is related to form factors that can be extracted from semileptonic D_q decays,

$$\frac{d\Gamma(D \to M_2 e\nu_e)}{dq^2} = \frac{G_F^2|V_{cq}|^2}{24\pi^3}|\mathbf{p}_{M_2}|^3|f_+(q^2)|^2, \quad (45)$$

where $\mathbf{p}_{M_2}$ is the hadron three-momentum in the D rest frame. Note that, in principle, Eq. (45) depends on two form factors (see below). We dropped the contribution from $f_-(q^2)$ because it is multiplied by m_e^2.

Theoretical parametrizations of semileptonic decays involve two nonperturbative quantities parametrizing the matrix element of a single hadronic current. Traditionally, the hadronic matrix elements for transitions to pseudoscalar hadrons are described in terms of two form factors, $f_+(q^2)$ and $f_-(q^2)$,

$$\langle M_2|\bar{q}\Gamma^\mu c|D\rangle = f_+^{D\to M_2}(q^2)P^\mu + f_-^{D\to M_2}(q^2)q^\mu, \quad (46)$$

where $P = p_D + p_{M_2}$ and $q = p_D - p_{M_2}$. An alternative parametrization is often used,

$$\langle M_2|\bar{q}\Gamma^\mu c|D\rangle = \left(P^\mu - \frac{m_D^2 - m_{M_2}^2}{q^2}q^\mu\right)f_+^{D\to M_2}(q^2) + \frac{m_D^2 - m_{M_2}^2}{q^2}q^\mu f_0^{D\to M_2}(q^2), \quad (47)$$

with $f_0^{D\to M_2}(q^2) = f_+^{D\to M_2}(q^2) + f_-^{D\to M_2}(q^2)q^2/(m_D^2 - m_{M_2}^2)$. Form factors have been evaluated at specific q^2 points in a variety of phenomenological models, where the shape is typically assumed from some model arguments.

Clearly, naive factorization of Eq. (42), while convenient, cannot be correct, as it assumes that scale and scheme dependence of a product of quark bilinears is the same as that of a four-fermion operator, which it is not. The situation can in principle be corrected, at least in the heavy-quark limit. In B decays, a QCD factorization formula has been written that takes into account perturbative QCD corrections (Beneke *et al.*, 1999). However, it is not clear that this approach is applicable to charm decays, as charm quark might be too light for this approach to be applicable. Nevertheless, even naive factorization provides a convenient way to estimate D meson decay rates.

Besides decay amplitudes for D mesons, which can be computed using the factorization arguments above, both flavor-flow and $SU(3)_F$ amplitudes can also be estimated. For example, contrary to Eq. (31), the corresponding relation for charged D meson decays,

$$\frac{\mathcal{A}(D^+ \to K^0\pi^+)}{\mathcal{A}(D^+ \to \bar{K}^0\pi^+)} = -\tan^2\theta_C\frac{\mathcal{C}'' + \mathcal{A}''}{\mathcal{C} + \mathcal{T}} = \frac{\mathcal{C} + (C_2/C_1)\mathcal{E}}{\mathcal{C} + \mathcal{T}}, \quad (48)$$

cannot be fixed by symmetry arguments alone. However, the factorization approach can be used to estimate this ratio. In particular,

$$\mathcal{T} = f_\pi(m_D^2 - m_K^2)f_+^{D\to K}(m_\pi^2)a_1, \quad (49)$$

$$\mathcal{C} = f_K(m_D^2 - m_\pi^2) f_+^{D\to\pi}(m_\pi^2) a_2, \tag{50}$$

$$\mathcal{T}'' = f_K(m_D^2 - m_\pi^2) f_+^{D\to\pi}(m_K^2) a_1, \tag{51}$$

$$\mathcal{C}'' = f_\pi(m_D^2 - m_K^2) f_+^{D\to K}(m_\pi^2) a_2, \tag{52}$$

where $a_{1,2} = C_{1,2} + C_{2,1}/N_c$. Note that some analyses employ $a_{1,2} \to a_{1,2}^{\rm eff}$, which are fitted from the data and treated as universal fit parameters. This way of calculating charm hadronic decay matrix elements is sometimes called the "modified factorization" approach. The argument for doing this is an attempt to include unknown nonperturbative corrections to Eq. (49). While this approach defines a convenient model to deal with hadronic decays, there is no reason to believe that soft contributions are universal in all transitions.

Calculations of $\mathcal{E}$ and $\mathcal{A}$ amplitudes in factorization are much more complicated. It was argued (Gao, 2007) that they can be estimated using methods similar to those employed in B decays (Beneke *et al.*, 1999). Numerically, the calculation of the ratio of Eq. (48) amounts to

$$\frac{\mathcal{A}(D^+ \to K^0\pi^+)}{\mathcal{A}(D^+ \to \bar{K}^0\pi^+)} = -\tan^2\theta_C r_s e^{i\phi_s}, \tag{53}$$

with $r_s \approx 1.521$ and $\phi_s \approx 103°$ for $C_2/C_1 \approx -0.5$. This ratio will be used to estimate decay asymmetries with kaons later in this paper.

V. CABIBBO-FAVORED D^0 AND D^+ DECAYS

The absolute branching fractions for decays of the ground state charmed mesons are important as they are used to normalize many B- and D-meson decays. For example, the determination of $|V_{cb}|$ from $B \to D^*\ell\nu$ (Richman and Burchat, 1995) depends directly on the determination of the D branching fractions used to reconstruct the final state.

To measure the absolute branching fractions we need to have a mechanism to determine the number of D mesons produced. As the cross sections for producing D mesons are not directly calculable we have to count the D mesons in the data sample. Broadly speaking there are two methods employed for this D counting. At threshold MARK-III and CLEO-c used a tagging technique described in Sec. III.A, where one D meson is fully reconstructed and tags the existence of another $\bar{D}$ in the event. At higher energies the presence of a D^{*+} meson can be tagged using the "slow pion" in the $D^{*+} \to D^0\pi^+$ decay. The slow pion in this decay is often denoted π_s. This slow pion tagging technique was used by several experiments including CLEO and ALEPH to count the number of $D^{*+} \to D^0\pi^+$ decays in charm jets produced in e^+e^- collisions. A variation of this idea was used by ARGUS, CLEO, and *BABAR* where D^* mesons produced in semileptonic B decays, $\bar{B}^0 \to D^{*+}\ell^-\bar{\nu}$, are tagged by the presence of a slow pion and a lepton. These different techniques are discussed in this section.

Before the CLEO-c measurement of the $D^+ \to K^-\pi^+\pi^+$ branching fraction using tagging as described in Sec. V.C there was a statistics limited study by MARK-III (Adler *et al.*, 1988) and model-dependent analyses. CLEO (Balest *et al.*, 1994) reconstructed the two decay chains $D^{*+} \to D^0\pi^+$, $D^0 \to K^-\pi^+$ and $D^{*+} \to D^+\pi^0$, $D^+ \to K^-\pi^+\pi^+$. This allowed CLEO to measure the ratio of produced $K^-\pi^+\pi^+$ to $K^-\pi^+$ final states, which can be expressed as

$$\frac{N_{K\pi\pi}}{N_{K\pi}} = \frac{\mathcal{B}(D^{*+} \to D^+\pi^0)\mathcal{B}(D^+ \to K^-\pi^+\pi^+)\epsilon(K\pi\pi)}{\mathcal{B}(D^{*+} \to D^0\pi^+)\mathcal{B}(D^0 \to K^-\pi^+)\epsilon(K\pi)}, \tag{54}$$

where $\epsilon(K\pi\pi)$ and $\epsilon(K\pi)$ are the efficiencies for reconstructing the $D^+ \to K^-\pi^+\pi^+$ and $D^0 \to K^-\pi^+$ final states, respectively, including the D^{*+}. To extract the $D^+ \to K^-\pi^+\pi^+$ branching fraction CLEO used the measured $D^0 \to K^-\pi^+$ branching fraction and the ratio

$$\frac{\mathcal{B}(D^{*+} \to D^+\pi^0)}{\mathcal{B}(D^{*+} \to D^0\pi^+)}. \tag{55}$$

The determination of this ratio is discussed by Butler *et al.* (1992) and Bartelt *et al.* (1998); it ultimately relies on isospin conservation. Though the errors are expected to be small they are hard to quantify.

A. Absolute D^0 branching fractions using slow pion tagging

The method of tagging $D^{*+} \to D^0\pi^+$ decays in jets produced in $e^+e^- \to c\bar{c}$ interactions by the presence of a slow pion from the D^* decay is sometimes referred to as the HRS technique after the first experiment that used this method. As the Q value of the $D^{*+} \to D^0\pi^+$ decay is only about 5 MeV and the produced pion has a momentum of only 39 MeV in the D^* rest frame it can at most contribute this amount to the transverse momentum with respect to the thrust axis. Experimentally, the slow pion from the D^{*+} decay closely follows the original D^* direction. Because of the soft track associated with this decay, the pion tends to bend out from the jet in the magnetic field of the tracking system.

The HRS experiment (Abachi *et al.*, 1988) used 300 pb^{-1} of data collected at $E_{\rm c.m.} = 29$ GeV. For candidate slow pions the transverse momentum p_T is calculated with respect to the thrust axis determined from the particles in the opposite hemisphere with respect to the slow pion candidate under consideration. The choice of using only tracks in the opposite hemisphere for the calculation of the thrust axis is to avoid any possible bias due to the decay of the D meson. In Fig. 10 the p_T^2 distribution is shown in two ranges of the fractional momentum $x_F = 2p_\parallel/E_{\rm c.m.}$ of the slow pion, where $p_\parallel$ is the component of the slow pion momentum that is parallel to the thrust axis. In the low fractional momentum range ($0.03 < x_F < 0.06$) a clear excess is seen at low values of the transverse momentum due to slow pions from $D^{*+} \to D^0\pi^+$ decays. This excess is not present in the higher x_F range as slow pions from D^{*+} decays do not populate this range. The HRS Collaboration used the excess at low p_t^2 to determine that they had 1584 ± 110 $D^{*+} \to D^0\pi^+$ decays in their sample. Next a D^0 is reconstructed in the $D^0 \to K^-\pi^+$ channel. The D^0 candidate is combined with the slow pion and the mass difference $M_{K\pi\pi_s} - M_{K\pi}$ is required to be in the range 0.143 to 0.148 GeV. The yield was determined by fitting the $M_{K\pi}$ mass distribution. A total of 56 ± 9 events were observed. The efficiency for finding the $K\pi$ pair, given that the π_s is found, is determined to be 79% giving a branching fraction of $\mathcal{B}(D^0 \to K^-\pi^+) = (4.5 \pm 0.8 \pm 0.5)\%$. The

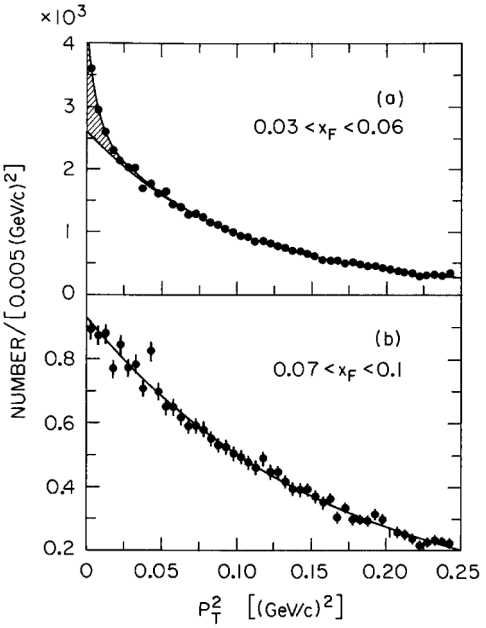

FIG. 10. The p_T^2 distribution for data from the HRS Collaboration. (a) The fractional slow pion momentum in the range $0.03 < x_F < 0.06$; (b) the fractional momentum range $0.07 < x_F < 0.1$. In the low momentum range where we expect slow pions from D^* decays a clear excess at low p_t^2 is seen. From Abachi *et al.*, 1988.

largest systematic uncertainty quoted is bias due to event selection criteria. This uncertainty is evaluated by changing the event selection criteria to remove the thrust and collinearity criteria used. The analysis was limited by statistics.

The same technique as pioneered above by the HRS Collaboration was used by ALEPH (Decamp *et al.*, 1991; Barate *et al.*, 1997), CLEO (Akerib *et al.*, 1993), and ARGUS (Albrecht *et al.*, 1994b). ALEPH used a sample of e^+e^- data collected from 1991 to 1994 at LEP near the Z pole. CLEO and ARGUS used samples of 1.79 fb^{-1} and 355 pb^{-1}, respectively, of e^+e^- data collected near the $\Upsilon(4S)$ resonance.

ALEPH followed the HRS approach closely. They analyzed the data in six ranges of the slow pion momentum, from 1.0 to 4.0 GeV. The transverse momentum squared distributions in the six momentum bins are shown in Fig. 11. A $D^0 \to K^-\pi^+$ candidate is searched for in events with a slow pion, and candidates where $0.1435 < M_{K\pi\pi_s} - M_{K\pi} < 0.1475$ GeV are accepted. In Table IV the yields and branching fractions from the ALEPH analysis are summarized. The results from the different momentum bins are combined, including correlations, to obtain the final result

$$\mathcal{B}(D^0 \to K^-\pi^+) = (3.90 \pm 0.09 \pm 0.12)\%. \tag{56}$$

This result includes corrections (1.9%) due to final-state radiation. The largest systematic uncertainties come from the background shape in extracting the inclusive D^* yield and the modeling of the angle between the D^* and the jet thrust axis.

ARGUS used the same technique to count $D^{*+} \to D^0\pi^+$ decays. To extract the $D^{*+} \to D^0\pi^+$ yield ARGUS plotted the distributions of $|\cos\theta|$, where θ is the angle between the slow pion candidate and the thrust axis of the jet in the opposite hemisphere. Figure 12 shows the $|\cos\theta|$ distribution in two ranges of the slow pion momentum. In the momentum range 0.2 to 0.3 GeV a clear excess of events near $|\cos\theta| = 1$ is seen from $D^{*+} \to D^0\pi^+$ decays. In the range 0.4 to 0.5 GeV no excess is seen as this is above the momentum where we have slow pions from D^{*+} decays. From a fit to the

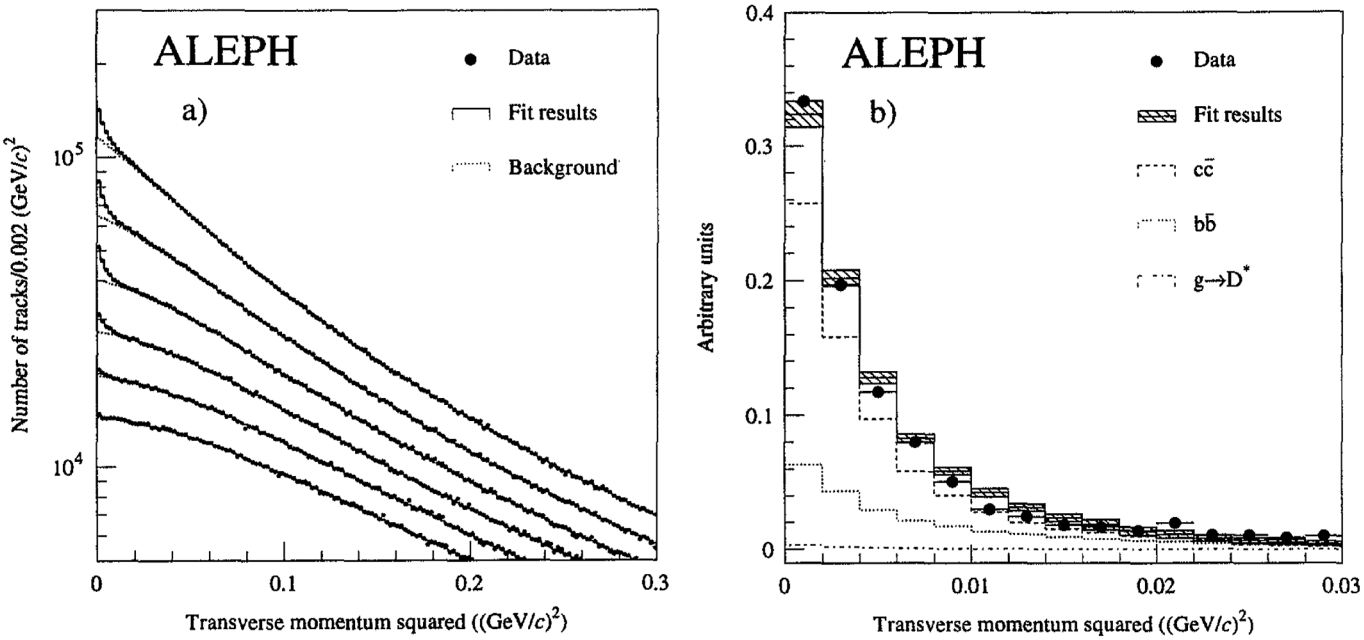

FIG. 11. The p_t^2 distribution for data from the ALEPH experiment. (a) The transverse slow pion momentum squared in six equal momentum bins from 1.0 to 4.0 GeV. The 1.0 to 1.5 GeV momentum bin is the uppermost and the 3.5 to 4.0 GeV bin is the lowest. The slow pion from $D^{*+} \to D^0\pi^+$ is clearly visible in the lower momentum range. (b) The transverse momentum distributions from different sources of D^* mesons. From Barate *et al.*, 1997.

TABLE IV. Event yields and branching fractions for the ALEPH study (Barate *et al.*, 1997) of the $D^0 \to K^-\pi^+$ decay in bins of the slow pion momentum. The first column is the momentum range, the second and third columns show the $D^{*+} \to D^0\pi^+$ yield determined from the slow pion transverse momentum and the $D^0 \to K^-\pi^+$ yields, respectively. The last column shows the $D^0 \to K^-\pi^+$ branching fraction.

Momentum range (GeV)	$N_{D^{*+}\to D^0\pi^+}$	$N_{D^0\to K^-\pi^+}$	$\mathcal{B}(D^0 \to K^-\pi^+)$ (%)
1.0–1.5	79 038.2 ± 2021.9 ± 12 018.0	2472.9 ± 55.5 ± 11.0	4.400 ± 0.150 ± 1.041
1.5–2.0	56 393.2 ± 1140.4 ± 921.6	1558.3 ± 41.4 ± 5.4	3.990 ± 0.133 ± 0.139
2.0–2.5	35 303.4 ± 855.8 ± 842.2	913.8 ± 30.9 ± 2.8	3.768 ± 0.157 ± 0.150
2.5–3.0	12 287.8 ± 674.7 ± 535.1	321.5 ± 18.2 ± 1.3	3.758 ± 0.296 ± 0.206
3.0–3.5	3497.4 ± 499.2 ± 630.4	115.7 ± 10.9 ± 0.7	5.010 ± 0.857 ± 1.228
3.5–4.0	192.4 ± 366.8 ± 401.5	9.8 ± 3.3 ± 0.4	7.44 ± 14.2 ± 19.4

$|\cos\theta|$ distribution ARGUS determined a yield of 51 327 ± 757 $D^{*+} \to D^0\pi^+$ decays in the sample. The systematic uncertainty on this yield is estimated to be 5.9% by varying the signal shape parametrization. ARGUS reconstructed the D^0 in three channels and determined the following branching fractions:

$$\mathcal{B}(D^0 \to K^-\pi^+) = (3.41 \pm 0.12 \pm 0.28)\%, \tag{57}$$

$$\mathcal{B}(D^0 \to K^-\pi^+\pi^-\pi^+) = (6.80 \pm 0.27 \pm 0.57)\%, \tag{58}$$

$$\mathcal{B}(D^0 \to \bar{K}^0\pi^-\pi^+) = (5.03 \pm 0.39 \pm 0.49)\%. \tag{59}$$

The CLEO (Akerib *et al.*, 1993) study is similar to the ARGUS analysis. CLEO studied only the final state $D^0 \to K^-\pi^+$. They tagged 165 658 ± 1, 149 ± 2485 $D^{*+} \to D^0\pi^+$ decays and measured the branching fraction

$$\mathcal{B}(D^0 \to K^-\pi^+) = (3.95 \pm 0.08 \pm 0.17)\%. \tag{60}$$

This includes a correction of about 1% for the effects of final-state radiation. The largest contribution to the systematic uncertainty (± 4.0%) comes from the track reconstruction efficiency for the final $K\pi$ system.

These measurements are limited by systematic uncertainties on the determination of the number of $D^{*+} \to D^0\pi^+$ decays in the data sample. The yield is extracted by extrapolating the background into the signal region based on shapes determined from Monte Carlo simulations.

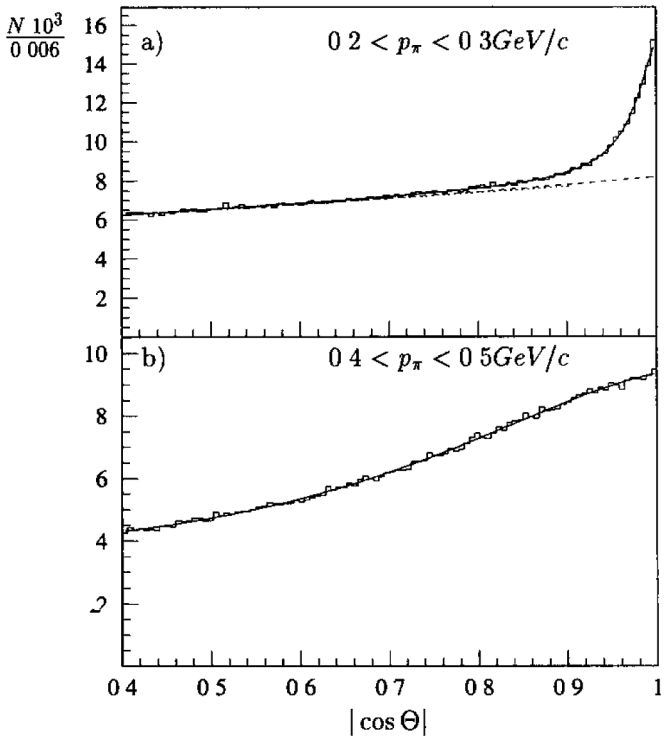

FIG. 12. The $|\cos\theta|$ distribution for data from the ARGUS experiment. (a) The distribution for the slow pion momentum in the range 0.2 to 0.3 GeV, and (b) for the range 0.4 to 0.5 GeV. From Albrecht *et al.*, 1994b.

B. Tagging with $\bar{B}^0 \to D^{*+}\ell^-\bar{\nu}$

Tagging semileptonic B decays with the presence of a lepton plus a slow pion was first used by ARGUS (Albrecht *et al.*, 1994a) and has since been used by CLEO (Artuso *et al.*, 1998) and most recently by *BABAR* (Aubert *et al.*, 2008b). The *BABAR* analysis used the largest data sample 210 fb^{-1} of e^+e^- data collected at the $\Upsilon(4S)$.

In the first study that used this technique ARGUS used a sample of 246 pb^{-1} of e^+e^- data collected at the $\Upsilon(4S)$ containing 209 000 ± 9500 $B\bar{B}$ pairs. They obtained the branching fractions

$$\mathcal{B}(D^0 \to K^-\pi^+) = (4.5 \pm 0.6 \pm 0.4)\%, \tag{61}$$

$$\mathcal{B}(D^0 \to K^-\pi^+\pi^+\pi^-) = (7.9 \pm 1.5 \pm 0.9)\%. \tag{62}$$

This measurement is clearly statistics limited; ARGUS reconstructed a sample of 2693 ± 183 ± 105 $D^{*+} \to D^0\pi^+$ candidates.

CLEO used a sample of 3.1 fb^{-1} of e^+e^- data collected at the $\Upsilon(4S)$ containing 3.3×10^6 $B\bar{B}$ events. A sample of 1.6 fb^{-1} of data collected below the $\Upsilon(4S)$ resonance was used for continuum subtraction. CLEO reconstructed 44 504 ± 360 inclusive events and 1165 ± 45 exclusive $D^0 \to K^-\pi^+$ decays and determined the branching fraction

$$\mathcal{B}(D^0 \to K^-\pi^+) = (3.81 \pm 0.15 \pm 0.16)\%. \tag{63}$$

This branching fraction does not include radiative corrections.

BABAR used 210 fb^{-1} of e^+e^- data collected at the $\Upsilon(4S)$ resonance, corresponding to 230×10^6 $B\bar{B}$ pairs, and 22 fb^{-1} collected 40 MeV below the resonance. The off-resonance

sample is used to subtract non-$B\bar{B}$ backgrounds. In this analysis the semileptonic B decay, $\bar{B}^0 \to D^{*+}\ell^-\bar{\nu}$ followed by $D^{*+} \to D^0\pi^+$, is used. *BABAR* used the lepton in the B decay and the slow pion from the D^* to count $\bar{B}^0 \to D^{*+}\ell^-\bar{\nu}$ decays followed by $D^{*+} \to D^0\pi^+$. *BABAR* used both electrons and muons in the momentum range $1.4 < |\mathbf{p}_\ell| < 2.3$ GeV/c. For the soft pion candidate the momentum is in the range $60 < |\mathbf{p}_{\pi_s}| < 190$ MeV. As the energy release in the $D^{*+} \to D^0\pi^+$ decay is small the reconstructed slow pion direction is used to approximate the direction of the D^{*+}. The momentum magnitude of the D^{*+} is parametrized as a linear function of the slow pion momentum. Using this estimate of the D^{*+} momentum, the missing mass squared of the neutrino is given by

$$M_\nu^2 = (E_{\text{beam}} - E_{D^*} - E_\ell)^2 - (\mathbf{p}_{D^*} + \mathbf{p}_\ell)^2, \tag{64}$$

where E_{beam} is half the center-of-mass energy and the momentum of the B is taken to be zero. The energies and momenta in this expression are evaluated in the e^+e^- center-of-mass frame. For signal candidates it is required that the charges of the slow pion and the lepton are opposite. For background studies *BABAR* considered same-charge candidates. *BABAR* extracted the number of $\bar{B}^0 \to D^{*+}\ell^-\bar{\nu}$ decays using the missing mass squared M_ν^2 against the D^* and the lepton. Besides the $\bar{B}^0 \to D^{*+}\ell^-\bar{\nu}$ signal events there are a few additional sources of events that peak near zero in the missing mass squared. *BABAR* included the following events as signal candidates: (1) $\bar{B} \to D^{*+}(n\pi)\ell^-\bar{\nu}$ (D^{**}), where $n \geq 1$; (2) $\bar{B} \to D^{*+}\bar{D}$, $\bar{D} \to \ell^- X$; (3) $\bar{B}^0 \to D^{*+}\tau^-\bar{\nu}$, $\tau^- \to \ell^-\bar{\nu}_\ell\nu_\tau$ (cascade); and (4) $\bar{B}^0 \to D^{*+}h^-$ (fake lepton), where h^- is a kaon or pion that has been misidentified as a lepton. The M_ν^2 distributions are shown in Fig. 13. A clear signal is observed for $M_\nu^2 > -2.0$ GeV^2. However, there are substantial backgrounds from combinatorics in $B\bar{B}$ events and in continuum production that need to be subtracted. The continuum background is modeled using off-resonance data and the $B\bar{B}$ combinatorial background, as well as the signal components, is modeled using Monte Carlo simulations. The signal yields are extracted from fits to the M_ν^2 distributions in the range from -10.0 to 2.5 GeV^2. The data are divided into ten different lepton momentum ranges to reduce sensitivity to the Monte Carlo simulation. In each lepton momentum bin the continuum yields are fixed by scaling the off-resonance sample to the luminosity of the on-resonance sample, while the number of events from the primary signal D^{**} and combinatorial $B\bar{B}$ are independently varied. The contributions from cascades and fake leptons are fixed from the simulation. These two contributions account for about 3% of the total inclusive signal.

Table V summarizes the event yields for the inclusive $\bar{B}^0 \to D^{*+}\ell^-\bar{\nu}$ reconstruction in the column labeled "Inclusive." *BABAR* found $N^{\text{incl}} = 2\,170\,640 \pm 3040 \pm 18\,100$ $\bar{B}^0 \to D^{*+}\ell^-\bar{\nu}$ decays followed by $D^{*+} \to D^0\pi^+$ in their data sample.

The next step in this analysis is to reconstruct the $D^0 \to K^-\pi^+$ decay. All reconstructed charged tracks in the event are considered except for the tracks associated with the lepton and slow pion candidates. Pairs of tracks with opposite charge are combined, and the track with the opposite charge with respect to the slow pion candidate is assigned the kaon mass.

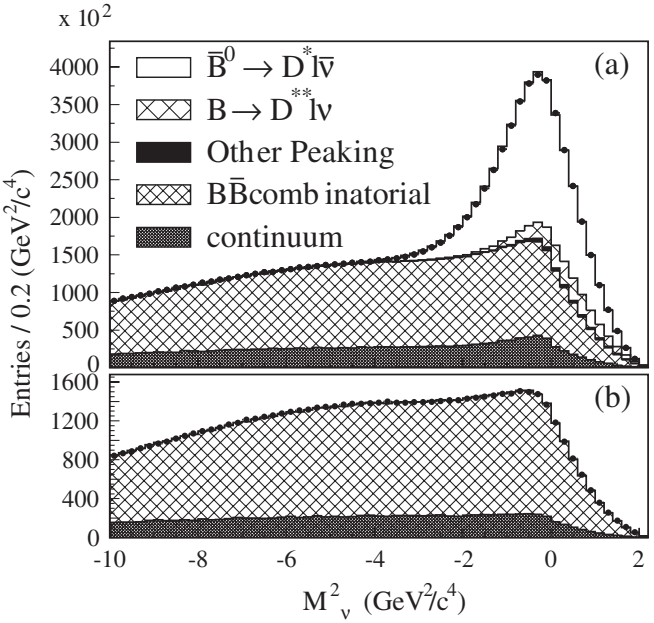

FIG. 13. The distribution of the missing mass squared M_ν^2 for (a) - right-sign events and (b) wrong-sign events. The wrong-sign events show that the simulation of the background shape is good. From Aubert *et al.*, 2008b.

The kaon candidate is required to satisfy loose kaon identification criteria that retain more than 80% of real kaons while rejecting 95% of pions. The kaon plus pion invariant mass is required to satisfy $1.82 < M_{K\pi} < 1.91$ GeV. Each D^0 candidate is combined with the slow pion and the mass difference $\Delta M = M(K^-\pi^+\pi_s^+) - M(K^-\pi^+)$ is computed. The signal is looked for in the range $142.4 < \Delta M < 149.9$ MeV.

Besides the signal events, the exclusive sample contains continuum, combinatorial $B\bar{B}$, uncorrelated peaking D^{*+}, and Cabibbo-suppressed decays. As for the inclusive sample, the continuum background is subtracted using the off-resonance sample. The combinatorial $B\bar{B}$ background is determined from simulated $B\bar{B}$ events, normalized in the ΔM sideband $153.5 < \Delta M < 162.5$ MeV. The background from uncorrelated peaking D^{*+} arises from events where the D^{*+} and lepton comes from different B mesons. This background peaks in ΔM but not in M_ν^2. This background is estimated using the sideband in M_ν^2. The backgrounds from Cabibbo-suppressed $D^0 \to K^-K^+$ and $D^0 \to \pi^-\pi^+$ decays are subtracted using simulated events.

TABLE V. Event yields for the inclusive $\bar{B}^0 \to D^{*+}\ell^-\bar{\nu}$ reconstruction and the exclusive analysis where the $D^0 \to K^-\pi^+$ final state is reconstructed in the *BABAR* analysis (Aubert *et al.*, 2008b) to determine the branching fraction for $D^0 \to K^-\pi^+$ decay. Errors are statistical only.

Source	Inclusive (10^6)	Exclusive (10^4)
Data	4.4124 ± 0.0021	4.727 ± 0.022
Continuum	0.46 ± 0.0021	0.309 ± 0.017
Combinatorial $B\bar{B}$	1.7817 ± 0.0007	0.819 ± 0.005
Peaking		0.163 ± 0.008
Cabibbo suppressed		0.055 ± 0.001
Signal	2.1706 ± 0.0030	3.381 ± 0.029

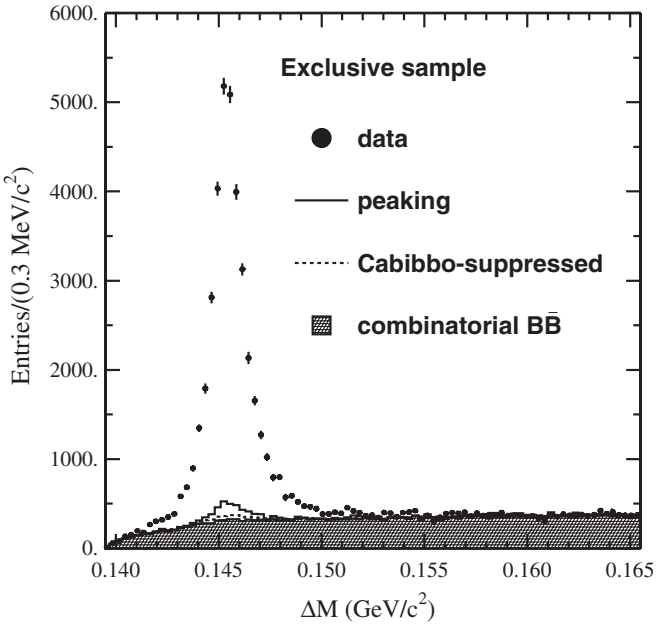

FIG. 14. The ΔM distribution for the reconstructed $D^0 \to K^-\pi^+$ candidates in events with a $\bar{B}^0 \to D^{*+}\ell^-\bar{\nu}$ tag. From Aubert *et al.*, 2008b.

The mass difference ΔM is shown in Fig. 14. The yields for this "exclusive" sample are given in Table V. After background subtraction *BABAR* found $N^{\rm excl} = (3.381 \pm 0.029) \times 10^4$ events, where the uncertainty is statistical only. The branching fraction for $D^0 \to K^-\pi^+$ is calculated using

$$\mathcal{B}(D^0 \to K^-\pi^+) = \frac{N^{\rm excl}}{N^{\rm incl}\xi\epsilon_{K\pi}}, \tag{65}$$

where $\epsilon_{K\pi} = (36.96 \pm 0.09)\%$ from simulation and $\xi = 1.033 \pm 0.002$ is the selection bias for the partial reconstruction. The selection bias stems from the fact that the reconstruction efficiency for the slow pion is larger in events where $D^0 \to K^-\pi^+$ than in generic D decays with more tracks.

BABAR considered many sources of systematic uncertainties that affects the measured $D^0 \to K^-\pi^+$ branching fraction. The most important uncertainties include selection bias ($\pm 0.35\%$), nonpeaking combinatorial background ($\pm 0.89\%$), peaking combinatorial background ($\pm 0.34\%$), tracking efficiency for kaon and pion ($\pm 1.00\%$), K^- identification ($\pm 0.70\%$), D^0 invariant mass selection ($\pm 0.56\%$), and final-state radiation in the $D^0 \to K^-\pi^+$ decay ($\pm 0.50\%$). The total systematic uncertainty is estimated to be $\pm 1.80\%$. *BABAR* obtained the final result

$$\mathcal{B}(D^0 \to K^-\pi^+) = (4.007 \pm 0.037 \pm 0.072)\%.$$

C. Absolute D hadronic branching fractions using double tags

CLEO-c (He *et al.*, 2005; Dobbs *et al.*, 2007) used a double tag technique, where by reconstructing one D in the event the presence of an additional $\bar{D}$ in the event is tagged. By determining how often the other D meson can be reconstructed in the event the branching fraction for the D decays can be calculated. This type of analysis was first pioneered by the Mark III Collaboration (Baltrusaitis *et al.*, 1986; Adler *et al.*, 1988). The CLEO-c analysis described here used the same basic idea.

The CLEO-c analysis determined the number of single tags, separately for D and $\bar{D}$ decays,

$$N_i = \epsilon_i \mathcal{B}_i N_{D\bar{D}} \tag{66}$$

and

$$\bar{N}_j = \bar{\epsilon}_j \mathcal{B}_j N_{D\bar{D}}, \tag{67}$$

where ϵ_i and $\mathcal{B}_i$ are the efficiencies and branching fractions for mode i and $N_{D\bar{D}}$ is the number of produced $D\bar{D}$ pairs. Although the yields are determined separately for D and $\bar{D}$ decays, it is assumed that the branching fractions are the same. Similarly, CLEO-c reconstructed double tags where both D mesons are reconstructed. The number of double tags found was given by

$$N_{ij} = \epsilon_{ij} \mathcal{B}_i \mathcal{B}_j N_{D\bar{D}}, \tag{68}$$

where i and j label the D and $\bar{D}$ mode used to reconstruct the event and ϵ_{ij} is the efficiency for reconstructing the final state. Combining the equations one can solve for $N_{D\bar{D}}$ as

$$N_{D\bar{D}} = \frac{N_i \bar{N}_j}{N_{ij}} \frac{\epsilon_{ij}}{\epsilon_i \bar{\epsilon}_j}. \tag{69}$$

This gives the number of produced $D\bar{D}$ events. Note that many systematic uncertainties cancel in the ratio of efficiencies. This includes, for example, track finding efficiencies and particle identification that are common to efficiencies in the denominator and numerator. However, systematic uncertainties from, for example, the determination of the yields do not cancel as they are not correlated. In this analysis CLEO-c determined all single tag and double tag yields in data and the efficiencies from Monte Carlo simulations. The branching fractions and $D\bar{D}$ yields are extracted from a combined fit to all measured data yields and efficiencies.

CLEO-c used three D^0 decay modes ($K^-\pi^+$, $K^-\pi^+\pi^0$, and $K^-\pi^+\pi^-\pi^+$) and six D^+ decay modes ($K^-\pi^+\pi^+$, $K^-\pi^+\pi^+\pi^0$, $K^0_S\pi^+$, $K^0_S\pi^+\pi^0$, $K^0_S\pi^+\pi^-\pi^+$, and $K^-K^+\pi^+$). The π^0 candidates are reconstructed in the $\gamma\gamma$ final state, and the K^0_S candidates are reconstructed in the $\pi^+\pi^-$ final state. Particle identification criteria are applied on kaons and pions (excluding pions in K^0_S candidates). A mode dependent selection criteria on ΔE, the candidate energy minus the beam energy, was applied. To extract the signal yields fits are performed to the $M_{\rm BC}$ distributions for the candidates that pass the selection criteria. The fit is described in Sec. III.A.3. The fit is performed separately for D and $\bar{D}$ candidates in each mode. These fits are shown in Fig. 15 where the D and $\bar{D}$ decays have been combined. Many backgrounds have been considered in this analysis and are discussed in detail by Dobbs *et al.* (2007). The single tag yields and backgrounds are summarized in Table VI.

The double tag yields are determined separately for the $45 = 3^2 + 6^2$ double tag modes. The same criteria on ΔE that was applied for the single tags are applied to the double tags. This ensures that the systematic uncertainty from the selection in single and double tag yields cancels in the ratio for the signal mode. To extract the number of double tag candidates a

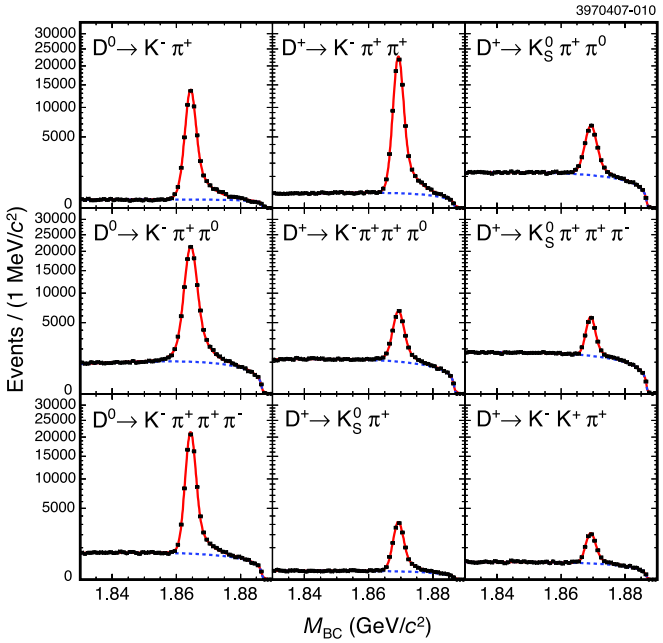

FIG. 15 (color online). Distributions of measured $M_{\rm BC}(D)$ and $M_{\rm BC}(\bar{D})$ values for single tag D^0 and D^+ candidates with D and $\bar{D}$ candidates combined in each plot. The points are data and the curves are fits to the data. In each plot, the dashed curve shows the background contributions and the solid curve shows the sum of the background and signal function. The number of events is shown on a square-root scale. From Dobbs *et al.*, 2007.

two-dimensional unbinned maximum likelihood fit is performed in the plane of $M_{\rm BC}(D)$ vs $M_{\rm BC}(\bar{D})$. This is illustrated in Fig. 16. The signal peaks at $M_{\rm BC}(\bar{D}) = M_{\rm BC}(D) = M_D$. Beam energy smearing affects both $M_{\rm BC}(\bar{D})$ and $M_{\rm BC}(D)$ in a correlated fashion to spread the signal along the $M_{\rm BC}(\bar{D})$ vs $M_{\rm BC}(D)$ diagonal. In addition, the effects of initial-state radiation will spread the signal along the same diagonal to larger values of $M_{\rm BC}(\bar{D})$ and $M_{\rm BC}(D)$. If all particles produced in the e^+e^- interaction are used to form the D and $\bar{D}$ candidates, but the particles are either from continuum or from a $D\bar{D}$ event but not assigned to the right D candidate (mispartitioning), the reconstructed $M_{\rm BC}(\bar{D})$ and $M_{\rm BC}(D)$ will lie on the diagonal. There are also events in which one of the two D candidates are misreconstructed. These events form horizontal and vertical bands in $M_{\rm BC}(\bar{D})$ vs $M_{\rm BC}(D)$.

The combined double tag data with the sum of the fits are shown in Fig. 17 for the $D^0\bar{D}^0$ and D^+D^- modes. There are a total of $13\,591 \pm 119$ $D^0\bar{D}^0$ double tags and 8870 ± 96 D^+D^- double tags. For most of the modes studied in this analysis the statistical uncertainty on the measured branching fraction is limited by the number of double tags. For the D^0 modes this statistical uncertainty is $\pm 0.88\%$ and for the D^+ modes this is $\pm 1.1\%$.

A detailed study of systematic uncertainties was performed. The signal shape systematic uncertainty for double tags is taken to be $\pm 0.2\%$, while for the single tags a range of systematic uncertainties from $\pm 0.3\%$ for $D^0 \to K^-\pi^+$ to $\pm 1.3\%$ for $D^+ \to K^-\pi^+\pi^+\pi^0$ is assigned. These systematic uncertainties were assigned based on trying alternative signal shape parametrizations in the fit. For the neutral D decays there is an uncertainty due to "double Cabibbo-suppressed interference." The source of this uncertainty comes from the interference between signal decays and decays where both the D^0 and $\bar{D}^0$ decay via doubly Cabibbo-suppressed decays. The relative size of this interference is $\Delta \approx 2R_{\rm ws}\cos 2\delta$, where $R_{\rm ws}$ is the ratio of the doubly Cabibbo-suppressed rate to the Cabibbo-favored rate, and δ is the relative strong phase between the doubly Cabibbo-suppressed amplitude and

TABLE VI. Single tag efficiencies, yields from data, and peaking background expectations. The efficiencies include the branching fractions for $\pi^0 \to \gamma\gamma$ and $K^0_S \to \pi^+\pi^-$ decays. The entries in the column labeled "Background" are the number of peaking events in the signal region produced by nonsignal events and the associated systematic uncertainty. The quoted yields include these background events. From Dobbs *et al.*, 2007.

Single tag mode	Efficiency (%)	Data yield	Background
$D^0 \to K^-\pi^+$	64.18 ± 0.19	$25\,760 \pm 165$	96 ± 27
$\bar{D}^0 \to K^+\pi^-$	64.90 ± 0.19	$26\,258 \pm 166$	96 ± 27
$D^0 \to K^-\pi^+\pi^0$	33.46 ± 0.12	$50\,276 \pm 258$	114 ± 10
$\bar{D}^0 \to K^+\pi^-\pi^0$	33.78 ± 0.12	$50\,537 \pm 259$	114 ± 10
$D^0 \to K^-\pi^+\pi^+\pi^-$	45.27 ± 0.16	$39\,709 \pm 216$	889 ± 135
$\bar{D}^0 \to K^+\pi^-\pi^-\pi^+$	45.81 ± 0.16	$39\,606 \pm 216$	889 ± 135
$D^+ \to K^-\pi^+\pi^+$	54.07 ± 0.18	$40\,248 \pm 208$	<1
$D^- \to K^+\pi^-\pi^-$	54.18 ± 0.18	$40\,734 \pm 209$	<1
$D^+ \to K^-\pi^+\pi^+\pi^0$	26.23 ± 0.18	$12\,844 \pm 153$	<1
$D^- \to K^+\pi^-\pi^-\pi^0$	26.58 ± 0.18	$12\,756 \pm 153$	<1
$D^+ \to K^0_S\pi^+$	45.98 ± 0.18	5789 ± 82	81 ± 22
$D^- \to K^0_S\pi^-$	46.07 ± 0.18	5868 ± 82	81 ± 22
$D^+ \to K^0_S\pi^+\pi^0$	23.06 ± 0.19	$13\,275 \pm 157$	113 ± 53
$D^- \to K^0_S\pi^-\pi^0$	22.93 ± 0.19	$13\,126 \pm 155$	113 ± 53
$D^+ \to K^0_S\pi^+\pi^+\pi^-$	31.70 ± 0.24	8275 ± 134	173 ± 83
$D^- \to K^0_S\pi^-\pi^-\pi^+$	31.81 ± 0.24	8285 ± 134	173 ± 83
$D^+ \to K^+K^-\pi^+$	45.86 ± 0.36	3519 ± 73	<1
$D^- \to K^-K^+\pi^-$	45.57 ± 0.35	3501 ± 73	<1

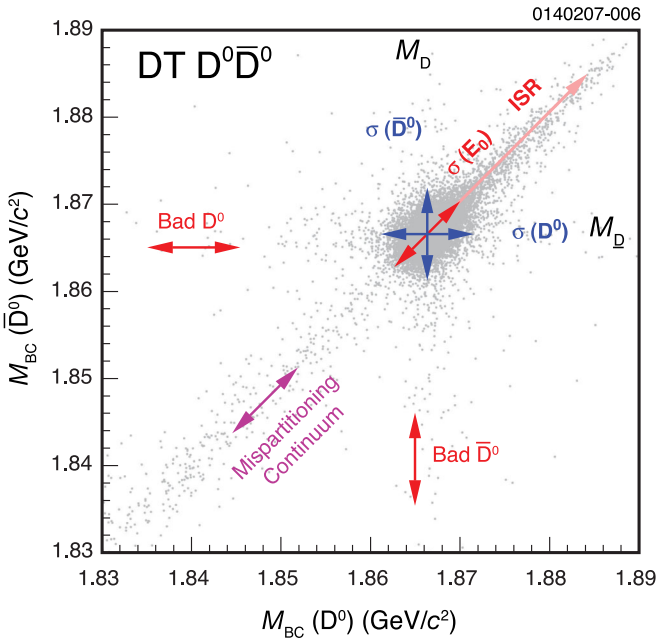

FIG. 16 (color online). Scatter plot of $M_{\rm BC}(\bar{D})$ vs $M_{\rm BC}(D)$ for $D^0\bar{D}^0$ double tag candidates. Signal candidates are concentrated at $M_{\rm BC}(\bar{D}) = M_{\rm BC}(D) = M_D$. The signal shape and different background contributions are discussed in the text. From Dobbs *et al.*, 2007.

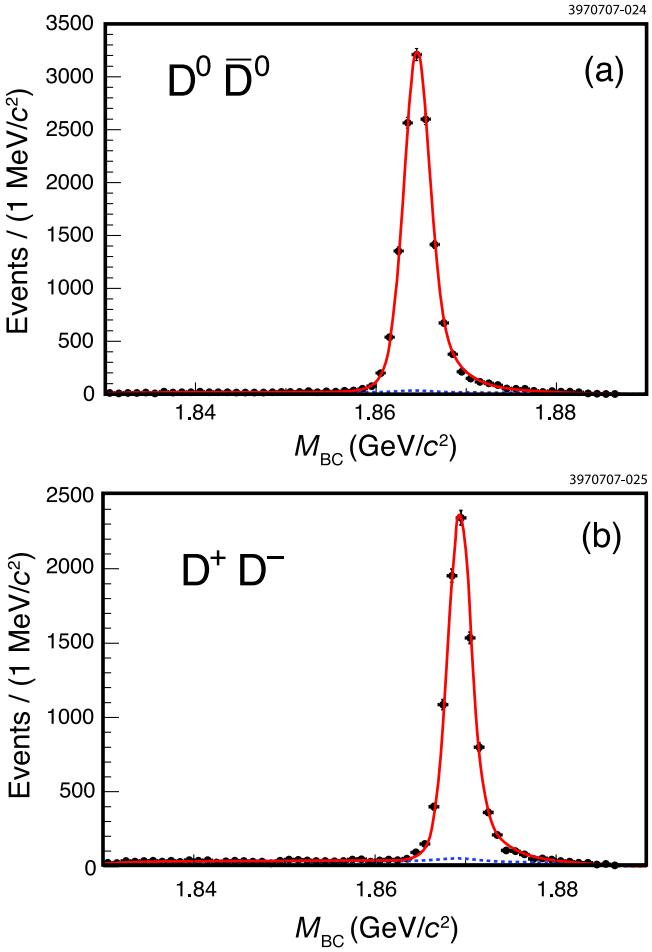

FIG. 17 (color online). Projections of the sum of the double tag candidate mass on the $M_{\rm BC}(D)$ axis for (a) the nine $D^0\bar{D}^0$ double tag modes and (b) the 36 D^+D^- double tag modes. The points show the data and the curves show the projection of the fit results. The dashed lines show the background contributions and the solid lines show the signal shape plus the background. From Dobbs *et al.*, 2007.

the Cabibbo-favored amplitude. CLEO-c assigned a systematic uncertainty of $\pm 0.8\%$ for this effect. This covered the range of allowed values of Δ for $R_{\rm ws} = 0.004$ and incorporated the uncertainties in δ.

For the charged track reconstruction CLEO-c assigned $\pm 0.3\%$ uncertainty and for charged kaons an additional $\pm 0.6\%$ added in quadrature. In addition CLEO-c assigned a $\pm 1.8\%$ uncertainty on the K^0_S reconstruction in the $\pi^+\pi^-$ final state and a $\pm 2.0\%$ uncertainty for the π^0 reconstruction in the $\gamma\gamma$ final state. These systematic uncertainties were discussed in Sec. III.A.4. Kaons and pions, except for pions in the reconstruction of $K^0_S \to \pi^+\pi^-$ candidates, are required to satisfy particle identification criteria. Uncertainties of $\pm 0.25\%$ and $\pm 0.3\%$ for pions and kaons, respectively, are assigned for the particle identification.

Multibody final states suffer from an uncertainty in the simulation of the efficiency due to imperfect modeling of the resonant substructure. The uncertainties associated with the three- or four-body final states were estimated by comparing the kinematic distributions in these decays between data and Monte Carlo simulations. Many three-body final states have been studied using Dalitz-plot fits and are well described in the Monte Carlo simulation (Lange, 2001). The Dalitz-plot analyses are described in Sec. IX.

Last, final-state radiation, as discussed in Sec. III.E, was considered. CLEO-c compared the signal efficiencies with and without FSR included in the Monte Carlo simulation. A systematic uncertainty of $\pm 30\%$ of the change due to not including final-state radiation was assigned. This gives the largest uncertainty of about 0.9% in the $D^0 \to K^-\pi^+$ mode.

The signal yields for single and double tags and the efficiencies determined from Monte Carlo simulations are combined in a χ^2 fit (Sun, 2006). This fit includes both statistical and systematic uncertainties. The fit extracts the branching fractions for the nine D decay modes studied in this analysis and the produced number of $D^0\bar{D}^0$ and D^+D^- pairs. The result of this fit is shown in Table VII. The χ^2 of the fit is 39.2 for 52 degrees of freedom, corresponding to a confidence level of 98%. The χ^2 includes systematic uncertainties.

The CLEO-c analysis obtained the main branching fraction results

$$\mathcal{B}(D^0 \to K^-\pi^+) = (3.891 \pm 0.035 \pm 0.059 \pm 0.035)\%, \tag{70}$$

$$\mathcal{B}(D^+ \to K^-\pi^+\pi^+) = (9.15 \pm 0.10 \pm 0.16 \pm 0.07)\%, \tag{71}$$

where the errors are statistical, systematic, and from final-state radiation, respectively. In addition, the $D\bar{D}$ yields determined from this analysis are used to normalize many other CLEO-c measurements. The cross sections for $D\bar{D}$ production are discussed in Sec. III.A.

D. Summary of $D^0 \to K^-\pi^+$

The absolute branching fraction for $D^0 \to K^-\pi^+$ has been measured by many different experiments, using different techniques as discussed in this section. The different measurements are summarized in Table VIII. The two most recent, and most precise, measurements are from CLEO-c and *BABAR*. They used different techniques but found branching fractions that are in good agreement. We adopt the PDG average

$$\mathcal{B}(D^0 \to K^-\pi^+) = 3.89 \pm 0.05. \tag{72}$$

These measurements are now limited by systematic uncertainties. There are many sources of systematic uncertainties that contribute. Some of these can be improved with additional data. Both CLEO-c and *BABAR* can increase the data samples used in their analyses.

E. Modes with K^0_L or K^0_S in the final states

It has commonly been assumed that $\Gamma(D \to K^0_S X) = \Gamma(D \to K^0_L X)$. However, as pointed out by Bigi and Yamamoto (1995), this is not generally true as for many D decays there are contributions from Cabibbo-favored and Cabibbo-suppressed decays that interfere and produce different rates to final states with K^0_S vs K^0_L. As an example consider $D^0 \to K^0_{S,L}\pi^0$. Contributions to these final states involve the Cabibbo-favored decay $D^0 \to \bar{K}^0\pi^0$ as well as the doubly

TABLE VII. Fitted branching fractions and $D\bar{D}$ pair yields. For $N_{D^0\bar{D}^0}$ and $N_{D^+D^-}$, uncertainties are statistical and systematic, respectively. For branching fractions and ratios, the systematic uncertainties are divided into the contribution from FSR (third uncertainty) and all others are combined (second uncertainty). The column of fractional systematic errors combines all systematic errors, including FSR. The last column $\Delta_{\rm FSR}$ is the relative shift in the fit results when FSR is not included in the Monte Carlo simulations used to determine efficiencies. From Dobbs *et al.*, 2007.

Parameter	Fitted value	Fractional error Stat. (%)	Fractional error Syst. (%)	$\Delta_{\rm FSR}$ (%)
$N_{D^0\bar{D}^0}$	$(1.031 \pm 0.008 \pm 0.013) \times 10^6$	0.8	1.3	+0.1
$\mathcal{B}(D^0 \to K^-\pi^+)$	$(3.891 \pm 0.035 \pm 0.059 \pm 0.035)\%$	0.9	1.8	−3.0
$\mathcal{B}(D^0 \to K^-\pi^+\pi^0)$	$(14.57 \pm 0.12 \pm 0.38 \pm 0.05)\%$	0.8	2.7	−1.1
$\mathcal{B}(D^0 \to K^-\pi^+\pi^+\pi^-)$	$(8.30 \pm 0.07 \pm 0.19 \pm 0.07)\%$	0.9	2.4	−2.4
$N_{D^+D^-}$	$(0.819 \pm 0.008 \pm 0.010) \times 10^6$	1.0	1.2	+0.1
$\mathcal{B}(D^+ \to K^-\pi^+\pi^+)$	$(9.15 \pm 0.10 \pm 0.16 \pm 0.07)\%$	1.1	1.9	−2.3
$\mathcal{B}(D^+ \to K^-\pi^+\pi^+\pi^0)$	$(5.98 \pm 0.08 \pm 0.16 \pm 0.02)\%$	1.3	2.8	−1.0
$\mathcal{B}(D^+ \to K^0_S\pi^+)$	$(1.526 \pm 0.022 \pm 0.037 \pm 0.009)\%$	1.4	2.5	−1.8
$\mathcal{B}(D^+ \to K^0_S\pi^+\pi^0)$	$(6.99 \pm 0.09 \pm 0.25 \pm 0.01)\%$	1.3	3.5	−0.4
$\mathcal{B}(D^+ \to K^0_S\pi^+\pi^+\pi^-)$	$(3.122 \pm 0.046 \pm 0.094 \pm 0.019)\%$	1.5	3.0	−1.9
$\mathcal{B}(D^+ \to K^+K^-\pi^+)$	$(0.935 \pm 0.017 \pm 0.024 \pm 0.003)\%$	1.8	2.6	−1.2
$\mathcal{B}(D^0 \to K^-\pi^+\pi^0)/\mathcal{B}(K^-\pi^+)$	$3.744 \pm 0.022 \pm 0.093 \pm 0.021$	0.6	2.6	+1.9
$\mathcal{B}(D^0 \to K^-\pi^+\pi^+\pi^-)/\mathcal{B}(K^-\pi^+)$	$2.133 \pm 0.013 \pm 0.037 \pm 0.002$	0.6	1.7	+0.5
$\mathcal{B}(D^+ \to K^-\pi^+\pi^+\pi^0)/\mathcal{B}(K^-\pi^+\pi^+)$	$0.654 \pm 0.006 \pm 0.018 \pm 0.003$	0.9	2.7	+1.4
$\mathcal{B}(D^+ \to K^0_S\pi^+)/\mathcal{B}(K^-\pi^+\pi^+)$	$0.1668 \pm 0.0018 \pm 0.0038 \pm 0.0003$	1.1	2.3	+0.5
$\mathcal{B}(D^+ \to K^0_S\pi^+\pi^0)/\mathcal{B}(K^-\pi^+\pi^+)$	$0.764 \pm 0.007 \pm 0.027 \pm 0.005$	0.9	3.5	+2.0
$\mathcal{B}(D^+ \to K^0_S\pi^+\pi^+\pi^-)/\mathcal{B}(K^-\pi^+\pi^+)$	$0.3414 \pm 0.0039 \pm 0.0093 \pm 0.0004$	1.1	2.7	+0.4
$\mathcal{B}(D^+ \to K^+K^-\pi^+)/\mathcal{B}(K^-\pi^+\pi^+)$	$0.1022 \pm 0.0015 \pm 0.0022 \pm 0.0004$	1.5	2.2	+1.1

Cabibbo-suppressed decay $D^0 \to K^0\pi^0$. However, we do not observe the K^0 and $\bar{K}^0$ but rather the K^0_S and K^0_L. As the amplitudes for $D^0 \to \bar{K}^0\pi^0$ and $D^0 \to K^0\pi^0$ interfere constructively to form the K^0_S final state, and destructively to form a K^0_L, we see a rate asymmetry between the K^0_L and K^0_S final states. Using $SU(3)_F$, and, in particular, the U-spin subgroup, one can predict the asymmetry in $D^0 \to K^0_{S,L}\pi^0$

$$R(D^0) \equiv \frac{\Gamma(D^0 \to K^0_S\pi^0) - \Gamma(D^0 \to K^0_L\pi^0)}{\Gamma(D^0 \to K^0_S\pi^0) + \Gamma(D^0 \to K^0_L\pi^0)} \approx 2\tan^2\theta_C = 0.109 \pm 0.001. \quad (73)$$

For the corresponding charged D mode, $D^+ \to K^0_{S,L}\pi^+$ a similar prediction based on SU(3) is not possible. Rather one has to rely on calculations based on factorization or other means of determination of decay amplitudes. For example, the flavor-flow diagram approach gives (Bhattacharya and Rosner, 2008)

$$R(D^+) = 2\tan^2\theta_C \mathrm{Re}\frac{C+A}{T+C} = -0.006^{+0.033}_{-0.028}. \quad (74)$$

We discuss the prediction of this ratio in factorization below.

Experimentally these channels are challenging as they involve final states with a K^0_L. CLEO-c studied these modes (He *et al.*, 2008). They inferred the presence of a K^0_L using a missing mass technique after vetoing events with a K^0_S decaying to either a $\pi^+\pi^-$ or $\pi^0\pi^0$ pair if there are tracks or π^0 candidates reconstructed in the event.

In addition to the challenge with the K^0_L final state, these decays are CP eigenstates and at the $\psi(3770)$ where CLEO-c recorded the data for their analysis one needs to disentangle the effects from quantum coherence with the rate asymmetry we are interested in here. The effect of the coherently produced $D^0\bar{D}^0$ pairs at the $\psi(3770)$ was discussed in Sec. III.A.1.

CLEO-c studied both $D^+ \to K^0_{S,L}\pi^+$ and $D^0 \to K^0_{S,L}\pi^0$. First the D^+ analysis is discussed as it does not involve the complication of quantum coherence. The branching fraction for $D^+ \to K^0_S\pi^+$ is from Dobbs *et al.* (2007). In this analysis only the branching fraction for $D^+ \to K^0_L\pi^+$ is directly measured. CLEO-c used a tag technique, in which one charged D is fully reconstructed. Six different charged D tags are used, and these modes are the same as in Dobbs *et al.* (2007) described in Sec. V.C. The tag D^- is combined with a π^+ and events consistent with a K^0_S are vetoed. An event is vetoed if an additional charged track or neutral pion, reconstructed in the $\pi^0 \to \gamma\gamma$ channel, was found. This veto

TABLE VIII. Summary of measurements of the $D^0 \to K^-\pi^+$ branching fraction measurements. Only the top six measurements are used in the average by the PDG.

Experiment	Reference	$\mathcal{B}(D^0 \to K^-\pi^+)$ (%)
CLEO-c	Dobbs *et al.* (2007)	$3.891 \pm 0.035 \pm 0.059 \pm 0.035$
BABAR	Aubert *et al.* (2008b)	$4.007 \pm 0.037 \pm 0.072$
CLEO II[a]	Artuso *et al.* (1998)	$3.82 \pm 0.07 \pm 0.12$
ALEPH	Barate *et al.* (1997)	$3.90 \pm 0.09 \pm 0.12$
ARGUS	Albrecht *et al.* (1994a)	$3.41 \pm 0.12 \pm 0.28$
ALEPH	Decamp *et al.* (1991)	$3.62 \pm 0.34 \pm 0.44$
CLEO-c	He *et al.* (2005)	$3.91 \pm 0.08 \pm 0.09$
CLEO II	Artuso *et al.* (1998)	$3.81 \pm 0.15 \pm 0.16$
CLEO II	Coan *et al.* (1998)	$3.69 \pm 0.11 \pm 0.16$
ARGUS	Albrecht *et al.* (1994b)	$4.5 \pm 0.6 \pm 0.4$
CLEO II	Akerib *et al.* (1993)	$3.95 \pm 0.08 \pm 0.17$
HRS	Abachi *et al.* (1988)	$4.5 \pm 0.8 \pm 0.5$
MARK-III	Adler *et al.* (1988)	$4.2 \pm 0.4 \pm 0.4$
MARK-II	Schindler *et al.* (1981)	4.1 ± 0.6
LGW	Peruzzi *et al.* (1977)	4.3 ± 1.0
Average		3.89 ± 0.05

[a]This is an average of the results by Akerib *et al.* (1993), Aubert *et al.* (2008b), and Coan *et al.* (1998).

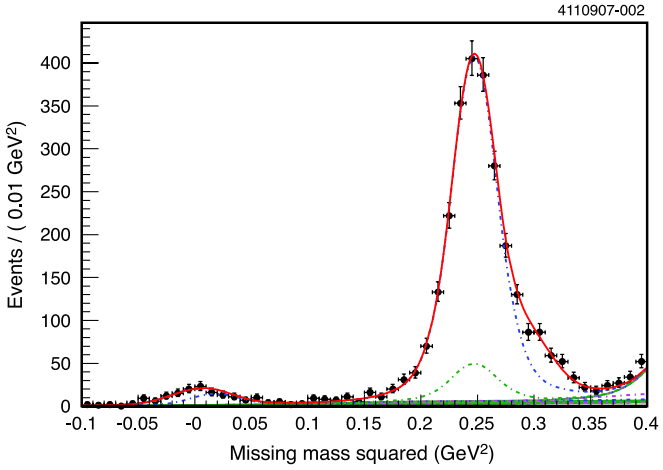

FIG. 18 (color online). Missing mass squared distribution for all six tag modes for $D^+ \to X\pi^+$. Events with extra tracks or π^0 candidates have been removed. From He *et al.*, 2008.

removes about 90% of the K_S^0 background as well as many other backgrounds while retaining 98% efficiency for signal events.

Figure 18 shows the invariant mass distribution recoiling against the tag D and charged pion. The signal peaks at a missing mass square of about 0.25 GeV^2 corresponding to the K_L^0. From the fit to the data CLEO-c extracts a signal of 2023 ± 54 events. With 165×10^3 charged D tags and an efficiency of 81.6% for finding the pion the branching fraction is calculated to be

$$\mathcal{B}(D^+ \to K_L^0\pi^+) = (1.460 \pm 0.040 \pm 0.035 \pm 0.005)\%, \tag{75}$$

where the errors are statistical, systematic, and from the branching fraction for $D^+ \to K_S^0\pi^+$. The largest contributions to the systematic uncertainty come from the extra track and π^0 veto ($\pm$ 1.1%) and the signal peak width ($\pm$ 1.6%). The sensitivity to the peak width comes from the $D^+ \to \eta\pi^+$ events just on the high side of the signal peak as seen in Fig. 18.

Combining the $D^+ \to K_L^0\pi^+$ branching fraction with the $D^+ \to K_S^0\pi^+$ measured by Dobbs *et al.* (2007), CLEO-c obtained the asymmetry

$$R(D^+) = 0.022 \pm 0.016 \pm 0.018. \tag{76}$$

There is no evidence for a significant asymmetry in the $D^+ \to K_{S,L}^0\pi^+$ mode. Predictions for the asymmetry in charged D decays are more involved than for neutral D decays. Based on factorization, Gao (2007) predicted this asymmetry to be in the range of 0.035 to 0.044, which is consistent with the observed asymmetry.

For the $D^0 \to K_{S,L}^0\pi^0$ analysis the effects of the quantum coherence have to be accounted for. In addition, experimentally this mode is more challenging as the resolution for a π^0 is worse than for a charged pion. CLEO-c first measured the branching fraction for $D^0 \to K_S^0\pi^0$ without using a $\bar{D}^0$ tag. Next the branching fraction for $D^0 \to K_S^0\pi^0$ is measured in a tagged analysis where the $\bar{D}^0$ is reconstructed in three modes. Because of the coherence the branching fraction measured in the tagged analysis is $\mathcal{B}(D^0 \to K_S^0\pi^0)(1 - C_f)$, where $C_f = (R_f z_f + y)/(1 + R_{WS,f})$, as described in Sec. III.A.1. For the three tag modes C_f can now be calculated. Finally, the branching fraction for $D^0 \to K_L^0\pi^0$ is measured using the same three tag modes; each of the tag modes gives us $\mathcal{B}(D^0 \to K_L^0\pi^0)(1 + C_f)$, and using the measured values of C_f from above the branching fraction $\mathcal{B}(D^0 \to K_L^0\pi^0)$ can be determined.

TABLE IX. The efficiency is for the reconstruction of the $K_S^0\pi^0$ after the D tag has been found, the tag yield is the number of D tags reconstructed, the signal yield is the number of $D^0 \to K_S^0\pi^0$ candidates reconstructed against the tag D, and the tag bias is a correction due to the fact that it is easier to reconstruct the tag in events with the signal than in generic D decays. From He *et al.* (2008).

Tag mode	$K^+\pi^-$	$K^+\pi^-\pi^0$	$K^+\pi^-\pi^+\pi^-$
Efficiency (%)	31.74	31.29	29.97
Tag yield	47 440	63 913	71 040
Signal yield	155	203	256
Tag bias correction (%)	1.000	1.014	1.033
$\mathcal{B}(D^0 \to K_S^0\pi^0)(1 - C_f)$	1.03 ± 0.09	1.00 ± 0.09	1.16 ± 0.08

The K_S^0 is reconstructed in the $K_S^0 \to \pi^+\pi^-$ final state. There is a background from $D^0 \to \pi^+\pi^-\pi^0$. This background is subtracted using the K_S^0 mass sideband. The signal yield in this analysis is extracted using a cut-and-count technique. CLEO-c looked in a 3 standard deviation window around the nominal values for the beam-constrained mass and ΔE. A sideband in ΔE is used to subtract the combinatorial backgrounds. The number of $D^0\bar{D}^0$ pairs in the data sample is taken from Dobbs *et al.* (2007). CLEO-c obtained the branching fraction

$$\mathcal{B}(D^0 \to K_S^0\pi^0) = (1.240 \pm 0.017 \pm 0.031 \pm 0.047)\%, \tag{77}$$

where the last error is due to the π^0 reconstruction efficiency. In the asymmetry $R(D^0)$ this uncertainty will cancel.

Next the branching fraction for $\mathcal{B}(D^0 \to K_S^0\pi^0)$ is measured with a $\bar{D}^0$ tag. The three tag modes used are $\bar{D}^0 \to K^+\pi^-$, $\bar{D}^0 \to K^+\pi^-\pi^0$, and $\bar{D}^0 \to K^+\pi^-\pi^+\pi^-$. The results for the tagged analysis are summarized in Table IX. Similarly the tagged branching fraction for $D^0 \to K_L^0\pi^0$ was studied using a missing mass technique where the event was fully reconstructed except for the K_L^0. The results are summarized in Table X.

TABLE X. The efficiency is for the reconstruction of the $K_L^0\pi^0$, including the K_S^0 veto, after the D tag has been found, the tag yield is the number of D tags reconstructed, the signal yield is the number of $D^0 \to K_S^0\pi^0$ candidates reconstructed against the tag D, and the tag bias is a correction due to the fact that it is easier to reconstruct the tag in events with the signal than in generic D decays. From He *et al.* (2008).

Tag mode	$K^+\pi^-$	$K^+\pi^-\pi^0$	$K^+\pi^-\pi^+\pi^-$
Efficiency (%)	55.21	52.72	49.88
Tag yield	47 440	64 280	71 040
Signal yield	334.8	414.5	466.5
Tag bias correction (%)	1.000	1.037	1.057
$\mathcal{B}(D^0 \to K_L^0\pi^0)(1 + C_f)$	1.28 ± 0.08	1.03 ± 0.06	1.12 ± 0.06

TABLE XI. Summary of final states with three kaons. If there is more than one measurement, we quote the PDG average.

Mode	Reference	$\mathcal{B}$ (10^{-3})
$D^0 \to K_S^0 K^+ K^-$	*BABAR* (Aubert *et al.*, 2005a)	$4.72 \pm 0.03 \pm 0.15 \pm 0.27$
$D^0 \to K_S^0 K_S^0 K_S^0$	PDG average (Amsler *et al.*, 2008)	$0.96 \pm 0.12 \pm 0.05$
$D^0 \to K^+ K^- K^- \pi^+$	PDG average (Amsler *et al.*, 2008)	$0.221 \pm 0.033 \pm 0.009$
$D^0 \to K_S^0 K_S^0 K^{\mp} \pi^{\pm}$	FOCUS (Link *et al.*, 2005b)	$0.63 \pm 0.11 \pm 0.06 \pm 0.04$

Combining these measurements CLEO-c finds an average asymmetry for the neutral D decays

$$R(D^0) = 0.108 \pm 0.025 \pm 0.024, \tag{78}$$

which is in good agreement with the prediction.

F. Final states with three kaons

Final states with three kaons are not generally Cabibbo suppressed, but the smaller branching fractions for these decays are due to the small phase space available in these decays. These decays are summarized in Table XI. The decay $D^+ \to K^+ K^- K^+$ is Cabibbo suppressed and is included in Sec. VII.D. The limited phase space available was taken advantage of to measure the D^0 mass (Cawlfield *et al.*, 2007).

G. Summary of Cabibbo-favored D^0 and D^+ decays

In Table XII a summary of the Cabibbo-favored D^0 and D^+ decays is given. Assuming that $\Gamma(D \to K_S^0 X) = \Gamma(D \to K_L^0 X)$ for modes where the final states with a K_L^0 has not been explicitly measured, the Cabibbo-favored branching fractions add up to $(50.8 \pm 1.4)\%$ for D^0 meson decays and $(38.3 \pm 1.1)\%$ for D^+ decays. The mode $D^0 \to K^- \pi^+ \pi^0 \pi^0$ is not included here. An early measurement by MARK-III (Adler *et al.*, 1988) reported a large branching fraction of $(15 \pm 5)\%$. The PDG is not using this result anymore in their summary and there have not been any newer measurements. However, CLEO-c used this mode for tagging D^0 decays in their studies of semileptonic decays (Ge *et al.*, 2009b). They provided enough information that the branching fraction $\mathcal{B}(D^0 \to K^- \pi^+ \pi^0 \pi^0) = (7.90 \pm 0.14)\%$ can be calculated. The error quoted includes only the statistical error and the uncertainty from the $D^0 \to K^- \pi^+$ normalization mode. In particular, experimental systematic uncertainties are not included and hence this is not included in the summary. But it does show that there is a substantial rate to the $D^0 \to K^- \pi^+ \pi^0 \pi^0$ final state.

TABLE XII. Summary of branching fractions for Cabibbo-favored D^0 and D^+ decays. Averages are from Amsler *et al.* (2008).

Mode	Branching fraction
$D^0 \to K^- \pi^+$	$(3.89 \pm 0.05)\%$
$D^0 \to K_S^0 \pi^0$	$(1.22 \pm 0.06)\%$
$D^0 \to K_L^0 \pi^0$	$(1.00 \pm 0.07)\%$
$D^0 \to K_S^0 \pi^+ \pi^-$	$(2.99 \pm 0.17)\%$
$D^0 \to K^- \pi^+ \pi^0$	$(13.9 \pm 0.5)\%$
$D^0 \to K^- \pi^+ \pi^+ \pi^-$	$(8.10 \pm 0.20)\%$
$D^0 \to K_S^0 \pi^+ \pi^- \pi^0$	$(5.4 \pm 0.6)\%$
$D^0 \to K^- \pi^+ \pi^+ \pi^- \pi^0$	$(4.2 \pm 0.4)\%$
$D^0 \to K_S^0 \eta \pi^0$	$(5.6 \pm 1.2) \times 10^{-3}$
$D^0 \to K_S^0 \pi^+ \pi^+ \pi^- \pi^-$	$(2.84 \pm 0.31) \times 10^{-3}$
$D^0 \to K^- \pi^+ \pi^+ \pi^+ \pi^- \pi^-$	$(2.2 \pm 0.6) \times 10^{-4}$
$D^+ \to K_S^0 \pi^+$	$(1.45 \pm 0.04)\%$
$D^+ \to K_L^0 \pi^+$	$(1.46 \pm 0.05)\%$
$D^+ \to K^- \pi^+ \pi^+$	$(9.22 \pm 0.21)\%$
$D^+ \to K_S^0 \pi^+ \pi^0$	$(6.8 \pm 0.5)\%$
$D^+ \to K^- \pi^+ \pi^+ \pi^0$	$(6.00 \pm 0.20)\%$
$D^+ \to K_S^0 \pi^+ \pi^+ \pi^-$	$(3.02 \pm 0.12)\%$
$D^+ \to K^- \pi^+ \pi^+ \pi^+ \pi^-$	$(5.6 \pm 0.5) \times 10^{-3}$

VI. CABIBBO-FAVORED D_s DECAYS

The determination of the absolute branching fraction scale for D_s decays has been a challenge since the discovery of D_s (Chen *et al.*, 1983). Until recently the focus has been on the final state $D_s^+ \to \phi \pi^+$, followed by $\phi \to K^- K^+$. This final state is easy to reconstruct with small backgrounds; the ϕ is a narrow resonance and the final state consists of all charged particles. However, this final state is not as ''clean'' as one would wish. There are non-ϕ contributions, such as the $f_0(980)$, to the $K^+ K^-$ mass near the ϕ mass that pollute the $D_s^+ \to \phi \pi^+$ signal. Of course, these decays are still real $D_s^+ \to K^+ K^- \pi^-$ decays. This is discussed further in Sec. IX.A.12 on the Dalitz-plot analysis of $D_s^+ \to K^+ K^- \pi^+$.

As measurements have gotten more precise the definition of what is measured has had to be made more precise. One of the most recent measurements by CLEO-c (Alexander *et al.*, 2008) does not quote a $D_s^+ \to \phi \pi^+$ branching fraction, but rather partial branching fractions in $K^+ K^-$ invariant mass regions near the ϕ. The first attempts at establishing the branching fraction scale for D_s^+ decays were based on model-dependent assumption about equal partial widths for semileptonic decays of the D_s^+ and D^+.

This section discusses the different approaches used to measure the D_s absolute branching fractions. The early measurements are described briefly and the more recent, and precise, measurements are described in more detail.

A. Model-dependent approaches

The NA14 experiment (Alvarez *et al.*, 1990) used the Lund model to estimate the ratio of D_s^+ to D^+ production cross sections, which allowed them to determine the $D_s^+ \to \phi \pi^+$ branching fractions. The CLEO Collaboration (Chen *et al.*, 1989) used estimates of the D_s^+ production rate to determine the branching fraction for $D_s^+ \to \phi \pi^+$.

Several experiments, CLEO (Alexander *et al.*, 1990a; Butler *et al.*, 1994), E687 (Frabetti *et al.*, 1993), ARGUS

(Albrecht *et al.*, 1991), and E691 (Anjos *et al.*, 1990), measured the ratio

$$\frac{\mathcal{B}(D_s^+ \to \phi \ell^+ \nu_\ell)}{\mathcal{B}(D_s^+ \to \phi \pi^+)}. \tag{79}$$

Using theoretical predictions for the ratio

$$\frac{\Gamma(D_s^+ \to \phi \ell^+ \nu_\ell)}{\Gamma(D^+ \to \bar{K}^{*0} \ell^+ \nu_\ell)} \tag{80}$$

and the measured D_s^+ and D^+ lifetimes these experiments determined the branching fraction for $D_s^+ \to \phi\pi^+$. Comparing these results requires some care as slightly different assumptions were made about the ratio of the semileptonic rates. Also, combining these measurements requires care as there are strong systematic correlations between the measurements due to the common, or at least similar, assumptions about partial rates for the semileptonic decays.

All of these measurements use model-dependent assumptions and have associated systematic uncertainties that are hard to quantify. These model-dependent measurements are typically no longer used in averages, e.g., by the Particle Data Group (Amsler *et al.*, 2008). With larger data samples model-independent measurements become possible.

B. The branching ratio for $D_s \to \phi\pi$ from $B \to D_s^* D^*$

The first statistically significant (see Sec. VI.D), model-independent measurement of the absolute D_s^+ branching fraction was performed by CLEO (Artuso *et al.*, 1996). They used 2.5 fb^{-1} of e^+e^- data collected at the $\Upsilon(4S)$ resonance, corresponding to 2.7×10^6 $B\bar{B}$ pairs, to study $B \to D_s^* D^*$ decays. The same technique was used by

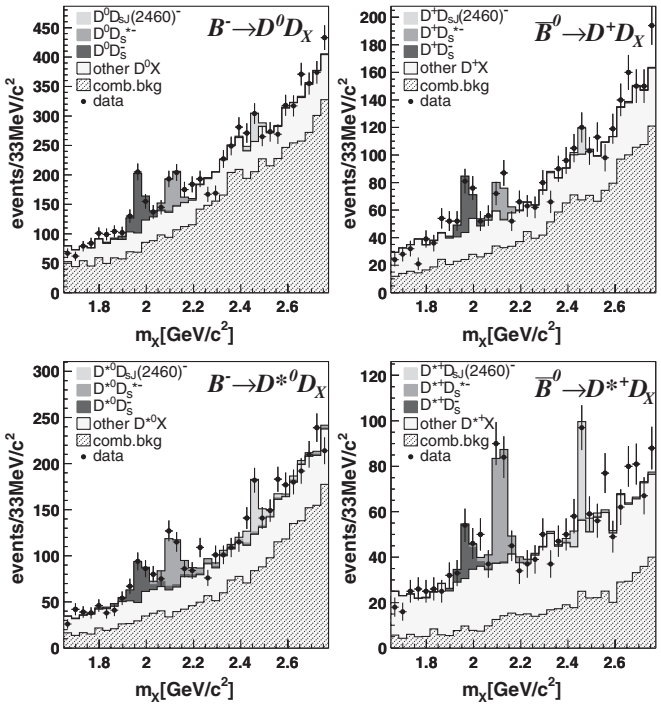

FIG. 19. The recoil mass against a D or D^* in B decays. Top left: $B^- \to D^0 D_X$; top right: $\bar{B}^0 \to D^+ D_X$; lower left: $B^- \to D^{*0} D_X$; and lower right: $\bar{B}^0 \to D^{*+} D_X$. From Aubert *et al.*, 2006c.

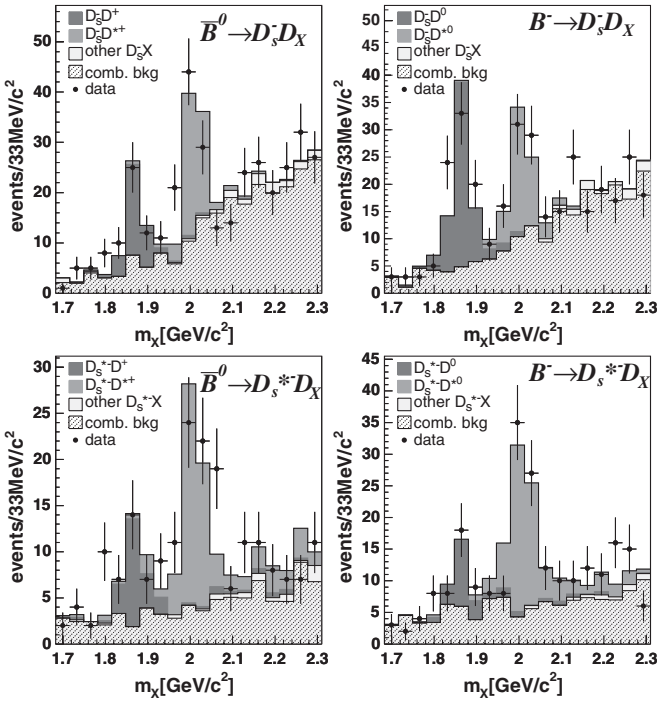

FIG. 20. The recoil mass against a D_s or D_s^*. Top left: $\bar{B}^0 \to D_S^- D_X$; top right: $B^- \to D_S^- D_X$; lower left: $\bar{B}^0 \to D_s^{*-} D_X$; and lower right: $B^- \to D_s^{*-} D_X$. From Aubert *et al.*, 2006c.

BABAR (Aubert *et al.*, 2005c). They analyzed a sample with $(123 \pm 1) \times 10^6$ $B\bar{B}$ pairs.

In these analyses the decay $B \to D_s^* D^*$ is reconstructed in two different ways. First, the D_s^* is fully reconstructed using $D_s^{*+} \to D_s^+ \gamma$ followed by $D_s^+ \to \phi\pi^+$ and the D^* is partially reconstructed using the slow pion from the D^* decay. Second, the D^* is fully reconstructed and the $D_s^{*+} \to D_s^+ \gamma$ is identified only through the presence of the γ. From this study *BABAR* quoted $\mathcal{B}(D_s^+ \to \phi\pi^+) = (4.81 \pm 0.52 \pm 0.38)\%$ and CLEO $\mathcal{B}(D_s^+ \to \phi\pi^+) = (3.59 \pm 0.77 \pm 0.48)\%$.

More recently, *BABAR* (Aubert *et al.*, 2006c) presented results based on 210 fb^{-1} of data where they used a tag technique in which one B meson is fully reconstructed. In events with one fully reconstructed B meson candidate *BABAR* reconstructs one additional $D^{(*)}$ or $D_{s(J)}^{(*)}$ meson. Then they looked at the recoil mass against this reconstructed candidate. The recoil masses are shown in Figs. 19 and 20.

From these data *BABAR* extracted $\mathcal{B}(D_{sJ}(2460)^- \to D_s^{*-}\pi^0) = (56 \pm 13 \pm 9)\%$ and $\mathcal{B}(D_{sJ}(2460)^- \to D_s^{*-}\gamma) = (16 \pm 4 \pm 3)\%$ in addition to $\mathcal{B}(D_s^- \to \phi\pi^+) = (4.52 \pm 0.48 \pm 0.68)\%$. *BABAR* combined this measurement with their previous measurement discussed above to obtain $\mathcal{B}(D_s^- \to \phi\pi^+) = (4.62 \pm 0.36 \pm 0.50)\%$.

C. Study of $D_s^+ \to K^+K^-\pi^+$ in continuum production

Belle (Abe *et al.*, 2007) used 552.3 fb^{-1} of e^+e^- data to study the process $e^+e^- \to D_s^{*+} D_{s1}^-$ followed by $D_{s1}^- \to D^{*0}K^-$ and $D_s^{*+} \to D_s^+ \gamma$. The large data sample allowed Belle to study this exclusive final state in continuum production of D_s mesons. The final state is reconstructed in two ways, by partially reconstructing either the D_{s1} or the D_s^*.

Belle obtained the preliminary branching fraction $\mathcal{B}(D_s^+ \to K^+K^-\pi^+) = (4.0 \pm 0.4 \pm 0.4)\%$ which is of comparable statistical precision to the other methods discussed above.

D. Absolute branching fractions for hadronic D_s decays using double tags

CLEO-c (Alexander *et al.*, 2008) determined the absolute hadronic branching fractions for D_s meson decays using a double tag technique similar to what was done for the D hadronic branching fractions. The same technique was used by MARK-III (Adler *et al.*, 1990b) and BES (Bai *et al.*, 1995). These initial studies were limited by statistics; MARK-III observed no events and placed an upper limit while BES observed two events and reported a branching fraction of

$$\mathcal{B}(D_s^+ \to \phi\pi^+) = (3.9^{+5.1+1.8}_{-1.9-1.1})\%. \tag{81}$$

The BES analysis used 22.3 pb^{-1} recorded at $E_{\text{c.m.}} = 4.03$ GeV.

The CLEO-c analysis used a sample of 298 pb^{-1} of e^+e^- collision data recorded at a center-of-mass energy of 4170 MeV. At this energy D_s mesons are produced, predominantly, as $D_s^+D_s^{*-}$ or $D_s^-D_s^{*+}$ pairs. The eight hadronic final states considered in this analysis by CLEO-c are $K_S^0K^+$, $K_S^0K^-\pi^+\pi^+$, $K^+K^-\pi^+$, $K^+\pi^-\pi^+$, $K^+K^-\pi^+\pi^0$, $\pi^+\pi^-\pi^+$, $\eta\pi^+$, and $\eta'\pi^+$. The analysis proceeds similar to the D hadronic branching fraction analysis described in Sec. V.C. Yields and efficiencies for single tags (separately for D_s^+ and D_s^-) and double tags are extracted. The π^0 or γ from the D_s^* decay is not reconstructed in this analysis. The yields in terms of the efficiencies, branching fractions, and data sample size are given by

$$y_i = N_{D_s^*D_s}\mathcal{B}_i\epsilon_i, \tag{82}$$

$$y_{\bar{j}} = N_{D_s^*D_s}\mathcal{B}_j\epsilon_{\bar{j}}, \tag{83}$$

$$y_{i\bar{j}} = N_{D_s^*D_s}\mathcal{B}_i\mathcal{B}_j\epsilon_{i\bar{j}}, \tag{84}$$

where i indicates a D_s^+ and $\bar{j}$ indicates a D_s^-. In this analysis a total of 16 single tags and 64 double tags are used. The event selection is detailed by Alexander *et al.* (2008). A D_s candidate is referred to as "indirect" if it comes from the decay of the D_s^* in the $e^+e^- \to D_sD_s^*$ interaction. Otherwise the D_s is said to be "direct." The D_s candidates are identified based on their momenta and invariant mass. The direct D_s has a fixed momentum in the e^+e^- rest frame, whereas the indirect D_s has momenta in a range due to the extra boost from the $D_s^* \to D_s(\gamma, \pi^0)$ decay. The recoil mass M_{rec} is defined by

$$M_{\text{rec}}^2 \equiv (E_0 - \sqrt{\mathbf{p}_{D_s}^2 + M_{D_s}^2})^2 - (\mathbf{p}_0 - \mathbf{p}_{D_s})^2, \tag{85}$$

where $(E_0, \mathbf{p}_0)$ is the e^+e^- center-of-mass four-vector, $\mathbf{p}_{D_s}$ is the measured D_s momentum, and M_{D_s} is the nominal D_s mass. For direct D_s candidates M_{rec} peaks at the D_s^* mass of 2.112 GeV, while for indirect D_s candidates M_{rec} is spread about evenly over ± 60 MeV around this peak. CLEO-c requires that D_s candidates in a double tag, and for most single tags, satisfies $M_{\text{rec}} > 2.051$ GeV. For the three single tag modes, $K^-K^+\pi^+\pi^0$, $\pi^+\pi^+\pi^-$, and $K^+\pi^+\pi^-$, with more substantial backgrounds, it is required that M_{rec} be greater than 2.099, 2.101, and 2.099 GeV, respectively. Note that this cut eliminates events from $e^+e^- \to D_s^+D_s^-$ as these events peak at $M_{\text{rec}} = M_{D_s}$. A number of vetoes are applied to reject fake candidates, primarily from D^*D^* events.

The single tag signal yields are extracted from the D_s invariant mass distributions. The single tag event yields in data are shown in Fig. 21. At most one single tag candidate per mode and charge are accepted per event. If more than one candidate passes the selection criteria, the candidate with the value of M_{rec} closest to $M_{D_s^*}$ is selected. The data are fit to a signal shape and a background shape. The signal shape is determined from Monte Carlo simulations, but the D_s mass is allowed to float in the fit.

The double tag yields are extracted by a cut-and-count procedure in the plot of the invariant mass of the D_s^+ vs D_s^-. All double tag candidates are shown in Fig. 22. At most one double tag candidate is allowed per event. If there is more than one candidate, the combination with the average mass $\hat{M} \equiv [M(D_s^+) + M(D_s^-)]/2$ closest to M_{D_s} is kept. The combinatorial background has structure in $\hat{M}$, but is more uniform in $\Delta M \equiv M(D_s^+) - M(D_s^-)$. The signal region is defined by $|\hat{M} - M_{D_s}| < 12$ MeV and $|\Delta M| < 30$ MeV and the sideband region is defined by $|\hat{M} - M_{D_s}| < 12$ MeV and $50 < |\Delta M| < 140$ MeV. In this analysis the individual double tag yields and efficiencies are determined. The signal and sideband regions are shown in Fig. 22.

All yields and efficiencies are combined in a likelihood fit to extract the D_s branching fractions. The branching fraction results from this fit are presented in Table XIII. In addition to the branching fractions, CLEO-c determined the number of $D_sD_s^*$ pairs produced in their data sample to be $N_{D_sD_s^*} = (2.93 \pm 0.14 \pm 0.06) \times 10^5$. Combined with the luminosity

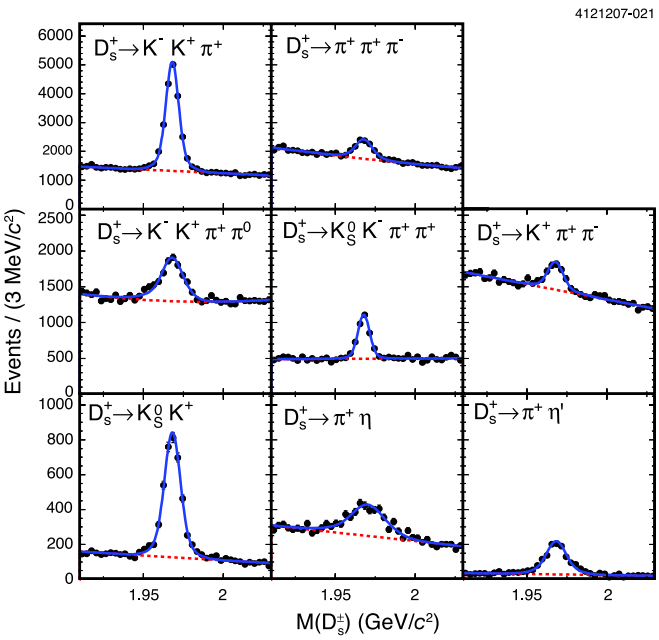

FIG. 21 (color online). Single tag yields for D_s modes used in the CLEO-c analysis. Charge conjugate modes are combined. From Alexander *et al.*, 2008.

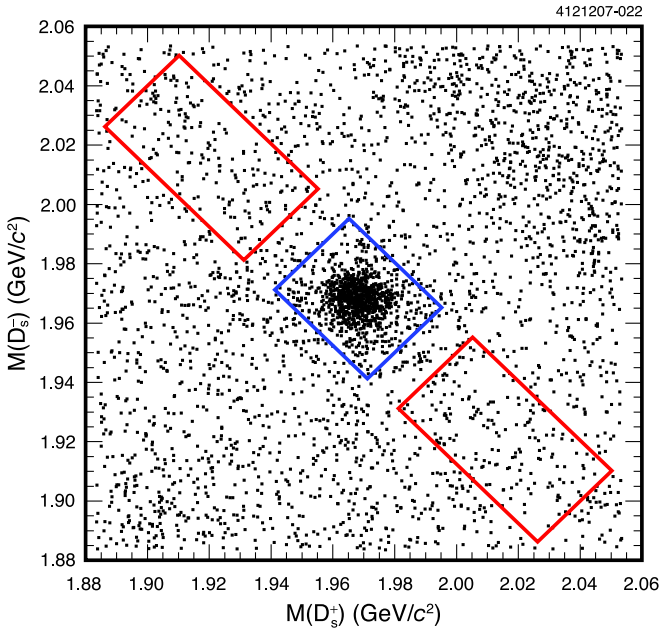

FIG. 22 (color online). Double tag yields for D_s modes used in the CLEO-c analysis. The signal region is indicated by the rectangle in the center and the two sideband regions are the diagonally offset rectangles. There are 1089 double tag candidates in the signal region and 339 candidates in the background region. With the signal-to-background region size of 1:3 this gives a signal-to-background ratio close to 9:1. From Alexander *et al.*, 2008.

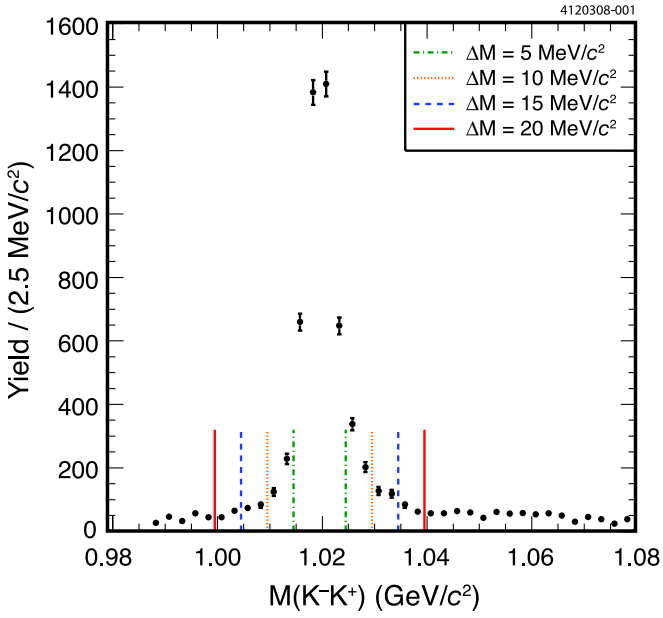

FIG. 23 (color online). The K^-K^+ invariant mass near the ϕ resonance in $D_s^+ \to K^-K^+\pi^+$ events from the CLEO-c double tag analysis. The single tag fit procedure used in the CLEO-c analysis is applied to extract the yield in each $M(K^-K^+)$ bin; hence backgrounds are subtracted and the yields shown are for the $D_s^+ \to K^-K^+\pi^+$ signal. The ϕ resonance is clear above an additional broad component. Indicated in the plot are the different mass windows considered by CLEO-c for their partial branching fractions. From Alexander *et al.*, 2008.

$\mathcal{L}_{\rm int} = (298 \pm 3)$ pb^{-1}, they obtained the cross section $\sigma_{D_sD_s^*}(E_{\rm c.m.} = 4.17\,{\rm GeV}) = 0.983 \pm 0.046 \pm 0.021 \pm 0.010$ nb, where the last systematic is due to the uncertainty in the luminosity.

CLEO-c does not quote a $D_s^+ \to \phi\pi^+$ branching fraction. The reason for this is that at the precision of this measurement the branching fraction for $D_s^+ \to \phi\pi^+$ is not a well-defined quantity. Figure 23 shows the K^+K^- invariant mass near the ϕ resonance. The combination of the relatively broad ϕ resonance and interference with other resonances, such as the $f_0(980)$, requires a complete amplitude analysis to determine the different contributions. Instead, CLEO-c provided partial branching fractions in different mass windows around the ϕ resonance. These partial branching fractions, given in four K^+K^- mass windows centered at the ϕ mass, are presented in Table XIV.

Systematic uncertainties from tracking efficiencies, π^0 and K_S^0 reconstruction, and particle identification are common in this analysis to those from the analysis of the D^0 and D^+ absolute branching fractions discussed in Sec. V.C. In addition, for modes containing an η in the final state an uncertainty of $\pm 4.0\%$ is applied per η. Other large systematic uncertainties in this analysis include the uncertainties from the signal line shape and the background parametrization in the fits for the yields. These uncertainties are explored by using alternative fits.

The CLEO-c analysis provided the to-date best determination of the hadronic branching fractions for D_s mesons. This analysis is statistics limited; the statistical uncertainty in the $D_s^+ \to K^+K^-\pi^+$ mode is 4.2% and the systematic uncertainty about 3%. The largest systematic uncertainties come from the yield extraction. Both the statistical and systematic uncertainties improve with additional data. This analysis was based on 298 pb^{-1}; CLEO-c recorded a total of 589 pb^{-1} of data at this energy.

TABLE XIII. Branching fractions for D_s decays determined by the CLEO-c analysis described by Alexander *et al.* (2008).

Mode	Branching fraction $\mathcal{B}$ (%)	$\mathcal{B}/\mathcal{B}(D_s^+ \to K^+K^-\pi^+)$	$\mathcal{A}_{CP}$ (%)
$\mathcal{B}(D_s^+ \to K_S^0K^+)$	$1.49 \pm 0.07 \pm 0.05$	$0.270 \pm 0.009 \pm 0.008$	$+4.9 \pm 2.1 \pm 0.9$
$\mathcal{B}(D_s^+ \to K^+K^-\pi^+)$	$5.50 \pm 0.23 \pm 0.16$	1	$+0.3 \pm 1.1 \pm 0.8$
$\mathcal{B}(D_s^+ \to K^+K^-\pi^+\pi^0)$	$5.65 \pm 0.29 \pm 0.40$	$1.03 \pm 0.05 \pm 0.08$	$-5.9 \pm 4.2 \pm 1.2$
$\mathcal{B}(D_s^+ \to K_S^0K^-\pi^+\pi^+)$	$1.64 \pm 0.10 \pm 0.07$	$0.298 \pm 0.014 \pm 0.011$	$-0.7 \pm 3.6 \pm 1.1$
$\mathcal{B}(D_s^+ \to \pi^+\pi^-\pi^+)$	$1.11 \pm 0.07 \pm 0.04$	$0.202 \pm 0.011 \pm 0.009$	$+2.0 \pm 4.6 \pm 0.7$
$\mathcal{B}(D_s^+ \to \pi^+\eta)$	$1.58 \pm 0.11 \pm 0.18$	$0.288 \pm 0.018 \pm 0.033$	$-8.2 \pm 5.2 \pm 0.8$
$\mathcal{B}(D_s^+ \to \pi^+\eta')$	$3.77 \pm 0.25 \pm 0.30$	$0.69 \pm 0.04 \pm 0.06$	$-5.5 \pm 3.7 \pm 1.2$
$\mathcal{B}(D_s^+ \to K^+\pi^+\pi^-)$	$0.69 \pm 0.05 \pm 0.03$	$0.125 \pm 0.009 \pm 0.005$	$+11.2 \pm 7.0 \pm 0.9$

TABLE XIV. Partial branching fractions in the mode $D_s^+ \to K^+K^-\pi^+$ for events with a K^+K^- invariant mass within ΔM MeV of the ϕ, $|m_{K^+K^-} - m_\phi| < \Delta M$. From the CLEO-c study described by Alexander *et al.* (2008).

ΔM	Partial branching fraction (%)
5	$1.69 \pm 0.08 \pm 0.06$
10	$1.99 \pm 0.10 \pm 0.05$
15	$2.14 \pm 0.10 \pm 0.05$
20	$2.24 \pm 0.11 \pm 0.06$

E. Summary of Cabibbo-favored D_s^+ decays

The previous sections discussed the key measurements that established the absolute branching fraction scale for D_s^+ meson decays. These measurements evolved from model-dependent determinations, e.g., making use of equal semileptonic widths as for the D^+ decay, to model-independent measurements using tagging techniques. Also as the measurements have become more precise we need to be more precise about what is measured. For example, the often-used normalization mode $D_s^+ \to \phi\pi^+$ suffers from a contamination from the $D_s^+ \to f_0(980)\pi^+$ under the $\phi\pi^+$ signal. The results for the Cabibbo-favored modes are summarized in Table XV.

VII. CABIBBO-SUPPRESSED DECAYS OF D^0, D^+, AND D_s^+ MESONS

A. Theoretical issues

Studies of hadronic singly Cabibbo-suppressed decays of charmed mesons are important for several reasons. First, these decays hold the potential for future observation of direct [i.e., not associated with $D^0\bar{D}^0$ mixing (Bianco *et al.*, 2003; Petrov, 2004; Gedalia and Perez, 2010] CP violation in the D system. In the standard model, this is due to the fact that the final-state particles contain at least one pair of a quark and antiquark of the same flavor, making a contribution possible from penguin-type amplitudes. Those amplitudes provide an access to the third generation of quarks (b quarks in the loops), needed for observation of CP violation in the standard model (Buccella *et al.*, 1993; Bianco *et al.*, 2003). New physics can also make an entrance through those transitions, affecting both the amplitudes and CP-violating asymmetries (Grossman, Kagan, and Nir, 2007). Second, it offers new ground for studying strong dynamics in hadronic decays, in particular, the issue of flavor $SU(3)_F$ breaking in D decays. For example, one of the famous failures of the applications of $SU(3)_F$ symmetry involves the prediction that the decay rates for $D^0 \to K^+K^-$ and $D^0 \to \pi^+\pi^-$ are equal. In reality, the first rate is about 3 times larger than the second one. Other puzzles include the fact that the rates for decays such as $D^+ \to K^{*+}\bar{K}^{*0}$ are so much enhanced by strong dynamics that their values appear to be as large as the ones of Cabibbo-favored decays. One popular explanation for such phenomena includes resonant final-state interactions (Kamal and Verma, 1987; Chau and Cheng, 1989) that affect not only D decays, but also $D^0\bar{D}^0$ mixing (Golowich and Petrov, 1998; Falk, Nir, and Petrov, 1999). There are also other explanations (Savage, 1991; Chau and Cheng, 1992). In order to study those phenomena it is convenient to select a base formalism for studies of hadronic transitions.

TABLE XV. Summary of branching fractions for Cabibbo-favored D_s^+ decays. Averages taken from Amsler *et al.* (2008) unless otherwise noted.

Mode	Branching fraction
$D_s^+ \to K^+K_S^0$	$(1.49 \pm 0.09)\%$
$D_s^+ \to K^+K^-\pi^+$	$(5.50 \pm 0.28)\%$
$D_s^+ \to K^+K^-\pi^+\pi^0$	$(5.6 \pm 0.5)\%$
$D_s^+ \to K_S^0K^+\pi^+\pi^-$	$(9.6 \pm 1.3) \times 10^{-3}$
$D_s^+ \to K_S^0K^-\pi^+\pi^+$	$(1.64 \pm 0.12)\%$
$D_s^+ \to K^+K^-\pi^+\pi^+\pi^-$	$(8.8 \pm 1.6) \times 10^{-3}$
$D_s^+ \to K_S^0K_S^0\pi^+\pi^+\pi^-$	$(8.4 \pm 3.5) \times 10^{-4}$
$D_s^+ \to \pi^+\pi^+\pi^-$	$(1.11 \pm 0.08)\%$
$D_s^+ \to \pi^+\pi^+\pi^-\pi^0$	$<14\%$
$D_s^+ \to \pi^+\pi^+\pi^+\pi^-\pi^-$	$(8.0 \pm 0.9) \times 10^{-3}$
$D_s^+ \to \pi^+\pi^+\pi^+\pi^-\pi^-\pi^0$	$(4.9 \pm 3.2)\%$
$D_s^+ \to \eta\pi^+$	$(1.58 \pm 0.21)\%$
$D_s^+ \to \omega\pi^+$ [a]	$(2.3 \pm 0.5) \times 10^{-3}$
$D_s^+ \to \omega\pi^0\pi^+$ [a]	$(2.78 \pm 0.70)\%$
$D_s^+ \to \omega\pi^+\pi^-\pi^+$ [a]	$(1.58 \pm 0.46)\%$
$D_s^+ \to \omega\pi^+\eta$ [a]	$<2.13\%$
$D_s^+ \to \eta\rho^+$	$(13.0 \pm 2.2)\%$
$D_s^+ \to \eta'\pi^+$	$(3.8 \pm 0.4)\%$
$D_s^+ \to \eta'\rho^+$	$(12.2 \pm 2.0)\%$

[a]Includes results from Ge *et al.* (2009b).

It is convenient to use the topological diagram approach to predict unknown branching ratios for singly Cabibbo-suppressed decays. The analysis, done by Chiang, Luo, and Rosner (2003) and repeated by Bhattacharya and Rosner (2008) and Bhattacharya *et al.* (2009) with updated experimental data, is displayed in Tables XVI, XVII, XVIII, and XIX.

1. $D \to PP$ transitions

A topological diagram approach to singly Cabibbo-suppressed transitions can make use of the information obtained from the fits of CF decays discussed above. In particular, the ratio of primed (SCS) to unprimed (CF) amplitudes is fixed, it is just $\lambda' = \tan\theta_C = 0.23$. Table XVI, from Bhattacharya and Rosner (2008), presents the most recent compilation of the branching ratios, amplitudes, and representations in terms of reduced amplitudes for singly Cabibbo-suppressed charm decays involving pions and kaons. The extracted topological amplitudes, in units of 10^{-7} GeV, are

$$T' = 6.44, \tag{86}$$

$$C' = -4.15 - 2.25i, \tag{87}$$

$$E' = -1.76 + 3.48i, \tag{88}$$

$$A' = 0.55 - 1.14i. \tag{89}$$

The deviations from flavor SU(3) in Table XVI are discussed.

Note that the decay $D^0 \to K^0\bar{K}^0$ is forbidden by $SU(3)_F$. Estimates of $SU(3)_F$-breaking effects lead to predictions for $\mathcal{B}(D^0 \to K^0\bar{K}^0)$ that are consistent with experimental observations, but are by no means reliable (Lipkin, 1980; Pham,

TABLE XVI. Branching ratios, amplitudes, decomposition in terms of reduced amplitudes, and predicted branching ratios for singly Cabibbo-suppressed charm decays involving pions and kaons. Predictions for the branching ratios are from Bhattacharya and Rosner (2008).

Meson	Decay mode	$\mathcal{B}$ (10^{-3})	p^* (MeV)	$\lvert\mathcal{A}\rvert$ $(10^{-7}$ GeV)	Rep.	Predicted $\mathcal{B}$ (10^{-3})
D^0	$\pi^+\pi^-$	1.40 ± 0.02	921.9	4.61 ± 0.03	$-(T' + E')$	2.23
	$\pi^0\pi^0$	0.80 ± 0.08	922.6	3.49 ± 0.17	$-(C' - E')/\sqrt{2}$	1.27
	K^+K^-	3.93 ± 0.07	791.0	8.35 ± 0.08	$(T' + E')$	1.92
	$K^0\bar{K}^0$	0.37 ± 0.06	788.5	2.57 ± 0.35	0	0
D^+	$\pi^+\pi^0$	1.24 ± 0.07	924.7	2.73 ± 0.08	$-(T' + C')/\sqrt{2}$	0.87
	$K^+\bar{K}^0$	6.17 ± 0.20	792.6	6.58 ± 0.11	$T' - A'$	5.12
D_s^+	π^+K^0	2.44 ± 0.30	915.7	5.84 ± 0.36	$-(T' - A')$	2.56
	π^0K^+	0.75 ± 0.28	917.1	3.24 ± 0.60	$-(C' + A')/\sqrt{2}$	0.87

TABLE XVII. Real and imaginary parts of amplitudes for SCS charm decays involving η and η', in units of 10^{-7} GeV. From Chiang, Luo, and Rosner (2003).

Amplitude	Expression	Re	Im	$\lvert\mathcal{A}_{\rm exp}\rvert$
$-\sqrt{6}\mathcal{A}(D^0 \to \pi^0\eta)$	$2E' - C' + SE'$	0.63	9.21	7.79 ± 0.54
$\frac{\sqrt{3}}{2}\mathcal{A}(D^0 \to \pi^0\eta')$	$\frac{1}{2}(C' + E') + SE'$	−2.95	0.62	3.54 ± 0.35
$\frac{3}{2\sqrt{2}}\mathcal{A}(D^0 \to \eta\eta)$	$C' + SE'$	−4.14	−2.25	5.91 ± 0.34
$-\frac{3\sqrt{2}}{7}\mathcal{A}(D^0 \to \eta\eta')$	$\frac{1}{7}(C' + 6E') + SE'$	−2.10	2.66	3.48 ± 0.38
$\sqrt{3}\mathcal{A}(D^+ \to \pi^+\eta)$	$T' + 2C' + 2A' + SA'$	−0.75	−6.77	8.21 ± 0.26
$-\frac{\sqrt{6}}{4}\mathcal{A}(D^+ \to \pi^+\eta')$	$\frac{1}{4}(T' - C' + 2A') + SA'$	2.92	−0.01	3.72 ± 0.15
$-\sqrt{3}\mathcal{A}(D_s^+ \to \eta K^+)$	$-(T' + 2C') + SA'$	1.85	4.50	8.05 ± 0.88
$\frac{\sqrt{6}}{4}\mathcal{A}(D_s^+ \to \eta' K^+)$	$\frac{1}{4}(2T' + C' + 3A') + SA'$	2.59	−1.41	3.43 ± 0.57

1987; Dai *et al.*, 1999; Eeg, Fajfer, and Zupan, 2001). We discuss those below.

Final states with η and η' require additional consideration: in particular, new topological amplitudes, flavor-singlet singlet exchange SE' and singlet annihilation SA'. The amplitudes C and E extracted from Cabibbo-favored charm decays imply values of $C' = \lambda' C$ and $E' = \lambda' E$ which may be used in constructing amplitudes for singly Cabibbo-suppressed D^0 decays involving η and η'.

2. $D \to PV$ transitions

A similar technique can be applied to describe $D \to PV$ transitions. In this case, similar topological amplitudes are denoted by a subscript V. We present the most recent results in Table XVIII (Bhattacharya *et al.*, 2009).

B. Cabibbo-suppressed D^0 and D^+ decays

Experimentally, Cabibbo-suppressed or doubly Cabibbo-suppressed decays of D^0 or D^+ mesons are almost always measured relative to a Cabibbo-favored normalization mode. This includes most CLEO-c analyses as the branching fractions for Cabibbo-suppressed modes are typically suppressed by $|V_{cd}/V_{cs}|^2 \approx 0.05$ and the statistics in these modes using a tagged analysis would be limited. In some cases, e.g., the CLEO-c analysis of $D^0 \to K\bar{K}$ final states (Bonvicini *et al.*, 2008a), CLEO normalized against the number of produced $D\bar{D}$ events and directly measured the branching fraction.

1. Two-body decays of D^0 and D^+

There is a substantial amount of data on the two-body decays of D^0 and D^+. The first measurements of Cabibbo-suppressed D^0 decays were for $D^0 \to K^-K^+$ and $D^0 \to \pi^-\pi^+$ by the Mark II experiment (Abrams *et al.*, 1979b). Since the first observation of these modes they have been measured by many experiments with increased precision. In these measurements the $D^0 \to K^-K^+$ and $D^0 \to \pi^-\pi^+$ branching fractions are measured relative to the $D^0 \to K^-\pi^+$ yield. Experiments operating above the $c\bar{c}$ threshold tag the D^0 by looking at the D^0-D^{*+} mass difference in the decay $D^{*+} \to D^0\pi^+$.

The results for the $D^0 \to K^-K^+$ and $D^0 \to \pi^-\pi^+$ decays are summarized in Table XIX. The most precise measurement is that of CDF (Acosta *et al.*, 2005); in the $D^0 \to K^-K^+$ they reconstructed about 16 000 signal candidates.

As can be seen from Table XIX, the rate for $D^0 \to K^+K^-$ is larger than the rate for $D^0 \to \pi^+\pi^-$ by a factor of 3. In the $SU(3)_F$ (or in the U-spin) symmetry limit, those rates should be the same. $SU(3)_F$ is, in general, expected to work to 30%, so this is a rather severe violation of this symmetry.

This problem has been around since the 1980s (Lipkin, 1980; Chau and Cheng, 1986), yet it still received no completely satisfactory solution. While the one popular explanation for this puzzle involves final-state interactions [e.g., a presence of a resonance that couples stronger to K^+K^- compared to $\pi^+\pi^-$ state or other type (Donoghue and Holstein, 1980; Chau and Cheng, 1986], it might be tempting

TABLE XVIII. Branching ratios and invariant amplitudes for singly Cabibbo-suppressed decays of charmed mesons to one pseudoscalar and one vector meson. From Bhattacharya and Rosner, 2009.

Meson	Decay mode	Representation	$\mathcal{B}$a (%)	p^* (MeV)	$\lvert\mathcal{A}\rvert$ (10^{-6})
D^0	$\pi^+\rho^-$	$-(T'_V + E'_P)$	0.497 ± 0.023	763.8	1.25 ± 0.03
	$\pi^-\rho^+$	$-(T'_P + E'_V)$	0.980 ± 0.040	763.8	1.76 ± 0.04
	$\pi^0\rho^0$	$\frac{1}{2}(E'_P + E'_V - C'_P - C'_V)$	0.373 ± 0.022	764.2	1.08 ± 0.03
	K^+K^{*-}	$T'_V + E'_P$	0.153 ± 0.015	609.8	0.97 ± 0.05
	K^-K^{*+}	$T'_P + E'_V$	0.441 ± 0.021	609.8	1.65 ± 0.04
	$K^0\bar{K}^{*0}$	$E'_V - E'_P$	<0.18	605.3	
	$\bar{K}^0K^{*0}$	$E'_P - E'_V$	<0.09	605.3	
	$\pi^0\phi$	$\frac{1}{\sqrt{2}}C'_P$	0.124 ± 0.012	644.7	0.81 ± 0.04
	$\pi^0\omega$	$\frac{1}{2}(E'_P + E'_V - C'_P + C'_V)$		761.2	
	$\eta\rho^0$	$\frac{1}{\sqrt{6}}(2C'_V - C'_P - E'_P - E'_V)$		652.0	
	$\eta\omega$	$-\frac{1}{\sqrt{6}}(2C'_V + C'_P + E'_P + E'_V)$	0.221 ± 0.023	648.1	1.07 ± 0.11
	$\eta\phi$	$\frac{1}{\sqrt{3}}(C'_P - E'_P - E'_V)$	0.014 ± 0.005	488.8	0.41 ± 0.15
	$\eta'\rho^0$	$\frac{1}{2\sqrt{3}}(E'_P + E'_V + C'_P + C'_V)$		342.5	
	$\eta'\omega$	$\frac{1}{2\sqrt{3}}(E'_P + E'_V + C'_P - C'_V)$		333.5	
D^+	$\rho^0\pi^+$	$\frac{1}{\sqrt{2}}(A'_P - A'_V - C'_P - T'_V)$	0.082 ± 0.015	767	0.32 ± 0.03
	$\omega\pi^+$	$-\frac{1}{\sqrt{2}}(A'_P + A'_V + C'_P + T'_V)$	<0.034	764	
	$\phi\pi^+$	C'_P	0.620 ± 0.070	647	1.13 ± 0.06
	$\bar{K}^{*0}K^+$	$(T'_V - A'_V)$	0.435 ± 0.048	611	1.03 ± 0.06
	$\pi^0\rho^+$	$\frac{1}{\sqrt{2}}(A'_V - A'_P - C'_V - T'_P)$		767	
	$\eta\rho^+$	$\frac{1}{\sqrt{3}}(A'_V + A'_P + 2C'_V + T'_P)$	<0.7	656	
	$\eta'\rho^+$	$\frac{1}{\sqrt{6}}(C'_V - A'_V - A'_P - T'_P)$	<0.5	349	
	$\bar{K}^0K^{*+}$	$(T'_P - A'_P)$	3.18 ± 1.38	612	2.78 ± 0.60
D_s^+	π^+K^{*0}	$(A'_V - T'_V)$	0.225 ± 0.039	773	0.79 ± 0.07
	π^0K^{*+}	$-\frac{1}{\sqrt{2}}(C'_V + A'_V)$		775	
	ηK^{*+}	$\frac{1}{\sqrt{3}}(T'_P + 2C'_V + A'_P - A'_V)$		661	
	$\eta' K^{*+}$	$\frac{1}{\sqrt{6}}(2T'_P + C'_V + 2A'_P + A'_V)$		337	
	$K^0\rho^+$	$(A'_P - T'_P)$		743	
	$K^+\rho^0$	$-\frac{1}{\sqrt{2}}(C'_P + A'_P)$	0.27 ± 0.05	745	0.92 ± 0.09
	$K^+\omega$	$-\frac{1}{\sqrt{2}}(C'_P - A'_P)$		741	
	$K^+\phi$	$T'_V + C'_P + A'_V$	<0.057	607	

[a]Amsler *et al.* (2008).

TABLE XIX. Measurements of $D^0 \to K^-K^+$ and $D^0 \to \pi^-\pi^+$. The branching fractions have been recalculated using $\mathcal{B}(D^0 \to K^-\pi^+) = (3.89 \pm 0.05)\%$.

Experiment	$\mathcal{B}(D^0 \to K^-K^+)$ (10^{-3})	$\mathcal{B}(D^0 \to \pi^-\pi^+)$ (10^{-3})
CLEO-c (Rubin *et al.*, 2006; Bonvicini *et al.*, 2008a)	$4.08 \pm 0.08 \pm 0.09$	$1.41 \pm 0.04 \pm 0.03$
BES II (Ablikim *et al.*, 2005)	$4.75 \pm 0.43 \pm 0.17$	
CDF (Acosta *et al.*, 2005)	$3.859 \pm 0.043 \pm 0.069$	$1.40 \pm 0.02 \pm 0.03$
FOCUS (Link *et al.*, 2003)	$3.863 \pm 0.054 \pm 0.074$	$1.37 \pm 0.05 \pm 0.03$
CLEO II (Csorna *et al.*, 2002)	$4.05 \pm 0.13 \pm 0.13$	$1.36 \pm 0.06 \pm 0.07$
E791 (Aitala *et al.*, 1998a)	$4.24 \pm 0.12 \pm 0.13$	$1.56 \pm 0.08 \pm 0.12$
CLEO II (Asner *et al.*, 1996)	$4.51 \pm 0.27 \pm 0.28$	
E687 (Frabetti *et al.*, 1994a)	$4.24 \pm 0.27 \pm 0.35$	
E691 (Anjos *et al.*, 1991)	$4.16 \pm 0.39 \pm 0.39$	
CLEO (Alexander *et al.*, 1990b)	$4.55 \pm 0.39 \pm 0.28$	
Average	3.98 ± 0.07	1.40 ± 0.03

to try to understand the issue in factorization (Sanda, 1980; Chau and Cheng, 1992), neglecting for a moment the annihilation diagram contribution,

$$\frac{\mathcal{A}_{K\bar{K}}}{\mathcal{A}_{\pi\bar{\pi}}} = \frac{f_K}{f_\pi}\frac{m_D^2 - m_K^2}{m_D^2 - m_\pi^2}\frac{F^{DK}(m_K^2)}{F^{D\pi}(m_\pi^2)}. \tag{90}$$

With the recent lattice evaluations $f_K/f_\pi = 1.218 \pm 0.002^{+0.011}_{-0.024}$ from a lattice QCD calculation with domain-wall fermions (Beane *et al.*, 2007) [which is consistent with experimental determinations of the decay constants that can also be used, see Artuso *et al.* (2008) and Bianco *et al.* (2003)], assuming a modified pole dominance for the form factors $F^{DK}(m_K^2)$ and $F^{D\pi}(m_\pi^2)$, and extracting them from semileptonic D decays [see Artuso *et al.* (2008) for a recent review and Besson *et al.* (2009) for recent determination of parameters], we get

$$\mathcal{A}_{K\bar{K}} \simeq 1.32\mathcal{A}_{\pi\bar{\pi}}. \tag{91}$$

It is interesting to note that the effect of $SU(3)_F$ breaking in the decay constants works in the *opposite* direction to the effect due to different phase space of K^+K^- and $\pi^+\pi^-$ final states (Chau and Cheng, 1992). In other words, factorization predicts about 30% breaking of $SU(3)_F$ in spectator amplitudes [cf. Chau and Cheng (1992)]. Clearly, this is not sufficient for the resolution of the puzzle.

There is a recent suggestion (Bianco *et al.*, 2003) attributing this effect to the difference between $SU(3)_F$ breaking in exclusive versus inclusive modes. This fact can also be interpreted in terms of final-state interactions, as final-state interactions do not simply enhance a given decay channel, but rather redistribute the strength of different channels composing the inclusive decay rate. The fact that the ratio of $\Gamma(D \to KK\pi\pi)$ and $\Gamma(D \to 4\pi)$ exhibits behavior opposite to the ratio of $\Gamma(D \to KK)$ and $\Gamma(D \to \pi\pi)$ (see Tables XXII and XXIII) buttresses this conclusion. The presence of final-state interaction-enhanced exchange amplitude is also crucial for the explanation of this phenomenon. A number of other two-body final states to pseudoscalars have been studied. These decays are summarized in Table XX.

The most complete study of D mesons decays to final states containing η and η' mesons is done by CLEO-c (Artuso *et al.*, 2008). This analysis uses 281 pb^{-1} of data collected at the $\psi(3770)$ resonance. In this study CLEO-c makes use of single tags; the modes studied here have sufficiently small branching fractions so that using D tagging is not useful. The π^0 and η mesons are reconstructed in the $\gamma\gamma$ final state. In addition, for modes with two η mesons in the final state ($\eta\eta$ and $\eta\eta'$) the $\eta \to \pi^+\pi^-\pi^0$ channel is used to reconstruct η mesons. The η' is reconstructed in the channel $\eta' \to \eta\pi^+\pi^-$. It is required that $402 < M_{\eta\pi^+\pi^-} - M_\eta < 418$ MeV.

TABLE XX. Measurements of D^0 and D^+ decays to Cabibbo-suppressed, nonstrange, two-body final states. The averages are from Amsler *et al.* (2008).

Mode	$\mathcal{B}$ (10^{-3})
$D^0 \to \pi^+\pi^-$	1.40 ± 0.02
$D^0 \to \pi^0\pi^0$	0.80 ± 0.08
$D^0 \to \eta\pi^0$	0.57 ± 0.14
$D^0 \to \omega\pi^0$	<0.26
$D^+ \to \pi^0\pi^+$	1.24 ± 0.07
$D^+ \to \pi^+\eta$	3.39 ± 0.29
$D^+ \to \pi^+\omega$	<0.34

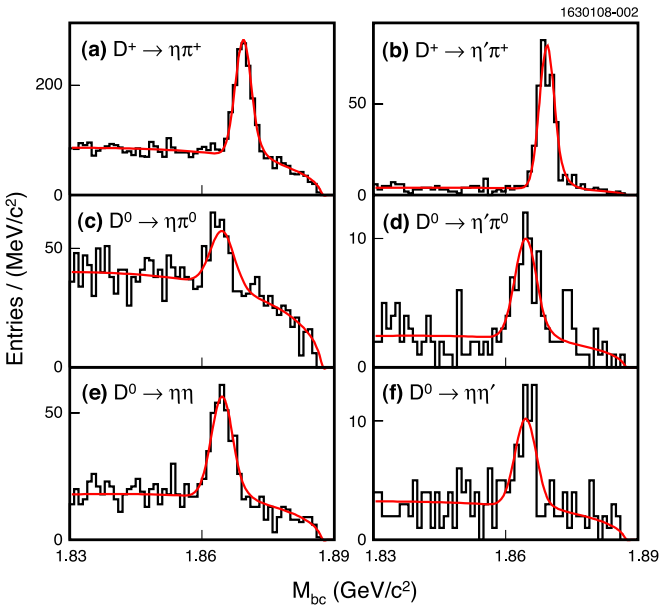

FIG. 24 (color online). Yields for (a) $D^+ \to \eta\pi^+$, (b) $D^+ \to \eta'\pi^+$, (c) $D^0 \to \eta\pi^0$, (d) $D^0 \to \eta'\pi^0$, (e) $D^0 \to \eta\eta$, and (f) $D^0 \to \eta\eta'$. From Artuso *et al.*, 2008.

The yields are extracted by fitting the $M_{\rm BC}$ distributions after selecting events consistent with $\Delta E = 0$. In Figs. 24 and 25 the observed signals are shown. The significances for all modes are over 4σ except for the $D^0 \to \eta'\pi^+\pi^-$ mode where the significance is estimated to be 3.2σ. The observed

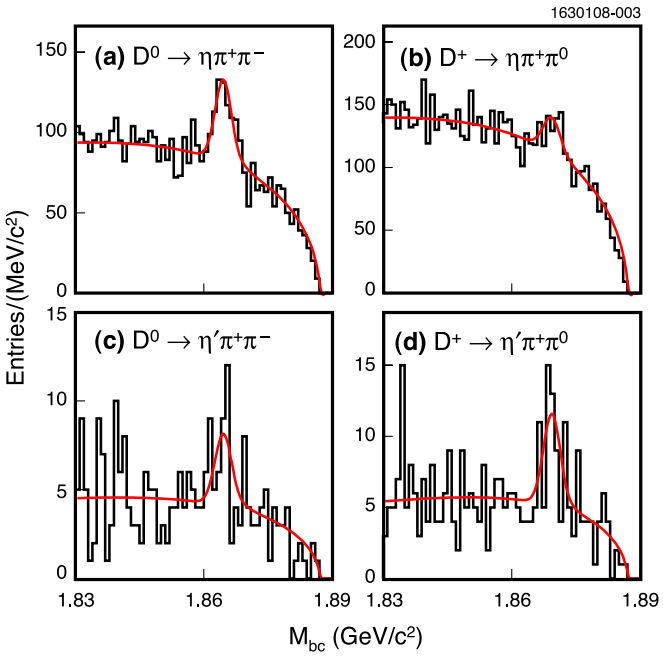

FIG. 25 (color online). Yields for (a) $D^0 \to \eta\pi^+\pi^-$, (b) $D^+ \to \eta\pi^+\pi^0$, (c) $D^0 \to \eta'\pi^+\pi^-$, and (d) $D^+ \to \eta'\pi^+\pi^0$. From Artuso *et al.*, 2008.

TABLE XXI. Yields and branching fractions for D meson decays to final states with η and η' mesons. From Artuso *et al.* (2008).

Mode	Yield	Branching fraction (10^{-4})
$\mathcal{B}(D^+ \to \eta\pi^+)$	1033 ± 42	$34.3 \pm 1.4 \pm 1.7$
$\mathcal{B}(D^+ \to \eta'\pi^+)$	352 ± 20	$44.2 \pm 2.5 \pm 2.9$
$\mathcal{B}(D^0 \to \eta\pi^0)$	156 ± 24	$6.4 \pm 1.0 \pm 0.4$
$\mathcal{B}(D^0 \to \eta'\pi^0)$	50 ± 9	$8.1 \pm 1.5 \pm 0.6$
$\mathcal{B}(D^0 \to \eta\eta)$	255 ± 22	$16.7 \pm 1.4 \pm 1.3$
$\mathcal{B}(D^0 \to \eta\eta')$	46 ± 9	$12.6 \pm 2.5 \pm 1.1$
$\mathcal{B}(D^0 \to \eta\pi^+\pi^-)$	257 ± 32	$10.9 \pm 1.3 \pm 0.9$
$\mathcal{B}(D^+ \to \eta\pi^+\pi^0)$	149 ± 34	$13.8 \pm 3.1 \pm 1.6$
$\mathcal{B}(D^0 \to \eta'\pi^+\pi^-)$	21 ± 8	$4.5 \pm 1.6 \pm 0.5$
$\mathcal{B}(D^+ \to \eta'\pi^+\pi^0)$	33 ± 9	$15.7 \pm 4.4 \pm 2.5$

yields and branching fractions are summarized in Table XXI. These data make it possible to constrain new singlet-exchange SE' amplitudes introduced in Sec. VII.A.1. In order to do that, one can rewrite four equations for D^0 decay amplitudes to the final states with $\eta^{(\prime)}$:

$$-\sqrt{6}\mathcal{A}(D^0 \to \eta\pi^0) = 2E' - C' + SE', \tag{92}$$

$$\frac{\sqrt{3}}{2}\mathcal{A}(D^0 \to \eta'\pi^0) = \frac{1}{2}(E' + C') + SE', \tag{93}$$

$$\frac{3}{2\sqrt{2}}\mathcal{A}(D^0 \to \eta\eta) = C' + SE', \tag{94}$$

$$-\frac{3\sqrt{2}}{7}\mathcal{A}(D^0 \to \eta'\eta') = \frac{1}{7}(C' + 6E') + SE'. \tag{95}$$

It is interesting to note that the right-hand sides of Eqs. (92)–(95) determine a vector in a complex plane. Since both amplitudes and phases of C' and E' are known from Eq. (86), these four equations contain a common complex offset SE'. Since only the magnitudes of the right-hand sides of these equations are known, they each define a circle in the complex plane with the radius given by that magnitude. Plotting them on the same graph then determines SE'.

This is done in Fig. 26. Notice that all circles intersect in two points, which determine two possible solutions for SE'. The smaller values for $SE' = (-0.7 \pm 0.4) \times 10^{-7}$ GeV $+ i(-1.0 \pm 0.6) \times 10^{-7}$ GeV are theoretically preferable, as SE' is an Okubo-Zweig-Iizuka–(OZI) suppressed amplitude (Zweig, 1964; Iizuka, 1966; Okubo, 1977).

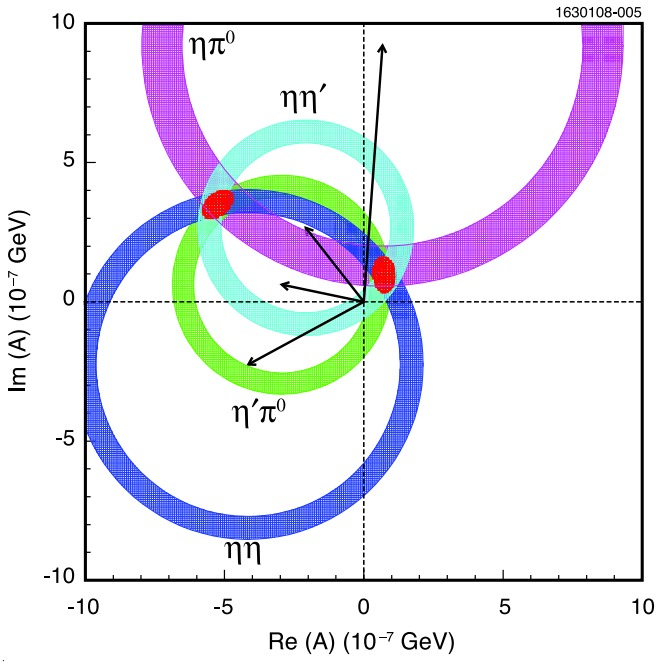

FIG. 26 (color online). Graphical representation of Eq. (92) used to determine SE' from the amplitude analysis for $D \to \eta^{(\prime)}\eta(\pi^0)$. Circles represent absolute values of the decay amplitudes. The intersection points provide two possible solutions for SE' (see text). From Artuso *et al.*, 2008.

2. Multibody decays with kaons and pions

Multibody decays of D^0 and D^+ mesons has also been extensively studied. While theoretical studies of those transitions are limited, some of those decays can be used in the Dalitz-plot analyses of $D^0\bar{D}^0$ mixing (Artuso, Meadows, and Petrov, 2008). Measurements of branching fractions to final states with three or more pions, including final states with η and ω mesons, can be found in Table XXII. In Sec. IX Dalitz-plot analyses of three-body final states are discussed.

In addition to the $D^0 \to KK$ decays discussed above, many other Cabibbo-suppressed decays with two kaons in the final states have been studied. Dalitz-plot analyses have been performed on some three-body final states as discussed in Sec. IX. The final states with two kaons are summarized in Table XXIII.

C. Cabibbo-suppressed D_s decays

The Cabibbo-suppressed D_s decays are final states with one or three kaons. The measured decays are listed in Table XXIV. This table also includes the doubly Cabibbo-suppressed decay $D^+ \to K^+K^+\pi^-$. CLEO-c (Adams *et al.*, 2007) performed a systematic study of two-body D_s decays.

D. Doubly Cabibbo-suppressed decays

The doubly Cabibbo-suppressed decays have two Cabibbo-suppressed weak couplings. Naively, the rates for the doubly Cabibbo-suppressed decays are smaller than the

TABLE XXII. Measurements of D^0 and D^+ decays to Cabibbo-suppressed final states with three or more pions in the final states. Final states with η and ω mesons are also included. Limits are given at 90% C.L. Averages from Amsler *et al.* (2008).

Mode	$\mathcal{B}$ (10^{-3})
$D^0 \to \pi^+\pi^-\pi^0$	14.1 ± 0.6
$D^0 \to \pi^+\pi^-\pi^+\pi^-$	7.44 ± 0.21
$D^0 \to \pi^+\pi^-\pi^+\pi^-\pi^0$	4.2 ± 0.5
$D^0 \to \pi^0\pi^0\pi^0$	<0.35
$D^0 \to \pi^+\pi^-\pi^0\pi^0$	10.0 ± 0.9
$D^0 \to \pi^+\pi^-\pi^+\pi^-\pi^+\pi^-$	0.42 ± 0.12
$D^+ \to \pi^+\pi^+\pi^-$	3.21 ± 0.19
$D^+ \to \pi^+\pi^0\pi^0$	4.6 ± 0.4
$D^+ \to \pi^+\pi^+\pi^-\pi^0$	11.4 ± 0.8
$D^+ \to \pi^+\pi^+\pi^-\pi^+\pi^-$	1.63 ± 0.16

TABLE XXIII. Measurements of branching fractions for D^0 and D^+ decays to Cabibbo-suppressed final states with two kaons. Averages from Amsler *et al.* (2008).

Mode	$\mathcal{B}$ (10^{-3})
$D^0 \to K_S^0 K^- \pi^+$	3.5 ± 0.5
$D^0 \to K_S^0 K^+ \pi^-$	2.7 ± 0.5
$D^0 \to K^+ K^- \pi^0$	3.29 ± 0.14
$D^0 \to K_S^0 K_S^0 \pi^0$	<0.59
$D^0 \to K^+ K^- \pi^+ \pi^-$	2.43 ± 0.012
$D^0 \to K_S^0 K_S^0 \pi^+ \pi^-$	1.30 ± 0.24
$D^0 \to K_S^0 K^- \pi^+ \pi^+ \pi^-$	<0.15
$D^0 \to K^+ K^- \pi^+ \pi^- \pi^0$	3.1 ± 2.0
$D^+ \to K^+ K^- \pi^+$	9.63 ± 0.31
$D^+ \to K^+ K_S^0 \pi^+ \pi^-$	1.69 ± 0.18
$D^+ \to K_S^0 K^- \pi^+ \pi^+$	2.32 ± 0.18
$D^+ \to K^+ K^- \pi^+ \pi^+ \pi^-$	2.3 ± 1.2

Cabibbo-favored decay rates by a factor of $\tan^4\theta_C \approx 2.8 \times 10^{-3}$. Since those rates are quite small, one may wonder if they can be affected by some kind of new physics contributions. It has been proven (Bergmann and Nir, 1999), however, that phenomenological constraints imply that the new physics contributions are quite small compared to the standard model amplitudes. Since all quarks in the decay vertex of the DCS diagram are of different flavors, the set of new physics models that could possibly affect those decays are indeed not that big.

The first observation of a doubly Cabibbo-suppressed decay was in the decay channel $D^0 \to K^+\pi^-$ (Cinabro *et al.*, 1994). Experimentally, the flavor, D^0 or $\bar{D}^0$, of the initial state is tagged by the charge of the slow pion in the decay $D^{*+} \to D^0\pi^+$. The simplest measurements observe the time integrated rate of D^0 and $\bar{D}^0$ decays. They do not separate direct decay contributions from mixing, where D^0 first oscillates into a $\bar{D}^0$ state and then decays via a Cabibbo-favored transition.

The D^0 doubly Cabibbo-suppressed decays that have been studied are summarized in Table XXV. The three most precise measurements of the $D^0 \to K^+\pi^-$ decay by CDF (Aaltonen *et al.*, 2008), *BABAR* (Aubert *et al.*, 2007b), and Belle (Zhang *et al.*, 2006) obtained branching ratios with respect to $D^0 \to K^-\pi^+$ of $(4.15 \pm 0.10) \times 10^{-3}$, $(3.53 \pm 0.08 \pm 0.04) \times 10^{-3}$, and $(3.77 \pm 0.08 \pm 0.05) \times 10^{-3}$, respectively. The agreement between these measurements is not good; the PDG applies a scale factor of 3.3 for the error on their average to obtain the average ratio of branching fractions to be $(3.80 \pm 0.18) \times 10^{-3}$.

TABLE XXIV. Cabibbo-suppressed D_s^+ decays.

Mode	Reference	$\mathcal{B}$ (10^{-3})
$D_s^+ \to K^+\pi^0$	Adams *et al.* (2007)	0.82 ± 0.22
$D_s^+ \to K_S^0\pi^+$	Adams *et al.* (2007) and Link *et al.* (2008)	1.25 ± 0.15
$D_s^+ \to K^+\eta$	Adams *et al.* (2007)	1.41 ± 0.31
$D_s^+ \to K^+\eta'$	Adams *et al.* (2007)	1.6 ± 0.5
$D_s^+ \to K^+\pi^+\pi^-$	Alexander *et al.* (2008)	6.9 ± 0.5
$D_s^+ \to K_S^0\pi^+\pi^+\pi^-$	Link *et al.* (2008)	3.1 ± 1.1
$D_s^+ \to K^+K^+K^-$	Link *et al.* (2002b)	0.49 ± 0.17
$D_s^+ \to K^+K^+\pi^-$	Link *et al.* (2005c)	0.29 ± 0.11

TABLE XXV. Doubly Cabibbo-suppressed D^0 decays. The second column ($\mathcal{B}$) shows the branching fraction for the decay and the third column (R) shows the ratio of the branching fraction with respect to the corresponding Cabibbo-favored decay. Averages from Amsler *et al.* (2008).

Mode	$\mathcal{B}$ (10^{-4})	R (10^{-3})
$D^0 \to K^+\pi^-$	1.48 ± 0.07	3.80 ± 0.18
$D^0 \to K^+\pi^-\pi^0$	3.05 ± 0.17	2.20 ± 0.10
$D^0 \to K^+\pi^-\pi^+\pi^-$	$2.62^{+0.21}_{-0.19}$	$3.23^{+0.25}_{-0.22}$

The decay $D^0 \to K^+\pi^-\pi^0$ was first observed by CLEO (Brandenburg *et al.*, 2001). The PDG average is dominated by the more recent measurements from *BABAR* (Aubert *et al.*, 2006b) and Belle (Tian *et al.*, 2005).

The first significant $D^0 \to K^+\pi^-\pi^+\pi^-$ observation was made by CLEO (Dytman *et al.*, 2001). The most recent and precise measurement of this decay was done by Belle (Tian *et al.*, 2005).

Both CLEO-c (Dytman *et al.*, 2006) and *BABAR* (Aubert *et al.*, 2006a) studied the doubly Cabibbo-suppressed decay $D^+ \to K^+\pi^0$. CLEO-c reconstructed candidates in a 281 pb^{-1} sample of e^+e^- data recorded at the $\psi(3770)$. *BABAR* used a sample of 124 fb^{-1} recorded at the $\Upsilon(4S)$. CLEO-c and *BABAR* found branching fractions in good agreement with each other, $\mathcal{B}(D^+ \to K^+\pi^0) = (2.24 \pm 0.36 \pm 0.15 \pm 0.08) \times 10^{-4}$ and $\mathcal{B}(D^+ \to K^+\pi^0) = (2.52 \pm 0.46 \pm 0.24 \pm 0.08) \times 10^{-4}$, respectively. The average branching fraction obtained is $(2.37 \pm 0.32) \times 10^{-4}$.

The final state $D^+ \to K^+\pi^+\pi^-$ was studied by E687 (Frabetti *et al.*, 1995b), E791 (Aitala *et al.*, 1997), and FOCUS (Link *et al.*, 2004b). The average branching fraction from these measurements is $\mathcal{B}(D^+ \to K^+\pi^+\pi^-) = (6.2 \pm 0.7) \times 10^{-4}$.

The decay $D^+ \to K^+K^+K^-$ was observed by FOCUS (Link *et al.*, 2002b). They measured the ratio of branching fractions $\mathcal{B}(D^+ \to K^+K^+K^-)/\mathcal{B}(D^+ \to K^-\pi^+\pi^+) = (9.49 \pm 2.17 \pm 0.22) \times 10^{-4}$. This gives the branching fraction $\mathcal{B}(D^+ \to K^+K^+K^-) = (8.7 \pm 2.0) \times 10^{-5}$.

VIII. FINAL-STATE INTERACTIONS AND AMPLITUDE ANALYSIS

One of the simplest ways to analyze decays of D mesons is to employ the flavor-flow-diagram technique described earlier. One potential problem with the application of this technique[1] to charm decays involves the assignment of quark amplitudes ($\mathcal{T}$, $\mathcal{A}$, etc.) to a particular decay. The root of the problem involves inelastic final-state interactions.

A. Hadronic decays into meson states

Historically, the issue came up with decays of type $D^0 \to \phi K^0$, which have been claimed to originate entirely from quark exchange amplitudes. Thus, in the topological SU(3) or

[1]Similar problems could affect charm decay analysis using the factorization approximation.

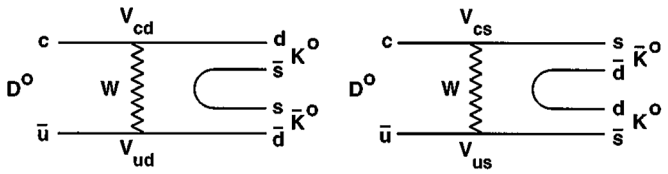

FIG. 27. The two quark diagrams that contribute to the decay $D^0 \to K_S^0 K_S^0$. Since $V_{cd} = -V_{us}$ the two amplitudes represented by these diagrams largely cancel. In the limit in which the d and s quark masses were the same the cancellation would have been exact.

flavor-flow analysis of this transition only an exchange amplitude $\mathcal{E}$ should be assigned to this decay. However, final-state interaction contributions of the type

$$D^0 \to \eta^{(\prime)} \bar{K}^{0*} \to \phi \bar{K}^0 \tag{96}$$

could proceed through the color-suppressed internal W-emission diagram $\mathcal{C}$ followed by strong-interaction rescattering $\eta^{(\prime)} \bar{K}^{0*} \to \phi \bar{K}^0$. This contribution is not optional, but is, in fact, required by unitarity (Donoghue, 1986). While in the example above partial cancellation occurs between the intermediate $\eta \bar{K}^{0*}$ and $\eta' \bar{K}^{0*}$ states (Lipkin, 1987), this cancellation is not generic. Similar processes are also possible in D_s meson decays (Fajfer *et al.*, 2003; Gronau and Rosner, 2009). If large, the contributions of this type could be important in the topological flavor-flow amplitude analysis of charm decays (Cheng, 2003).

One way to study the importance of inelastic final-state interaction contributions in charm decays is to seek guidance from experimental studies of "annihilation" decays, i.e., decays whose contribution is dominated by weak annihilation or exchange amplitudes in the topological flavor-flow analysis.

Another related decay mode that is interesting from this perspective is $D^0 \to K_S K_S$. Naively, there are two W exchange diagrams that contribute to this final state as illustrated in Fig. 27. Since $V_{cd} = -V_{us}$, these amplitudes interfere destructively, so in the flavor $SU(3)_F$ limit the branching ratio for this process is zero. Thus, in addition to being the "pure annihilation" decay, the rate of the $D^0 \to K_S K_S$ transition explicitly probes $SU(3)_F$-breaking corrections. It should be rather small.

Interestingly enough, a naive calculation of this decay rate in factorization gives exactly zero,

$$\begin{aligned}\mathcal{A}(D^0 \to K_S K_S) &= \tfrac{1}{2}\mathcal{A}(D^0 \to K^0 \bar{K}^0) \\ &= f_D p_D (p_{K^0} - p_{\bar{K}^0}) = 0,\end{aligned} \tag{97}$$

so $\mathcal{B}_{\rm fact}(D^0 \to K_S K_S) = 0$. As we discuss later in this section, experimental analyses of this transition, however, clearly yield a nonzero result.

The ratio of branching fractions $\mathcal{B}(K_S^0 K_S^0)/\mathcal{B}(K_S^0 \pi^+ \pi^-)$ was measured by CLEO (Alexander *et al.*, 1990b), E687 (Frabetti *et al.*, 1994c), CLEO II (Asner *et al.*, 1996), and FOCUS (Link *et al.*, 2005b). CLEO-c (Bonvicini *et al.*, 2008a) studied this decay using a single tag technique and normalized to the number of $D^0 \bar{D}^0$ events produced. These measurements are summarized in Table XXVI. Measurements of the branching ratios $\mathcal{B}(K_S^0 K_S^0)/\mathcal{B}(K_S^0 \pi^+ \pi^-)$ have been rescaled using $\mathcal{B}(K_S^0 \pi^+ \pi^-) = (2.99 \pm 0.17)\%$ (Amsler *et al.*, 2008).

The most recent, and most precise, measurement from CLEO-c gives the smallest central value. Given the large uncertainties in the earlier measurements there is no strong inconsistency between the different measurements. This clearly points to shortcomings of factorization calculation outlined above.

One way to understand this branching ratio would be to assume that nonfactorizable pieces, dropped in Eq. (97), dominate the branching ratio for $D^0 \to K_S^0 K_S^0$. There is, however, no reliable way to estimate those [see, however, Eeg, Fajfer, and Zupan (2001)]. Another way would be to accept that this and similar branching ratios are dominated by final-state interactions (Lipkin, 1980; Pham, 1987). Simple two-channel model estimates give

$$\Gamma(D^0 \to K^0 \bar{K}^0) = \Gamma(D^0 \to K^+ K^-) \tan^2[\tfrac{1}{2}(\delta_0 - \delta_1)], \tag{98}$$

where δ_0 and δ_1 are the phase shifts for $I = 0$ and $I = 1$ amplitudes. Estimates with other models of final-state interactions give comparable results (Dai *et al.*, 1999). While these estimates are by no means reliable, they serve as an indication of the importance of final-state interactions in charm hadronic decays.

B. Baryonic decay $D_s^+ \to p^+ \bar{n}$

Final states with baryons are not possible for the D^0 and D^+. The lightest neutral final state $p\bar{p}$ has a mass of 1876.54 MeV and is just above the D^0 and D^+ mass. However, the D_s^+ is kinematically allowed to decay to $p^+ \bar{n}$. This decay is also quite interesting because the flavors of all valence quarks that constitute the initial state ($c\bar{s}$) differ from the flavors of the final-state quarks composing the $p^+ \bar{n}$ pair. Thus, it is quite tempting to declare that the transition

TABLE XXVI. The observed branching fractions for $D^0 \to K_S^0 K_S^0$. The errors are statistical, systematic, and from normalization branching fraction $K_S^0 \pi^+ \pi^-$ when used.

Experiment	Events	$\mathcal{B}(D^0 \to K_S^0 K_S^0)$ (10^{-4})
CLEO-c (Bonvicini *et al.*, 2008a)	68 ± 15	$1.46 \pm 0.32 \pm 0.09$
FOCUS (Link *et al.*, 2005b)	79 ± 17	$4.31 \pm 0.96 \pm 0.48 \pm 0.24$
CLEO II (Asner *et al.*, 1996)	26	$3.02 \pm 0.66 \pm 0.48 \pm 0.17$
E687 (Frabetti *et al.*, 1994c)	20 ± 7	$11.7 \pm 3.9 \pm 3.9 \pm 0.7$
CLEO (Alexander *et al.*, 1990b)	5	$6.3^{+3.3}_{-2.4} \pm 0.6 \pm 0.4$
Average		1.93 ± 0.30

$D_s^+ \to p^+\bar{n}$ proceeds only via the weak annihilation graph (Pham, 1980a, 1980b; Chen, Cheng, and Hsiao, 2008).

A factorization ansatz can be employed in order to estimate the branching ratio for this process (Chen, Cheng, and Hsiao, 2008). It must be emphasized again that, contrary to hadronic B decays, simple factorization has not been proven in charm transitions, especially as applied to annihilation amplitudes. Nevertheless, a factorized decay amplitude is

$$A(D_s^+ \to p^+\bar{n}) = \frac{G_F}{\sqrt{2}} V_{cs}V_{ud}^* a_1 f_{D_s} p_{D_s}^\mu \langle p\bar{n}|\bar{u}\gamma_\mu(1-\gamma_5)d|0\rangle, \tag{99}$$

where $p_{D_s} = p_p + p_{\bar{n}}$ is the four-momentum of a D_s meson. The matrix element between the vacuum and the final state can be parametrized. We note that first vector current conservation implies that

$$p_{D_s}^\mu \langle p\bar{n}|\bar{u}\gamma_\mu(1-\gamma_5)d|0\rangle = (m_p + m_{\bar{n}})\langle p\bar{n}|\bar{u}\gamma_5 d|0\rangle, \tag{100}$$

so the decay amplitude can be parametrized as

$$A(D_s^+ \to p^+\bar{n}) = \frac{G_F}{\sqrt{2}} V_{cs}V_{ud}^* a_1 f_{D_s}\left(2m_N g_1^{p\bar{n}} + \frac{m_{D_s}^2}{2m_N} g_3^{p\bar{n}}\right)\bar{u}_p\gamma_5 v_{\bar{n}}, \tag{101}$$

where $g_i^{p\bar{n}}$ are the form factors parametrizing the baryon current, and m_N is the nucleon's mass. The two form factors $g_1^{p\bar{n}}$ and $g_3^{p\bar{n}}$ can be related to each other (Pham, 1980a, 1980b; Chen, Cheng, and Hsiao, 2008),

$$g_3^{p\bar{n}}(p_{D_s}^2) = -\frac{4m_N^2}{p_{D_s}^2 - m_\pi^2} g_1^{p\bar{n}}(p_{D_s}^2), \tag{102}$$

so that the decay amplitude takes the form

$$A(D_s^+ \to p^+\bar{n}) = \frac{2G_F}{\sqrt{2}} V_{cs}V_{ud}^* a_1 f_{D_s} m_N\left(\frac{m_\pi}{m_{D_s}}\right)^2 g_1^{p\bar{n}}\bar{u}_p\gamma_5 v_{\bar{n}}. \tag{103}$$

This amplitude leads to the estimate of the decay branching ratio $\mathcal{B}(D_s^+ \to p^+\bar{n})$ in the factorization approximation (Chen, Cheng, and Hsiao, 2008),

$$\mathcal{B}(D_s^+ \to p^+\bar{n})_{\rm th} = (0.4^{+1.1}_{-0.3}) \times 10^{-6}. \tag{104}$$

The theoretical error quoted in Eq. (104) is entirely due to the uncertainty in the form-factor value of $g_1^{p\bar{n}}(m_{D_s}^2)$ (Chen, Cheng, and Hsiao, 2008), which was obtained by extrapolation of the nucleon data with a particularly assumed shape of q^2 dependence. This estimate gives a rather small branching ratio, which nevertheless can be tested experimentally. CLEO-c studied this final state (Athar *et al.*, 2008).

As (anti)neutrons are hard to reconstruct, CLEO-c used a missing mass technique to identify this signal. All particles in the event, except for the (anti)neutron, are reconstructed and the signal is extracted by looking in the missing mass distribution of the events, which for signal will peak at the neutron mass.

CLEO-c used 325 pb^{-1} of e^+e^- annihilation data collected at a center-of-mass energy of 4170 MeV. CLEO-c used eight tag modes ($K^+K^-\pi^-$, $K_S^0K^-$, $\eta\pi^-$, $\eta'\pi^-$, $\phi\rho^-$, $\pi^-\pi^+\pi^-$, $K^{*-}K^{*0}$, and $\eta\rho^-$) to first reconstruct a D_s^- candidate. It is required that this D_s candidate has a reconstructed invariant mass which is within 2.5σ of the known D_s mass. Next, this candidate is combined with a photon. The recoil mass squared against the $D_s^-\gamma$ is calculated and required to be consistent with the mass of the D_s. Note that it does not matter if the photon came from the D_s^* that is the parent of the D_s^- or from the parent of the other D_s in the event. This missing mass squared distribution is fit to determine the number of tags; CLEO-c reported finding 16 995 D_s tags. This yield will be used as the denominator in the branching fraction calculation.

CLEO-c then searched for the proton candidate in the momentum range from 150 to 550 MeV. In this momentum range CLEO-c used dE/dx to identify the proton, where 550 MeV is below Cherenkov threshold. Kinematic fits are performed to the D_s^-, photon, and proton candidates. Applying these kinematic constraints improves the resolution on the missing mass by a factor of 2.

Figure 28 shows the distribution of the recoil mass against the proton. There are 13 candidate events consistent with the $D_s^+ \to p^+\bar{n}$ signal. From this yield, the number of tags, and the efficiency for reconstructing the proton, CLEO-c determined the branching fraction

$$\mathcal{B}(D_s^+ \to p^+\bar{n})_{\rm exp} = (1.30 \pm 0.36^{+0.12}_{-0.16}) \times 10^{-3}. \tag{105}$$

This result shows quite unambiguously that the factorization-ansatz estimate of Eq. (104) fails by more than 3 orders of magnitude. This could be because of the following two reasons. First, the use of a factorization ansatz could be

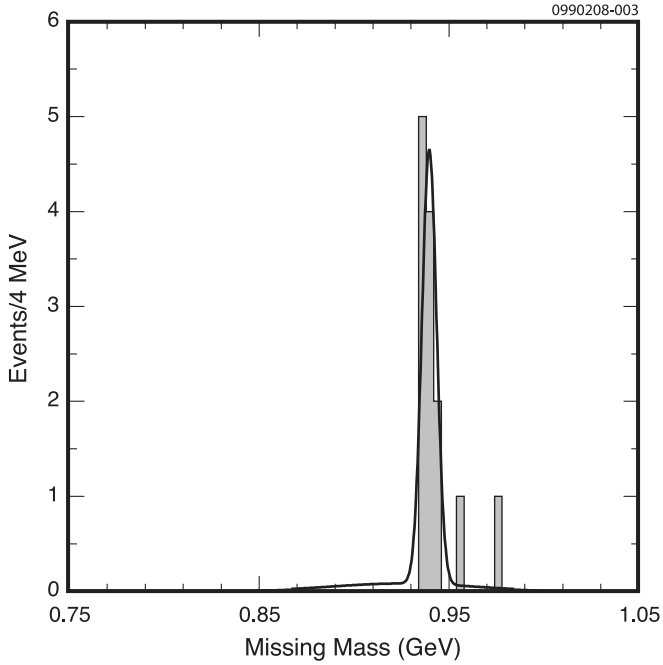

FIG. 28. The missing mass distribution for all $D_s^+ \to p^+\bar{n}$ candidates. CLEO-c saw 13 signal candidates. From Athar *et al.*, 2008.

completely misleading for the description of $D_s^+ \to p^+\bar{n}$. This could be due to the fact that the charm quark is too light for the factorization approach to be reliable. In fact, since the mass of the D_s lies right in the middle of the region populated by highly excited light-quark resonances, it is possible that the presence of nearby states could significantly affect the decay. In addition, the decay happens almost at the threshold for $p\bar{n}$ production, with no large energy release, something that factorization-based approaches usually require. Second, there could be other decay mechanisms that contribute to this transition besides annihilation. For example, inelastic rescattering discussed above could be responsible for the bulk of the result. An example of this mechanism would be a tree-level transition $D_s^+ \to \eta^{(\prime)}\pi^+$ with subsequent rescattering $\eta^{(\prime)}\pi^+ \to p^+\bar{n}$. It was argued (Chen, Cheng, and Hsiao, 2008) that this mechanism can provide a contribution that is consistent with the experimentally measured branching ratio. More work is definitely needed for a complete theoretical understanding of this and related processes.

IX. DALITZ DECAYS OF D MESONS

In this section multibody decays of D mesons are discussed. The most extensive studies of multibody decays are the Dalitz-plot studies performed in three-body decays. An overview is given of the analysis techniques used, and some of the final states that have been investigated are discussed. Last, a few four-body final states have also been investigated and they are discussed here.

A. Three-body Dalitz-plot analyses

Many hadronic three-body final states of D^0, D^+, and D_s^+ meson decays have been studied using a Dalitz-plot analysis in which the resonant substructure was probed. From these analyses we learn about the amplitudes and phases of the different components that contribute to these final states. It is seen that most three-body final states are dominated by pseudo-two-body decays.

There is an enormous number of applications of three-body decays of D mesons. One of the most important applications involves proper determination of branching fractions of quasi-two-body decays, such as $D \to \rho\pi$. Also, the possibility of determination of all relative decay amplitudes and phases in the Dalitz analysis of D^0 decays allows for novel studies of $D^0\bar{D}^0$ mixing and searches of CP violation in the charm system. Finally, Dalitz analyses of D decays offer unique ways to study formation of light-quark structures (such as σ and κ) that are not reachable in direct e^+e^--annihilation experiments.

In a Dalitz-plot analysis the dynamics of a decay is investigated by analyzing the kinematic distributions by plotting the data such that the event density is proportional to the matrix element squared (Dalitz, 1953). For the three-body decay $D \to abc$, where a, b, and c are pseudoscalars, the decay rate can be written (Amsler *et al.*, 2008)

$$d\Gamma = \frac{1}{32(2\pi)^3 M_D^3}|\mathcal{M}|^2 dm_{ab}^2 dm_{bc}^2, \tag{106}$$

where $\mathcal{M}$ is the decay matrix element and $m_{ij}^2 = (p_i + p_j)^2$ is the invariant mass squared of particles i and j. Note that for $\mathcal{M} = \text{const}$, the Dalitz plot in variables (m_{ab}^2, m_{bc}^2) of Eq. (106) represents a homogeneously filled shape. Any apparent structures would then represent interactions of the final-state particles.

1. Formalism for Dalitz-plot fits

In general, the amplitude for the process $D \to Rc$, $R \to ab$, where R is an intermediate resonance and a, b, and c are particles of arbitrary spin, can be written

$$\mathcal{M}_R(L, m_{ab}, m_{bc}) = \sum_\lambda \langle ab|R_\lambda\rangle T_R(m_{ab})\langle cR_\lambda|D\rangle, \tag{107}$$

where L is the spin of resonance R, and the sum is over the helicity states λ of R. It is customary to break the amplitude of Eq. (107) into three parts,

$$\mathcal{M}_R(L, m_{ab}, m_{bc}) = Z(L, \mathbf{p}, \mathbf{q})B_L^D(|\mathbf{p}|)B_L^R(|\mathbf{q}|)T_R(m_{ab}), \tag{108}$$

where Z depends on the spin of resonance R and describes the angular distribution of the decay products. If all final-state particles are spin 0, which is the case for all of the decays described here [see Eq. (106)], it reduces to Legendre's polynomials. The B_L's are the spin-dependent Blatt-Weisskopf penetration functions that incorporate effects due to the finite size of the final-state hadrons, and T_R is a function that describes dynamics of the final-state mesons that incorporate a prescription on how to treat the intermediate resonances R. The momenta $\mathbf{p}$ and $\mathbf{q}$ of c and a, respectively, are defined in the R rest frame, e.g., $|\mathbf{q}| = \sqrt{[m_R^2 - (m_a + m_b)^2][m_R^2 - (m_a - m_b)^2]}/2m_R$. The main difference between various analyses of Dalitz plots is related to the chosen model for T_R.

The most common description of Dalitz plots in three-body decays is the so-called isobar model. In this model amplitudes are added coherently for each resonance. A nonresonant contribution, which describes a direct decay of the D into a three-body final state, is usually added as a coherent contribution uniformly distributed across the Dalitz plot, making the total amplitude

$$\mathcal{M} = \mathcal{M}_{NR} + \sum_R \mathcal{M}_R(L, m_{ab}, m_{bc}). \tag{109}$$

In the isobar model each resonance is described by a Breit-Wigner line shape,

$$T_R(m_{ab}) = [m_R^2 - m_{ab}^2 - im_R\Gamma_{ab}(q)]^{-1}. \tag{110}$$

Here $\Gamma_{ab}(q)$ describes a momentum-dependent width of the resonance R, which generalizes the narrow-width approximation,

$$\Gamma_{ab}(q) = \Gamma_R\left(\frac{q}{q_0}\right)^{2L+1}\left(\frac{m_0}{m_{ab}}\right)B_L'(q, q_0)^2. \tag{111}$$

Resonant fractions, or fit fractions, are defined, for each resonance R, as

$$f_R = \frac{\int |\mathcal{M}_R|^2}{\int |\mathcal{M}_{NR} + \sum_R \mathcal{M}_R|^2}, \quad (112)$$

where the integration above is over the whole Dalitz plot. The sum of fractions, so defined, is not required to be unity. One must remember that the isobar model is breaking unitarity partly due to the result of interference terms, missing from the denominator, and partly due to kinematic limits imposed on the integrals (Edera, 2004).

The K-matrix model is used when a proper description of a Dalitz plot dominated by broad scalar resonances is needed. The K-matrix formalism is, by construction, unitary. It follows from a specific parametrization of the scattering matrix,

$$S_{if} = \delta_{if} + 2iT_{if} = \delta_{if} + 2i\{\rho_i\}^{1/2}\hat{T}_{if}\{\rho_f\}^{1/2}, \quad (113)$$

where $\hat{T}_{if}$ is a Lorentz-invariant scattering amplitude and $\rho_i = 2q_i/m_i$ are the diagonal elements of the (diagonal) phase-space matrix. Here $q_i = m_i\sqrt{1-4m_i^2/s}$ is the breakup momentum for decay channel i.

The K matrix represents a particular parametrization of $\hat{T}$,

$$\hat{T} = (\hat{I} - i\hat{K}\,\hat{\rho})^{-1}\hat{K}. \quad (114)$$

The final-state resonances appear in the K matrix as a sum of poles. A particular parametrization of the K matrix can be chosen, which incorporates data from scattering experiments. One useful parametrization of the K matrix can be found in Anisovich and Sarantsev (2003). A good description of the K-matrix formalism can be found in Chung *et al.* (1995). See also D. Asner's review in Amsler *et al.* (2008).

In addition to the isobar model and the K-matrix models presented above, several experiments used the model-independent partial wave analysis (MIPWA). This approach was first used by the E791 Collaboration (Aitala *et al.*, 2006). Instead of trying to describe the S wave as a sum of broad Breit-Wigner resonances, which often leads to unitarity violation when they overlap, or using the K-matrix parametrization, this method parametrizes the amplitude and phase by dividing the $\pi^+\pi^-$ mass spectrum into discrete slices. The amplitude and phase are interpolated using a relaxed cubic spline (Kölbig and Lipps, 1990).

2. Experimental considerations

When analyzing data using a Dalitz-plot analysis there are several experimental effects to consider. The reconstruction efficiency for the D candidates is not uniform across the Dalitz plot. The momentum spectrum of the observed particles will depend on the position in the Dalitz plot and affect the efficiency for finding and reconstructing the particles. The effect of efficiency variations across the Dalitz plot is typically incorporated using a Monte Carlo simulation and parametrization of the efficiency as a function of the Dalitz-plot variables.

The finite detector resolution is usually neglected as the resonances studied are mostly broad compared to the detector resolution. There are a few exceptions such as $\phi \to K^+K^-$ and $\omega \to \pi^+\pi^-$. In these cases the resolution function has to be convolved with the truth level probability distribution. A related effect is resolution effects near the phase-space boundary in the Dalitz plot. To avoid smearing near the phase-space boundary the final-state particles momenta can be recalculated using a constraint to the D mass. This forces the phase-space boundary to be strictly respected.

Experimentally we also have to consider backgrounds that pass the event selection criteria. The backgrounds can be classified into different categories. Combinatorial backgrounds where the selected particles do not all come from the decay of a D. This background may contain resonances, such as a K^* or ρ. We also have backgrounds where all candidates come from a D decay but are not signal. These backgrounds include final states with identical particles, e.g.,

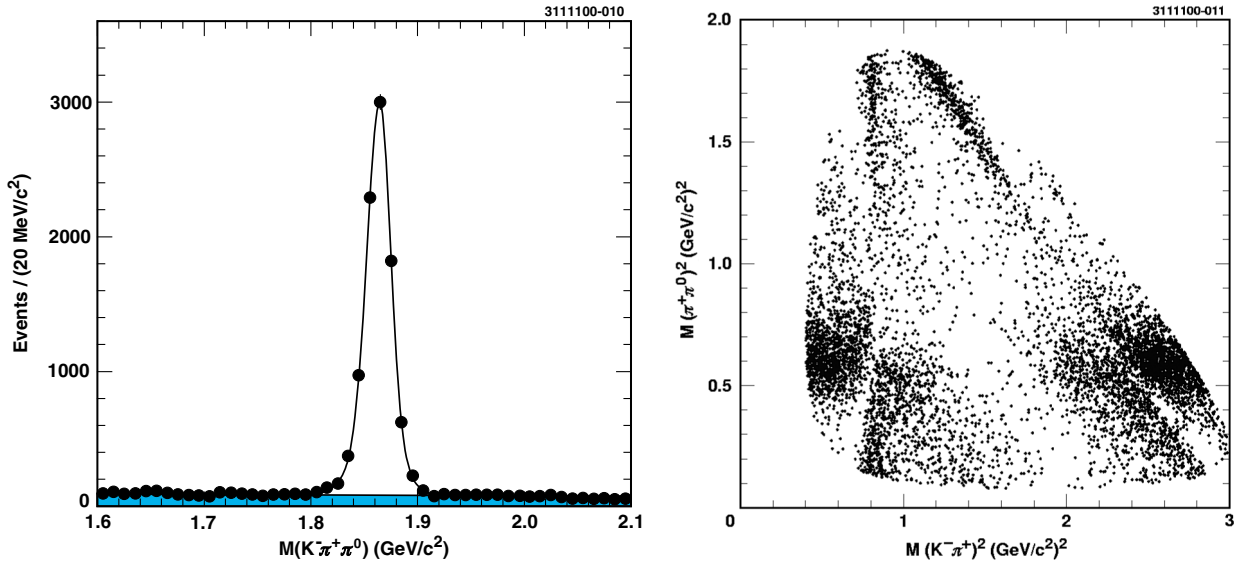

FIG. 29 (color online). The left plot shows the $D^0 \to K^-\pi^+\pi^0$ reconstructed mass distribution. The right plot shows the $M^2(\pi^+\pi^0)$ vs $M^2(K^-\pi^+)$ Dalitz plot for the 7070 $D^0 \to K^-\pi^+\pi^0$ candidates. From Kopp *et al.*, 2001.

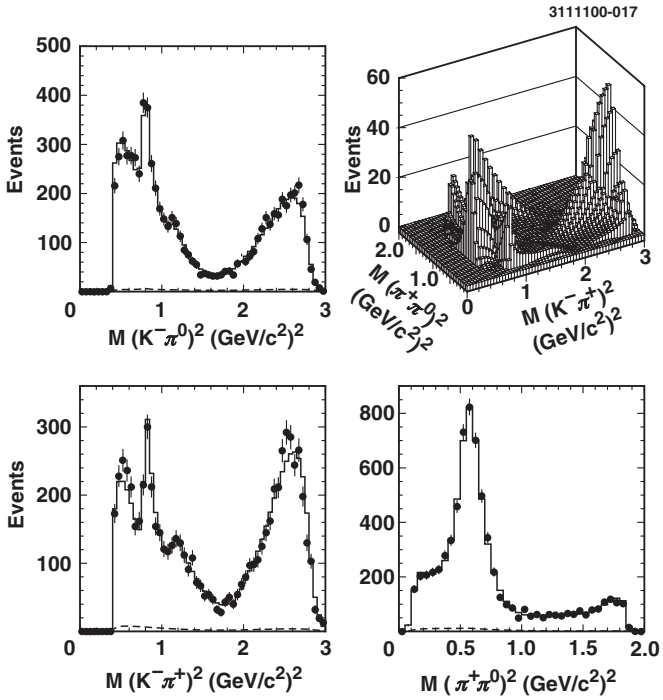

FIG. 30. The $D^0 \to K^-\pi^+\pi^0$ Dalitz fit. From Kopp *et al.*, 2001.

$D^0 \to K^0_S\pi^0$ contributing to $D^0 \to \pi^+\pi^-\pi^0$ or a $\bar{D}^0$ decay incorrectly identified as a D^0, or misidentified particles such as $D^+ \to \pi^-\pi^+\pi^+$ reconstructed as $D^+ \to K^-\pi^+\pi^+$.

In the following sections different Dalitz-plot analyses will be discussed. As in general it is impossible to average the results of different analyses, the most recent, or precise, results are discussed in more detail for each mode.

3. $D^0 \to K^-\pi^+\pi^0$

The decay $D^0 \to K^-\pi^+\pi^0$ was studied by the tagged photon spectrometer at Fermilab (Summers *et al.*, 1984), MARK-III (Adler *et al.*, 1987), E691 (Anjos *et al.*, 1993) E687 (Frabetti *et al.*, 1994b), and CLEO II (Kopp *et al.*, 2001). The first of these analyses was a simplified Dalitz analysis that did not include the interference. The data were fit to an incoherent sum of $K^-\rho^+$, $\bar{K}^{*0}\pi^0$, $K^{*-}\pi^+$, and nonresonant decays. The latest analysis by CLEO II has about a factor of 10 higher statistics than any of the earlier measurements.

The analysis by CLEO II used 4.7 fb^{-1} of e^+e^- collision data collected at $\sqrt{s} = 10.6$ GeV. The D^0 candidate is required to come from a $D^{*+} \to D^0\pi^+$ decay. The D^0 candidate is required to form a D^{*+} candidate which satisfies $144.9 < M(D^{*+}) - M(D^0) < 145.9$ MeV. The invariant mass distribution of the $K^-\pi^+\pi^0$ candidates and the 7070 event selected for the Dalitz-plot analysis are shown in Fig. 29. This sample has a purity of $(96.7 \pm 1.1)\%$. The large K^{*0}, ρ^+, and K^{*-} resonances and their interference is easily seen in the Dalitz plot and in the projections of the Dalitz-plot fit in Fig. 30. The results of the Dalitz-plot fit are summarized in Table XXVII. The $\rho(770)^+$ resonance dominates the Dalitz plot with a fit fraction of 78.8%.

4. $D^0 \to K^0_S\pi^+\pi^-$

The decay $D^0 \to K^0_S\pi^+\pi^-$ is of interest for the extraction of the CKM angle γ in the decays $B^\mp \to D^{(*)}K^\mp$ and $B^\mp \to \bar{D}^{(*)}K^\mp$ (Atwood, Dunietz, and Soni, 2001). When the decay of the D^0 or $\bar{D}^0$ in these decays is to a common final state, such as $K^0_S\pi^+\pi^-$, the two decays above interfere and this allows us to measure the CKM angle γ. To extract γ from this analysis a good understanding of the $D^0 \to K^0_S\pi^+\pi^-$ Dalitz plot is required.

This final state was investigated by many experiments. The first studies were performed by Adler *et al.* (1987), Frabetti *et al.* (1992, 1994b, Albrecht *et al.* (1993), and Anjos *et al.* (1993). CLEO was the first experiment to include doubly Cabibbo-suppressed decays in the Dalitz-plot analysis (Muramatsu *et al.*, 2002) of this decay. They used 10 resonances in their fit: $K^0_S\rho^0$, $K^0_S\omega$, $K^0_Sf_0(980)$, $K^0_Sf_2(1270)$, $K^0_Sf_0(1370)$, $K^*(892)^-\pi^+$, $K^*_0(1430)^-\pi^+$, $K^*_2(1430)^-\pi^+$, $K^*(1680)^-\pi^+$, and the Cabibbo-suppressed mode $K^*(892)^+\pi^-$. CLEO found a small fit fraction for the nonresonant contribution of $(0.9 \pm 0.4^{+1.0+1.7}_{-0.3-0.2})\%$. They also determined that the phase difference between the Cabibbo-allowed $K^*(892)^-\pi^+$ and the doubly Cabibbo-suppressed decay $K^*(892)^+\pi^-$ is consistent with 180° as expected from the Cabibbo factors. The significance of the $K^*(892)^+\pi^-$ resonance is 5.5 standard deviations in the study by CLEO.

Both *BABAR* (Aubert *et al.*, 2005b, 2008a) and Belle (Poluektov *et al.*, 2006; Abe *et al.*, 2008) studied this decay with samples well over an order of magnitude larger than CLEO in their program to determine the CKM angle γ. *BABAR* (Aubert *et al.*, 2008a) used a data sample of 351 fb^{-1} collected at the $\Upsilon(4S)$ to study the $D^0 \to K^0_S\pi^+\pi^-$ Dalitz plot. They reconstructed 487 000 $D^{*+} \to D^0\pi^+$, $D^0 \to K^0_S\pi^+\pi^-$ decays with a purity of 97.7%. The Dalitz plot is fit to a sum of eight different P and D wave

TABLE XXVII. Dalitz-plot parameters from CLEO II analysis of $D^0 \to K^-\pi^+\pi^0$,. The errors shown are statistical, experimental systematic, and modeling systematic, respectively. From Kopp *et al.* (2001).

Mode	Fit fraction	Phase (deg)
$\rho(770)^+K^-$	$0.788 \pm 0.019 \pm 0.013 \pm 0.046$	0.0 (fixed)
$K^*(892)^-\pi^+$	$0.161 \pm 0.007 \pm 0.007^{+0.026}_{-0.008}$	$163 \pm 2.3 \pm 3.1 \pm 4.3$
$\bar{K}^*(892)^0\pi^0$	$0.127 \pm 0.009 \pm 0.005 \pm 0.015$	$-0.2 \pm 3.3 \pm 2.2 \pm 7.0$
$\rho(1700)^+K^-$	$0.057 \pm 0.008 \pm 0.007 \pm 0.006$	$171 \pm 6 \pm 5^{+6.1}_{-55}$
$\bar{K}^*_0(1430)^0\pi^0$	$0.041 \pm 0.006 \pm 0.007^{+0.031}_{-0.005}$	$166 \pm 5 \pm 4.6 \pm 12$
$K^*_0(1430)^-\pi^+$	$0.033 \pm 0.006 \pm 0.007 \pm 0.012$	$55.5 \pm 5.8 \pm 3.3^{+4.2}_{-13}$
$K^*(1680)^-\pi^+$	$0.013 \pm 0.003 \pm 0.003 \pm 0.003$	$103 \pm 8 \pm 7 \pm 14$
Nonresonant	$0.075 \pm 0.009 \pm 0.006^{+0.056}_{-0.009}$	$31 \pm 4 \pm 5.5^{+14}_{-3.7}$

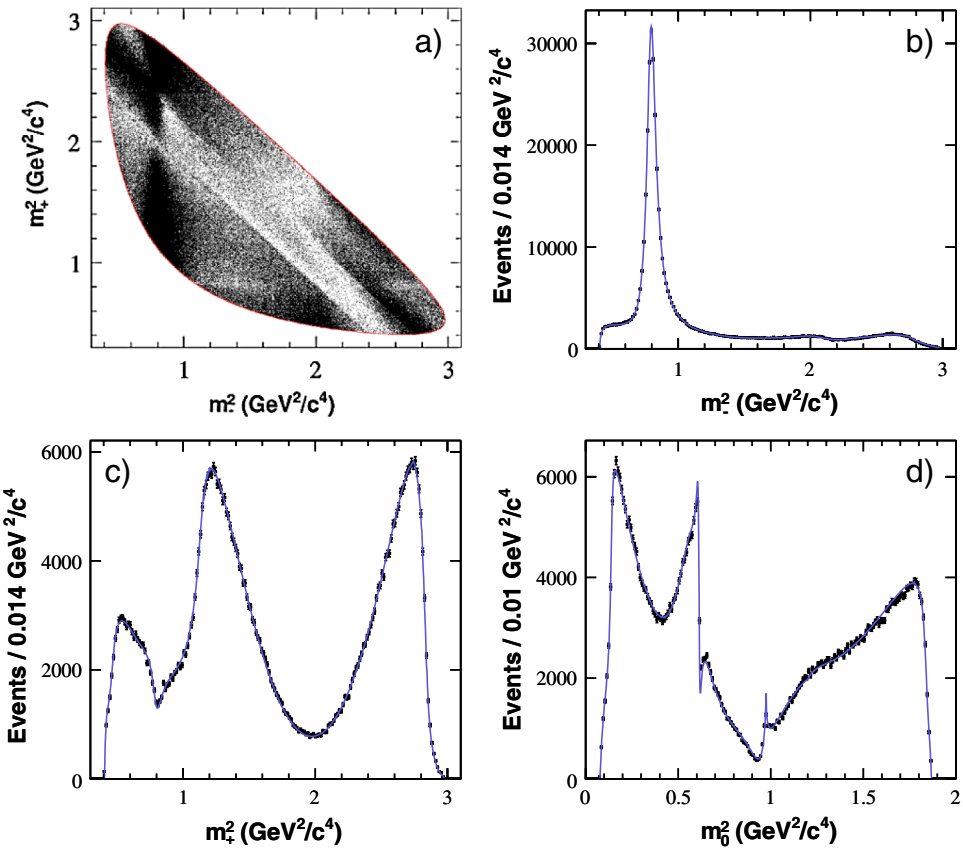

FIG. 31 (color online). *BABAR* $D^0 \to K^0_S\pi^+\pi^-$ Dalitz-plot analysis. From Aubert *et al.*, 2008a.

resonances. They used three Cabibbo-favored resonances $K^*(892)^-$, $K^*(1680)^-$, and $K_2^*(1430)^-$; two doubly Cabibbo-suppressed resonances $K^*(892)^+$ and $K_2^*(1430)^+$; and three CP eigenstates $\rho(770)^0$, $\omega(782)$, and $f_2(1270)$. The K-matrix formalism with the P-vector approximation is used to describe the contribution to the amplitude from the $\pi^+\pi^-$ S wave. The $K\pi$ S wave includes the $K_0^*(1430)^-$ and $K_0^*(1430)^+$ resonances and a nonresonant component. The data and the fit projections are shown in Fig. 31. The result of the fit is shown in Table XXVIII.

Belle (Poluektov *et al.*, 2006) used a 357 fb^{-1} sample collected at the $\Upsilon(4S)$ to study the $D^0 \to K^0_S\pi^+\pi^-$ Dalitz plot. They selected a sample of 271 621 events for their analysis with an estimated purity of 96.8%. They fit their data to a sum of 15 resonances plus a nonresonant amplitude. The data and projections of their fit are shown in Fig. 32. The result of their fit is summarized in Table XXIX. For the two σ resonances that are included in the fit Belle obtained $M_{\sigma_1} = 519 \pm 6$ MeV, $\Gamma_{\sigma_1} = 454 \pm 12$ MeV, $M_{\sigma_2} = 1050 \pm 6$ MeV, and $\Gamma_{\sigma_2} = 101 \pm 7$ MeV. The wide σ_1 resonance is highly correlated with the nonresonant component. Belle also reported a preliminary study (Abe *et al.*, 2008) using 605 fb^{-1} of data to study this Dalitz plot.

At this point the uncertainties in γ are limited by statistics. Contributions to the uncertainty on γ from these measurements are not limited by the Dalitz-plot uncertainty. But with

TABLE XXVIII. Dalitz-plot parameters from the *BABAR* analysis (Aubert *et al.*, 2008a) of $D^0 \to K^0_S\pi^+\pi^-$. The errors for the amplitudes and phases include only the statistical errors. The fit fractions quoted also include the systematic uncertainties. Upper limits on fit fractions are quoted at 95% confidence level.

Resonance	Amplitude	Phase (deg)	Fit fraction
$K^*(892)^-$	1.740 ± 0.010	139.0 ± 0.3	55.7 ± 2.8
$K_0^*(1430)^-$	8.2 ± 0.7	153 ± 8	10.2 ± 1.5
$K_2^*(1430)^-$	1.410 ± 0.022	138.4 ± 1.0	2.2 ± 1.6
$K^*(1680)^-$	1.46 ± 0.10	-174 ± 4	0.7 ± 1.9
$K^*(892)^+$	0.158 ± 0.003	-42.7 ± 1.2	0.46 ± 0.23
$K_0^*(1430)^+$	0.32 ± 0.06	143 ± 11	<0.05
$K_2^*(1430)^+$	0.091 ± 0.016	85 ± 11	<0.12
$\rho(770)^0$	1 (fixed)	0 (fixed)	21.0 ± 1.6
$\omega(782)$	0.0527 ± 0.0007	126.5 ± 0.9	0.9 ± 1.0
$f_2(1270)$	0.606 ± 0.026	157.4 ± 2.2	0.6 ± 0.7
$\pi\pi$ S wave			11.9 ± 2.6

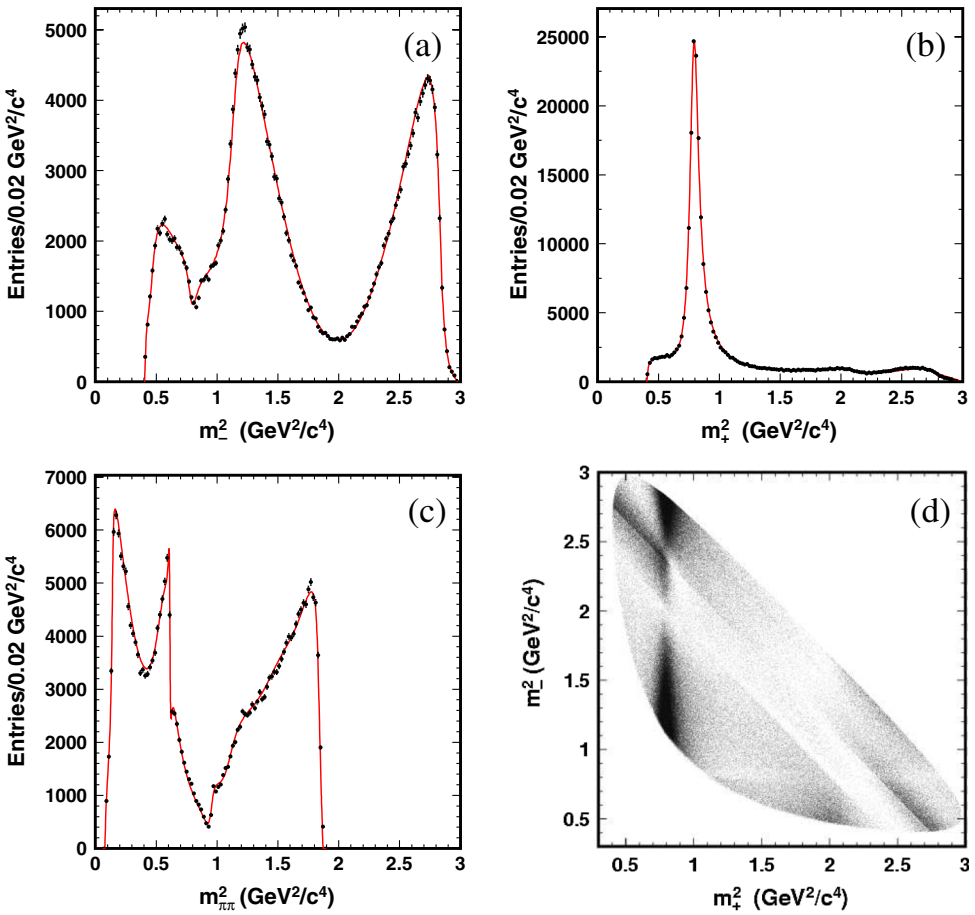

FIG. 32 (color online). Belle $D^0 \to K^0_S\pi^+\pi^-$ Dalitz-plot analysis. (a) $m^2(K^0_S\pi^+)$, (b) $m^2(K^0_S\pi^-)$, and (c) $m^2(\pi^-\pi^+)$ distributions, and (d) Dalitz-plot distribution. The points with error bars show the data and the smooth curve is the result of the fit. From Poluektov *et al.*, 2006.

TABLE XXIX. Dalitz-plot parameters from Belle analysis of $\bar{D}^0 \to K^0_S\pi^+\pi^-$, from Poluektov *et al.* (2006). Errors are statistical only.

Resonance	Amplitude	Phase (deg)	Fit fraction (%)
$K^0_S\sigma_1$	1.43 ± 0.07	212 ± 3	9.8
$K^0_S\rho^0$	1 (fixed)	0 (fixed)	21.6
$K^0_S\omega$	$(31.4 \pm 0.8) \times 10^{-3}$	110.8 ± 1.6	0.4
$K^0_S f_0(980)$	0.365 ± 0.006	201.9 ± 1.9	4.9
$K^0_S\sigma_2$	0.23 ± 0.02	237 ± 11	0.6
$K^0_S f_2(1270)$	1.32 ± 0.04	348 ± 2	1.5
$K^0_S f_0(1370)$	1.44 ± 0.10	82 ± 6	1.1
$K^0_S\rho(1370)^0$	0.66 ± 0.07	9 ± 8	0.4
$K^*(892)^+\pi^-$	1.644 ± 0.010	132.1 ± 0.5	61.2
$K^*(892)^-\pi^+$	0.144 ± 0.004	320.3 ± 1.5	0.55
$K^*(1410)^+\pi^-$	0.61 ± 0.06	113 ± 4	0.05
$K^*(1410)^-\pi^+$	0.45 ± 0.04	254 ± 5	0.14
$K^*_0(1430)^+\pi^-$	2.15 ± 0.04	353.6 ± 1.2	7.4
$K^*_0(1430)^-\pi^+$	0.47 ± 0.04	88 ± 4	0.43
$K^*_2(1430)^+\pi^-$	0.88 ± 0.03	318.7 ± 1.9	2.2
$K^*_2(1430)^-\pi^+$	0.25 ± 0.02	265 ± 6	0.09
$K^*(1680)^+\pi^-$	1.39 ± 0.27	103 ± 12	0.36
$K^*(1680)^-\pi^+$	1.2 ± 0.2	118 ± 11	0.11
Nonresonant	3.0 ± 0.3	164 ± 5	9.7

increased statistics the γ measurement should improve and a better understanding of the Dalitz plot is required. CLEO-c (Briere *et al.*, 2009) performed a CP- and flavor-tagged Dalitz-plot analysis using 818 pb^{-1} of data collected at the $\psi(3770)$ resonance. In this analysis the final states $K^0_S\pi^+\pi^-$ and $K^0_L\pi^+\pi^-$ are studied in decays where they recoil against a flavor-tagged, CP-tagged, or $K^0_S\pi^+\pi^-$ decay of the other D meson in the $\psi(3770)$ decay. The Dalitz plot is binned into eight regions and fit for the average interference between the D^0 and $\bar{D}^0$ in the bin. This allows the extraction of the relative strong phase between $D^0 \to K^0_s\pi^+\pi^-$ and $\bar{D}^0 \to K^0_s\pi^+\pi^-$, which is required for the extraction of the CKM angle γ. The CLEO-c measurement reduced the systematic uncertainty from the strong phase difference on the determination of γ to about 1.7°.

5. $D^0 \to \pi^-\pi^+\pi^0$

The Dalitz plot of $D^0 \to \pi^-\pi^+\pi^0$ was studied by *BABAR* as a means to extract information about the CKM parameter γ (Aubert *et al.*, 2007c) similar to what was done with $D^0 \to K^0_S\pi^+\pi^-$. CLEO also studied this decay (Muramatsu *et al.*, 2002). *BABAR* reconstructed 44 780 ± 250 signal events over a background of 830 ± 70 events. The Dalitz plot of these events is shown in Fig. 33. The three ρ bands are clearly

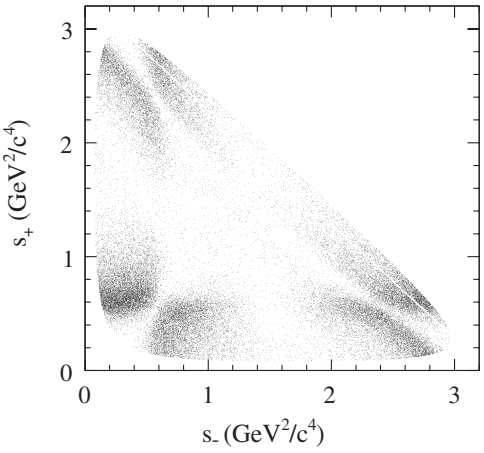

FIG. 33. *BABAR* Dalitz plot of $s_+ = m^2_{\pi^+\pi^0}$ vs $s_- = m^2_{\pi^-\pi^0}$ for the $D^0 \to \pi^+\pi^-\pi^0$ decay. From Aubert *et al.*, 2007c.

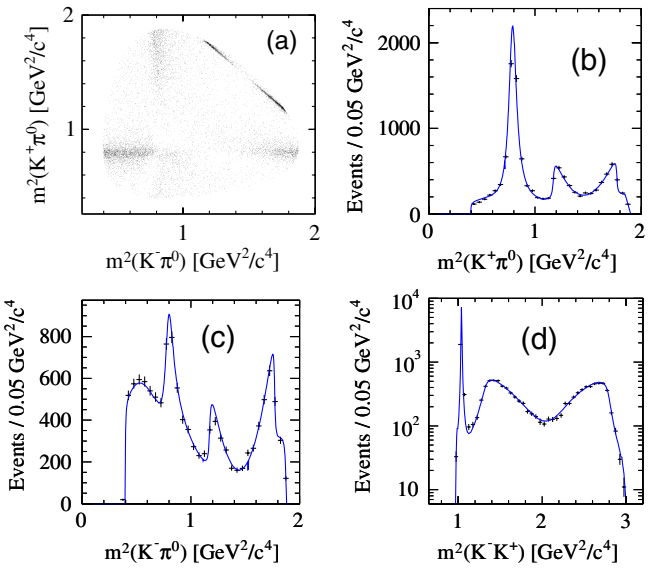

FIG. 34 (color online). *BABAR* $D^0 \to K^+K^-\pi^0$ Dalitz-plot analysis. From Aubert *et al.*, 2007a.

visible with a strong destructive interference. *BABAR* used 15 resonances plus a nonresonant contribution to fit the data. The results of the fit are summarized in Table XXX. The $\rho(770)$ resonances are clearly the strongest features on the Dalitz plot, with fit fractions adding to $(128.6 \pm 1.6)\%$. The $\rho(1700)$ resonances contribute with fit fractions of 3% to 5% each, much smaller than the dominant contributions. The remaining amplitudes, including nonresonant, are much smaller. The large, destructively interfering, $\rho\pi$ amplitudes are suggestive of an $I = 0$ dominated final state (Zemach, 1965). This is consistent with the observation that $D^0 \to 3\pi^0$ is strongly suppressed.

6. $D^0 \to K^+K^-\pi^0$

CLEO (Besson *et al.*, 2006) and *BABAR* (Aubert *et al.*, 2007a) both studied the Dalitz plot of this decay. The *BABAR* analysis used 358 fb^{-1} of e^+e^- collision data collected near the $\Upsilon(4S)$ resonance. A sample with a high purity of about 98.1% was selected for this study containing $11\,278 \pm 110$ $D^{*+} \to D^0\pi^+$ tagged candidates. The Dalitz plot and the best isobar fit is shown in Fig. 34. The isobar model allows for several different solutions that each give a similarly good description of the data. At low K^+K^- invariant mass an S-wave K^+K^- contribution is needed, but the fit cannot distinguish between an $a_0(980)$ and a $f_0(980)$. Similarly, at intermediate K^+K^- invariant mass either a $f_2'(1525)$ or an f_0 with a similar mass works. In the study of this Dalitz plot the relative amplitude and phase of the amplitudes for $D^0 \to K^{*-}K^+$ to $D^0 \to K^{*+}K^-$ can be measured. Defining r_D and δ_D by

$$r_D e^{i\delta_D} \equiv \frac{a_{D^0\to K^{*-}K^+}}{a_{D^0\to K^{*+}K^-}}, \tag{115}$$

BABAR obtained

$$r_D = 0.599 \pm 0.013(\text{stat}) \pm 0.011(\text{syst}) \tag{116}$$

and

$$\delta_D = -35.5^\circ \pm 1.9^\circ(\text{stat}) \pm 2.2^\circ(\text{syst}), \tag{117}$$

consistent with the earlier CLEO results.

TABLE XXX. Dalitz-plot parameters from *BABAR* analysis of $D^0 \to \pi^-\pi^+\pi^0$. From Aubert *et al.* (2007c).

Resonance	Amplitude ratio (%)	Phase (deg)	Fit fraction
$\rho(770)^+$	100 (fixed)	0 (fixed)	$67.8 \pm 0.0 \pm 0.6$
$\rho(770)^0$	$58.8 \pm 0.6 \pm 0.2$	$16.2 \pm 0.6 \pm 0.4$	$26.2 \pm 0.5 \pm 1.1$
$\rho(770)^-$	$71.4 \pm 0.8 \pm 0.3$	$-2.0 \pm 0.6 \pm 0.6$	$34.6 \pm 0.8 \pm 0.3$
$\rho(1450)^+$	$21 \pm 6 \pm 13$	$-146 \pm 18 \pm 24$	$0.11 \pm 0.07 \pm 0.12$
$\rho(1450)^0$	$33 \pm 6 \pm 4$	$10 \pm 8 \pm 12$	$0.30 \pm 0.11 \pm 0.07$
$\rho(1450)^-$	$82 \pm 5 \pm 4$	$16 \pm 3 \pm 3$	$1.79 \pm 0.22 \pm 0.12$
$\rho(1700)^+$	$225 \pm 18 \pm 14$	$-17 \pm 2 \pm 3$	$4.1 \pm 0.7 \pm 0.7$
$\rho(1700)^0$	$251 \pm 15 \pm 13$	$-17 \pm 2 \pm 2$	$5.0 \pm 0.6 \pm 1.0$
$\rho(1700)^-$	$100 \pm 11 \pm 7$	$-50 \pm 3 \pm 3$	$3.2 \pm 0.4 \pm 0.6$
$f_0(980)$	$1.50 \pm 0.12 \pm 0.17$	$-59 \pm 5 \pm 4$	$0.25 \pm 0.04 \pm 0.04$
$f_0(1370)$	$6.3 \pm 0.9 \pm 0.9$	$156 \pm 9 \pm 6$	$0.37 \pm 0.11 \pm 0.09$
$f_0(1500)$	$5.8 \pm 0.6 \pm 0.6$	$12 \pm 9 \pm 5$	$0.39 \pm 0.08 \pm 0.07$
$f_0(1710)$	$11.2 \pm 1.4 \pm 1.7$	$51 \pm 8 \pm 7$	$0.31 \pm 0.07 \pm 0.08$
$f_2(1270)$	$104 \pm 3 \pm 21$	$-171 \pm 3 \pm 4$	$1.32 \pm 0.08 \pm 0.10$
$\sigma(400)$	$6.9 \pm 0.6 \pm 1.2$	$8 \pm 4 \pm 8$	$0.82 \pm 0.10 \pm 0.10$
Nonresonant	$57 \pm 7 \pm 8$	$-11 \pm 4 \pm 2$	$0.84 \pm 0.21 \pm 0.12$

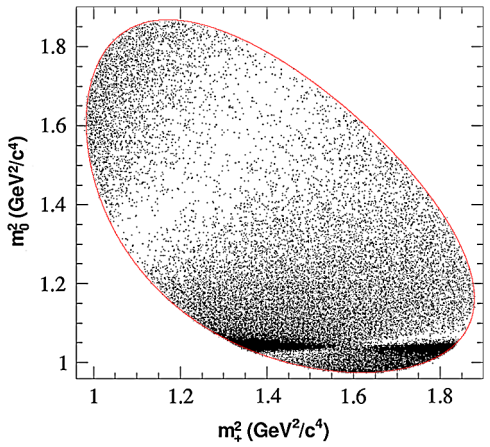

FIG. 35 (color online). Dalitz-plot distribution from the *BABAR* analysis of $D^0 \to K^+K^-K_S^0$. The invariant mass squares plotted are $m_0^2 = m^2(K^+K^-)$ and $m_+^2 = m^2(K^+K_S^0)$ for a D^0 decay and the charge conjugate particles are used for the $\bar{D}^0$ decay. From Aubert *et al.*, 2008a.

7. $D^0 \to K^+K^-K_S^0$

The $D^0 \to K^+K^-K_S^0$ mode was studied by *BABAR* (Aubert *et al.*, 2005a, 2008a) as part of an analysis for γ determination. *BABAR* used a sample of 69 000 reconstructed $D^0 \to K^+K^-K_S^0$ decays with a purity of 99.3%. The data, shown in Fig. 35, were fit to an isobar model which includes eight resonances. The result of this fit is summarized in Table XXXI. In the fit *BABAR* floated the mass and width of the $\phi(1020)$. The $a_0(980)$ resonance has a mass close to KK threshold, decays primarily to $\eta\pi$, and is described by a coupled channel Breit-Wigner line shape. The data are well described by the fit, and *BABAR* found a reduced χ^2 of 1.09 for 6856 degrees of freedom.

8. $D^0 \to K_S^0\eta\pi^0$

The decay $D^0 \to K_S^0\eta\pi^0$ was studied using a 9.0 fb^{-1} data sample collected using the CLEO II.V detector in e^+e^- collisions at the $\Upsilon(4S)$ resonance (Rubin *et al.*, 2004). The sample contained 155 $D^0 \to K_S^0\eta\pi^0$ candidate events. The two large contributions to this decay come from $K^*(892)^0\eta$ and $a_0(980)^0K_S^0$. The projections of the Dalitz-plot fit is shown in Fig. 36. Fixing the amplitude for $a_0(980)^0K_S^0$ to be 1 with a zero phase CLEO measured

TABLE XXXI. Dalitz-plot parameters from *BABAR* analysis of $D^0 \to K^+K^-K_S^0$. Errors are statistical only. From Aubert *et al.* (2008a).

Resonance	Amplitude	Phase (deg)	Fit fraction (%)
$K_S^0a_0(980)^0$	1	0	55.8
$K_S^0\phi(1020)^0$	0.227 ± 0.005	56.2 ± 1.0	44.9
$K_S^0f_0(1370)$	0.04 ± 0.06	2 ± 80	0.1
$K_S^0f_2(1370)$	0.261 ± 0.020	9 ± 6	0.3
$K_S^0a_0(1450)^0$	0.65 ± 0.09	95 ± 10	12.6
$K^-a_0(980)^+$	0.562 ± 0.015	179 ± 3	16.0
$K^-a_0(1450)^+$	0.84 ± 0.04	97 ± 4	21.8
$K^+a_0(1450)^-$	0.118 ± 0.015	138 ± 7	0.7

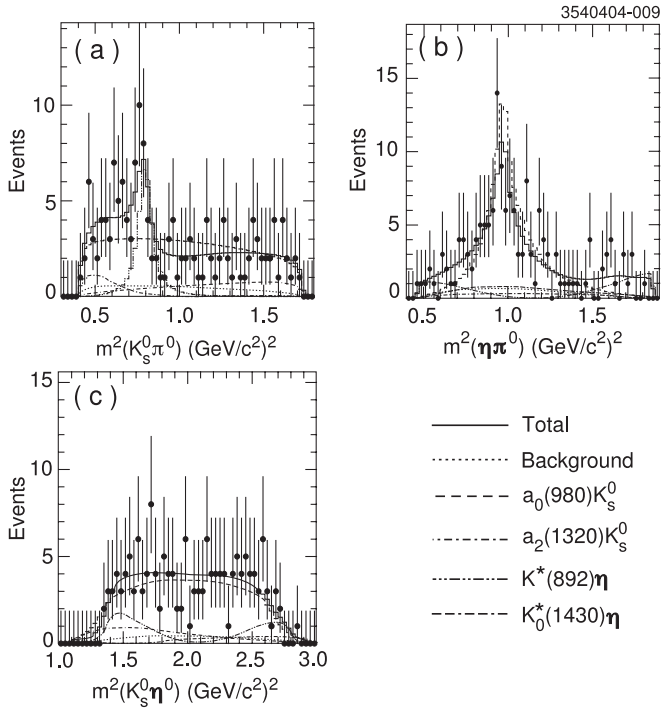

FIG. 36. CLEO $D^0 \to K_S^0\eta\pi^0$ Dalitz-plot analysis. From Rubin *et al.*, 2004.

$$a_{K^*(892)^0\eta} = 0.249 \pm 0.032 \pm 0.013 \pm 0.018, \quad (118)$$

$$\phi_{K^*(892)^0\eta} = (259 \pm 12 \pm 9 \pm 6)^\circ, \quad (119)$$

$$\mathrm{FF}(K^*(892)^0\eta) = 0.293 \pm 0.062 \pm 0.029 \pm 0.019, \quad (120)$$

$$\mathrm{FF}(a_0(980)^0K_S^0) = 1.19 \pm 0.09 \pm 0.20 \pm 0.16, \quad (121)$$

where the errors are statistical, systematic, and model dependent, respectively. For the model dependence CLEO considered alternative models where they added additional resonances. They considered four different alternative fits including a nonresonant component, $K_0^*(1430)\eta$, $K_0^*(1430)\eta + a_2(1320)K_S^0$, and $\kappa\eta$. The probabilities for these different fits were 6.4%, 19.4%, 64.7%, and 49.9%, respectively. The fit with only two resonances had a probability of 0.8%. From these alternative fits CLEO-c derived a fit fraction of $0.246 \pm 0.092 \pm 0.024 \pm 0.087$ for any additional components beyond the $K^*(892)^0\eta$ and $a_0(980)^0K_S^0$.

9. $D^+ \to K^-\pi^+\pi^+$

The decay $D^+ \to K^-\pi^+\pi^+$ is one of the largest decays of the D^+. CLEO-c measured the branching fraction to be $\mathcal{B}(D^+ \to K^-\pi^+\pi^+) = (9.15 \pm 0.10 \pm 0.16 \pm 0.07)\%$. The Dalitz plot for this decay was studied by several experiments, e.g., MARK-III (Adler *et al.*, 1987), NA14 (Alvarez *et al.*, 1991), E691 (Anjos *et al.*, 1993), E687 (Frabetti *et al.*, 1994b), E791 (Aitala *et al.*, 2002, 2006), CLEO-c (Bonvicini *et al.*, 2008b), and most recently by FOCUS (Link *et al.*, 2009). This Dalitz plot is interesting as the only clear resonant contribution from $K^*(892)^0$ only has a 12% fit fraction and a

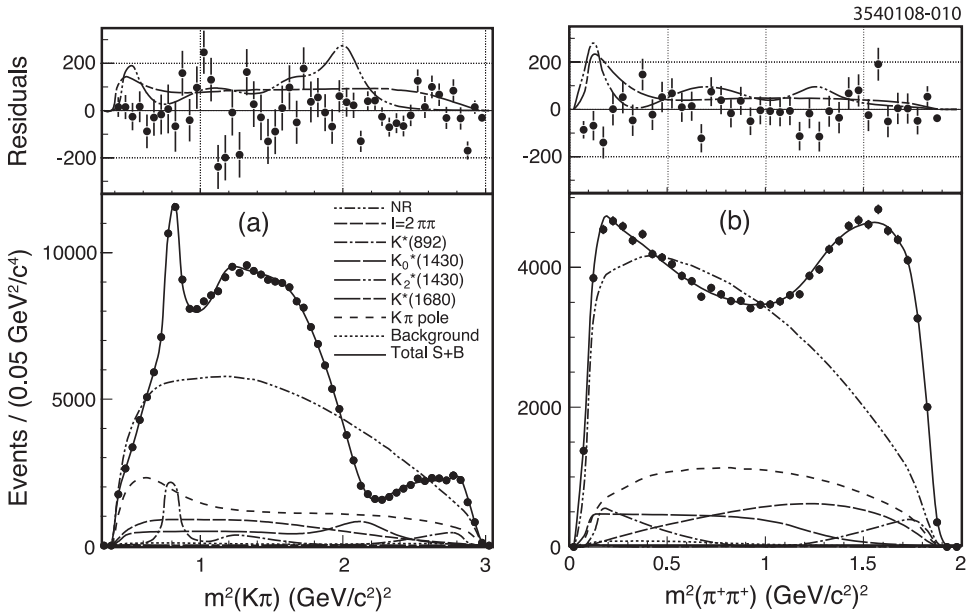

FIG. 37. Projections of the Dalitz-plot fit in the CLEO-c Dalitz-plot analysis of $D^+ \to K^-\pi^+\pi^+$ in (a) for $m^2(K\pi)$ (two entries per candidate), and (b) for $m^2(\pi^+\pi^+)$. The data are shown as points with error bars. The insets on top show the residuals between the data and as points with error bars. The small contributions in the fit from the $K^*(1680)$ and $K_2^*(1430)$ resonances are also shown in the insets enhanced by a factor of 10. From Bonvicini *et al.*, 2008b.

contribution of over 60% from the $K\pi$ S wave. E791 (Aitala *et al.*, 2002) obtained a good fit including a large low-mass $K^-\pi^+$ scalar resonance κ. This fit obtained fit fractions that were significantly different from earlier studies. E791 (Aitala *et al.*, 2006) reanalyzed the data using a model-independent partial wave analysis. The CLEO-c analysis also used the same model-independent partial wave analysis.

The CLEO-c study is based on 572 pb^{-1} of e^+e^- collision data collected at the $\psi(3770)$ resonance. The data sample selected for the Dalitz-plot analysis consists of 140 793 events with a background of about 1.1%. The projections of the Dalitz plot are shown in Fig. 37. The CLEO-c analysis found that in order to get a good description of the data, either in the isobar model or using the model-independent partial wave analysis for the $K\pi$ S wave, they need to include a $I = 2$ $\pi^+\pi^+$ S wave. CLEO-c implemented this $I = 2$ $\pi^+\pi^+$ S wave using either an analytic form or a model-independent partial wave analysis. The model-independent partial wave analysis results agree with the analytic form and both give a good fit. CLEO-c found a fit fraction of about 10% to 15% for the $I = 2$ $\pi^+\pi^+$ S wave. The almost constant $K\pi$ S-wave amplitude from threshold to about 1.4 GeV with a slow phase variation does not show evidence for a κ resonance.

The FOCUS analysis used a sample of 53 595 events with a purity of 98.8% to perform a model-independent partial wave analysis to study the $K\pi$ S wave. The result for the $K\pi$ S wave is consistent with CLEO-c, only small amplitude variations below 1.4 GeV, and a smoothly changing phase.

10. $D^+ \to \pi^+\pi^+\pi^-$

The $D^+ \to \pi^+\pi^+\pi^-$ decay was studied by E687 (Frabetti *et al.*, 1997), E691 (Anjos *et al.*, 1989), E791(Aitala *et al.*, 2001a), FOCUS (Link *et al.*, 2004a), and CLEO-c (Bonvicini *et al.*, 2007). The most recent analysis, with the largest data sample, is the CLEO-c analysis. The earlier analysis by E791 reported the need to add a $\sigma(500)$ Breit-Wigner to the $\pi^+\pi^-$ S wave in order to get an acceptable fit. FOCUS analyzed this mode using a K-matrix description of the $\pi^+\pi^-$ S wave. They obtained an acceptable fit, but did not rule out the need for a $\sigma(500)$. CLEO-c studied these decays with a sample of about 2600 signal events, excluding the K_S^0 events. The nominal fit using the isobar model supports the need for a $\sigma\pi^+$ component. The fit to the isobar model is shown in Fig. 38 and the result from the fit is summarized in Table XXXII.

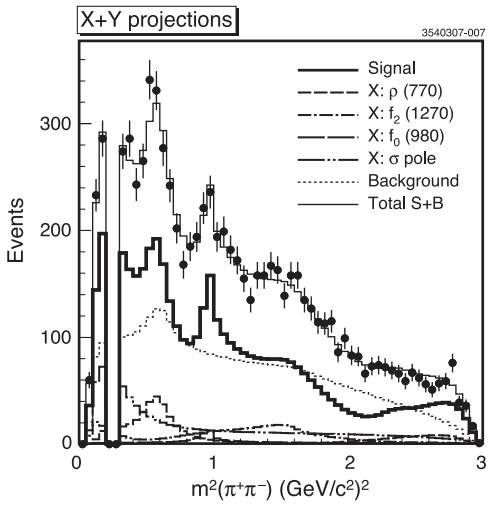

FIG. 38. CLEO-c $D^+ \to \pi^+\pi^-\pi^+$ Dalitz-plot analysis. From Bonvicini *et al.*, 2007.

TABLE XXXII. Dalitz-plot parameters obtained by the CLEO-c analysis of $D^+ \to \pi^+\pi^-\pi^+$. From Bonvicini *et al.* (2007).

Resonance	Amplitude	Phase (deg)	Fit fraction (%)
$\rho(770)^0\pi^+$	1 (fixed)	0 fixed	$20.0 \pm 2.3 \pm 0.9$
$f_0(980)\pi^+$	$1.4 \pm 0.2 \pm 0.2$	$12 \pm 10 \pm 5$	$4.1 \pm 0.9 \pm 0.3$
$f_2(1270)\pi^+$	$2.1 \pm 0.2 \pm 0.1$	$-123 \pm 6 \pm 3$	$18.2 \pm 2.6 \pm 0.7$
$f_0(1370)\pi^+$	$1.3 \pm 0.4 \pm 0.2$	$-21 \pm 15 \pm 14$	$2.6 \pm 1.8 \pm 0.6$
$f_0(1500)\pi^+$	$1.1 \pm 0.3 \pm 0.2$	$-44 \pm 13 \pm 16$	$3.4 \pm 1.0 \pm 0.8$
σ pole	$3.7 \pm 0.3 \pm 0.2$	$-3 \pm 4 \pm 2$	$41.8 \pm 1.4 \pm 2.5$

11. $D^+ \to K^+K^-\pi^+$

The Dalitz plot of the Cabibbo-suppressed decay $D^+ \to K^+K^-\pi^+$ was studied by E687 (Frabetti *et al.*, 1995a) and CLEO-c (Rubin *et al.*, 2008). The CLEO-c analysis used a sample about 20 times larger than E687. For the Dalitz analysis a sample with about 23 000 events was used with a purity of $(84.3 \pm 0.1)\%$.

The best fit (labeled "Fit B" in the CLEO-c paper) is shown in Fig. 39 and the result of the fit is summarized in Table XXXIII. The total fit fraction is $(86.1 \pm 1.1)\%$ and the fit had a $\chi^2/\text{dof} = 895/708$. CLEO-c also reported results from two additional fits with different $K\pi$ S-wave parametrizations. Instead of the $\kappa(800)$ they tried a nonresonant contribution and a parametrization from the LASS experiment (Aston *et al.*, 1988). Both of these fits were of similar quality.

12. $D_s^+ \to K^+K^-\pi^+$

The Dalitz plot for $D_s^+ \to K^+K^-\pi^+$ is of interest as it contains the large $D_s^+ \to \phi\pi^+$ contribution that traditionally was the reference branching fraction for D_s^+ decays. The decay $D_s^+ \to K^+K^-\pi^+$ was studied by E687 (Frabetti *et al.*, 1995a) using a sample of 701 events. This analysis showed evidence for a large $D_s^+ \to f_0(980)\pi^+$ contribution. FOCUS also reported a preliminary study of this Dalitz plot (Malvezzi, 2000). Most recently CLEO-c (Mitchell *et al.*, 2009) reported results from their study of the Dalitz plot in this decay.

The CLEO-c analysis used 586 pb^{-1} of e^+e^- collision data collected at $\sqrt{s} = 4.17$ GeV. In this analysis about 14 400 $D_s^+ \to K^+K^-\pi^+$ candidates are reconstructed with a background of about 15%. The invariant mass distribution for the $K^+K^-\pi^+$ candidates is shown in Fig. 40. The Dalitz plot is shown in Fig. 41. Clearly visible in this plot are the ϕ and K^{*0} resonances.

The data are fit to an isobar model including the $f_0(980)$, ϕ, $f_0(1370)$, $f_0(1710)$, $K^*(892)$, and $K_0^*(1430)$ resonances. CLEO-c found that all resonances studied by E687 are significant, but that in order to obtain a good fit they need to add an additional K^+K^- resonance. Several

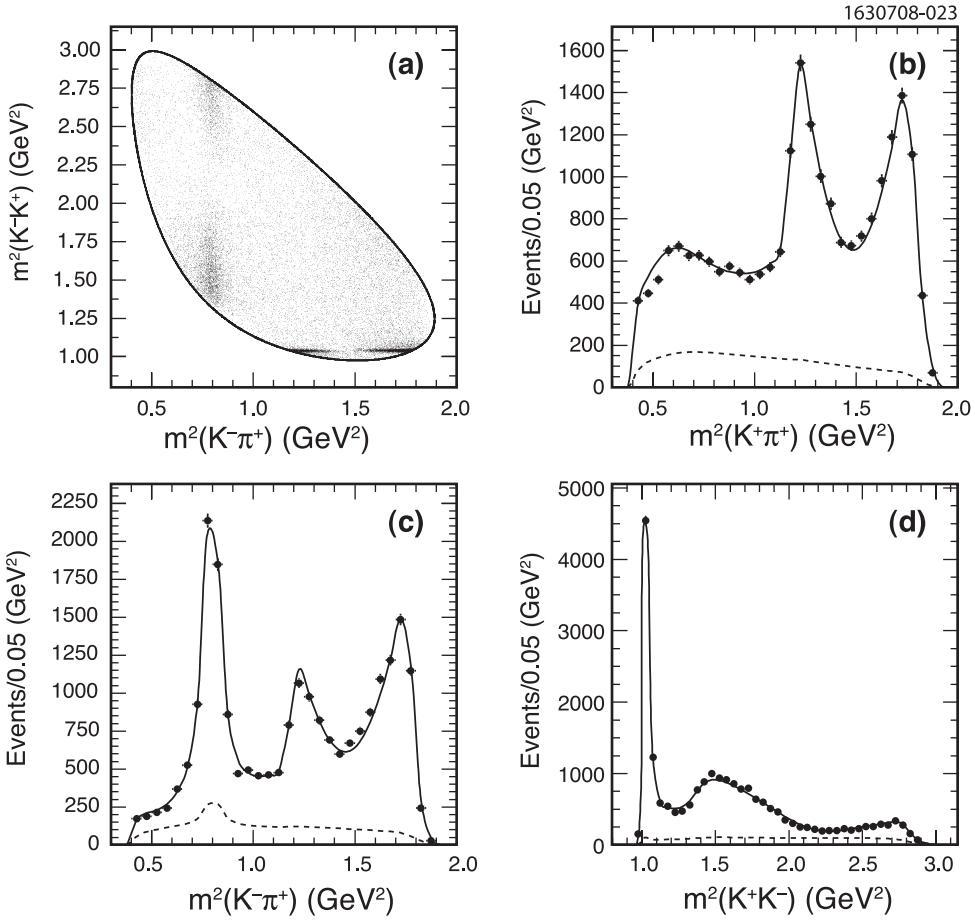

FIG. 39. CLEO-c $D^+ \to K^+K^-\pi^+$ Dalitz-plot analysis. (a) The Dalitz-plot distribution. (b)–(d) The projections of the fit (solid) lines and the data (points). The dashed lines show the background contribution. From Rubin *et al.*, 2008.

TABLE XXXIII. Dalitz-plot parameters from CLEO-c analysis of $D^+ \to K^+K^-\pi^+$; results are from their "fit B." From Rubin *et al.* (2008).

Resonance	Amplitude	Phase (deg)	Fit fraction (%)
$\bar{K}^*(892)^0K^+$	1 (fixed)	0 (fixed)	$25.7 \pm 0.5^{+0.4+0.1}_{-0.3-1.2}$
$\bar{K}_0^*(1430)^0K^+$	$4.56 \pm 0.13^{+0.10+0.42}_{-0.01-0.39}$	$70 \pm 6^{+1+16}_{-6-23}$	$18.8 \pm 1.2^{+0.6+3.2}_{-0.1-3.4}$
$\phi\pi^+$	$1.166 \pm 0.015^{+0.001+0.025}_{-0.009-0.009}$	$-163 \pm 3^{+1+14}_{-1-5}$	$27.8 \pm 0.4^{+0.1+0.2}_{-0.3-0.4}$
$a_0(1450)^0\pi^+$	$1.50 \pm 0.10^{+0.09+0.92}_{-0.06-0.33}$	$116 \pm 2^{+1+7}_{-1-14}$	$4.6 \pm 0.6^{+0.5+7.2}_{-0.3-1.8}$
$\phi(1680)\pi^+$	$1.86 \pm 0.20^{+0.02+0.62}_{-0.08-0.77}$	$-112 \pm 6^{+3+19}_{-4-12}$	$0.51 \pm 0.11^{+0.01+0.37}_{-0.04-0.15}$
$\bar{K}_2^*(1430)^0K^+$	$7.6 \pm 0.8^{+0.5+2.4}_{-0.6-4.8}$	$171 \pm 4^{+0+24}_{-2-11}$	$1.7 \pm 0.4^{+0.3+1.2}_{-0.2-0.7}$
$\kappa(800)\pi^+$	$2.30 \pm 0.13^{+0.01+0.52}_{-0.11-0.29}$	$-87 \pm 6^{+2+15}_{-3-10}$	$7.0 \pm 0.8^{+0.0+3.5}_{-0.6-1.9}$

resonant, or nonresonant, contributions give a similar improvement of the fit quality, though the $f_0(1370)$ gives the best fit and is used in the main result. The result of this fit is shown in Fig. 42. A summary of the amplitudes and phases extracted from this fit is shown in Table XXXIV. CLEO-c obtained a reasonably good fit $\chi^2/\text{dof} = 178/117$, using these resonances. It is interesting to note the large $f_0(980)$ contribution in the same mass regions as the $\phi(1020)$. As the $f_0(980)$ is spin zero and the $\phi(1020)$ is spin one the angular distributions are different for the produced K^+K^- pair for the two resonances.

13. $D_s^+ \to \pi^+\pi^-\pi^+$

The decay $D_s^+ \to \pi^+\pi^-\pi^+$ was studied by E791 (Aitala *et al.*, 2001b), FOCUS (Link *et al.*, 2004a), and *BABAR* (Aubert *et al.*, 2009). The *BABAR* analysis selected 13 179 events with a purity of 80%. The invariant mass distribution of the $D_s^+ \to \pi^+\pi^-\pi^+$ candidates is shown in Fig. 43 and the symmetrized Dalitz-plot distribution is shown in Fig. 44. The symmetrized plot shows two entries in the Dalitz plot for each candidate. The analysis by *BABAR* includes three resonances, $f_2(1270)\pi^+$, $\rho(770)\pi^+$, and $\rho(1450)\pi^+$. In addition to these P- and D-wave resonances the MIPWA is used for the $\pi^+\pi^-$ S wave. This method parametrizes the amplitude and phase by dividing the $\pi^+\pi^-$ mass spectrum into 29 slices. The results for the amplitudes and phases from the fit for the parametrization of the S wave clearly show the $f_0(980)$ resonance. There is also some evidence for the $f_0(1370)$ and $f_0(1500)$. In Table XXXV the summary of the fit is given. The S-wave parametrization accounts for a fit fraction of $(83.0 \pm 0.9 \pm 1.9)\%$. This decay also has an important contribution from a spin-2 resonance, $D_s^+ \to f_2(1270)\pi^+$.

B. Four-body decays

Similar to the three-body decays discussed in the previous section the resonant substructure can be studied in higher multiplicity final states. A four-body final state has a five-dimensional phase space which is hard to visualize.

MARK-III (Adler *et al.*, 1990a) studied the decay $D^0 \to K^-\pi^+\pi^-\pi^+$. They performed an unbinned maximum likelihood fit in the five-dimensional phase space to extract amplitudes for two-body decays. MARK-III selected a sample of 1281 ± 45 $D^0 \to K^-\pi^+\pi^-\pi^+$ candidates. The result of the fit to this samples is summarized in Table XXXVI. The largest two-body decay contributing to this final state is $D^0 \to K^-a_1(1260)^+$ with a fit fraction of $0.492 \pm 0.024 \pm 0.08$.

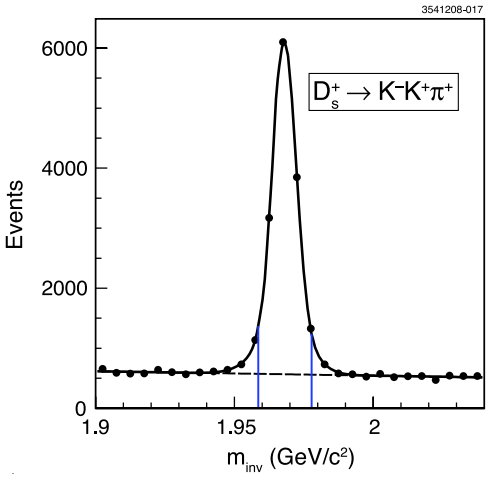

FIG. 40 (color online). The $K^+K^-\pi^+$ invariant mass for the signal candidates in the CLEO-c Dalitz-plot analysis of $D_s^+ \to K^+K^-\pi^+$. From Mitchell *et al.*, 2009.

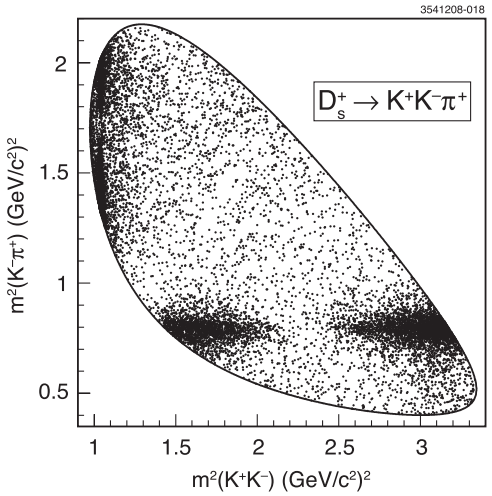

FIG. 41. The Dalitz plot for $D_s^+ \to K^+K^-\pi^+$ candidates in the CLEO-c analysis of $D_s^+ \to K^+K^-\pi^+$. From Mitchell *et al.*, 2009.

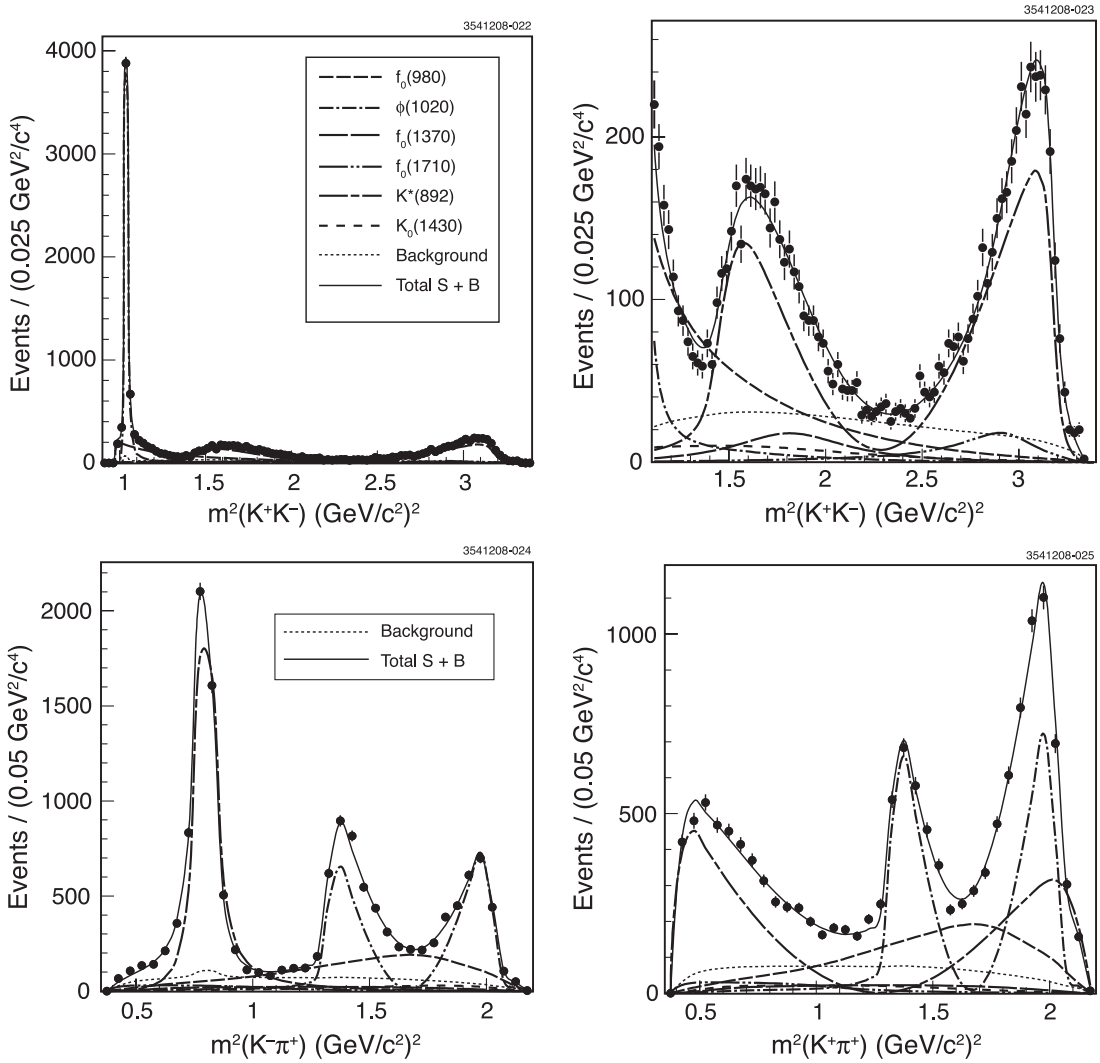

FIG. 42. The CLEO-c Dalitz-plot fit for $D_s^+ \to K^+K^-\pi^+$ candidates. From Mitchell *et al.*, 2009.

The fit gives a fit fraction of $0.242 \pm 0.025 \pm 0.06$ for nonresonant four-body final states, but it is likely that this includes contributions from other wide resonances.

The decay $D^0 \to K^+K^-\pi^+\pi^-$ was studied by E687 (Frabetti *et al.*, 1995c), E791 (Aitala *et al.*, 1998b), and FOCUS (Link *et al.*, 2005e). The FOCUS study used 1279 ± 48 events. They performed an unbinned maximum likelihood fit including ten resonances. The amplitudes are summarized in Table XXXVII. The dominant contribution to the decay

TABLE XXXIV. Dalitz-plot parameters from CLEO-c analysis of $D_s^+ \to K^-K^+\pi^+$. From Mitchell *et al.* (2009).

Resonance	Amplitude	Phase (deg)	Fit fraction (%)
$\bar{K}^*(892)^0K^+$	1 (fixed)	0 (fixed)	48.2 ± 1.2
$\bar{K}_0^*(1430)^0K^+$	1.76 ± 0.12	145 ± 8	5.3 ± 0.7
$f_0(980)\pi^+$	3.67 ± 0.13	156 ± 3	16.8 ± 1.1
$\phi(1020)\pi^+$	1.15 ± 0.02	-15 ± 4	42.7 ± 1.3
$f_0(1710)\pi^+$	1.27 ± 0.07	102 ± 4	4.4 ± 0.4

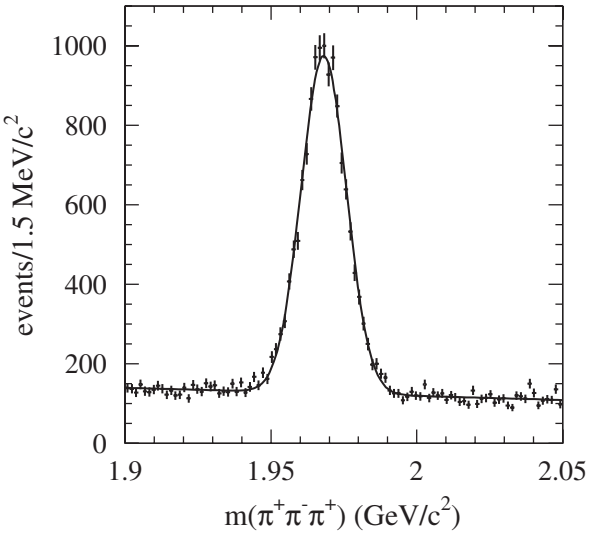

FIG. 43. The $\pi^+\pi^-\pi^+$ invariant mass for the signal candidates in the *BABAR* Dalitz-plot analysis of $D_s^+ \to \pi^+\pi^-\pi^+$. From Aubert *et al.*, 2009.

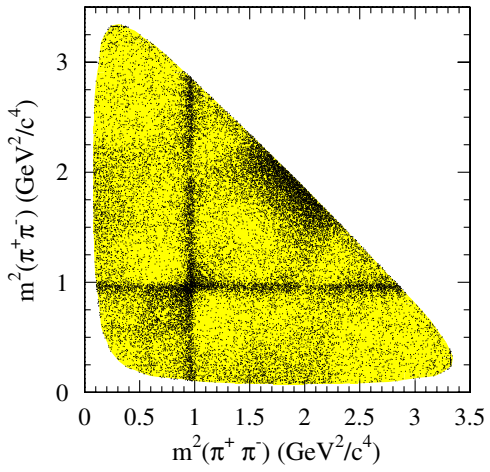

FIG. 44 (color online). The Dalitz plot for signal candidates in the *BABAR* Dalitz-plot analysis of $D_s^+ \to \pi^+\pi^-\pi^+$. From Aubert *et al.*, 2009.

rate, about 55%, comes from decays to intermediate states with an axial vector and a pseudoscalar. The second largest contribution, about 30%, comes from intermediate states with two vector mesons. The remaining contributions are from three-body intermediate states $D \to VPP$ and $D \to SPP$.

The decay $D^0 \to \pi^+\pi^-\pi^+\pi^-$ was studied by FOCUS (Link *et al.*, 2007). They performed a likelihood fit to a sample of 6153 events using an isobar model. The result of the fit is summarized in Table XXXVIII. The dominant contribution to the decay rate, about 60%, comes from decays to intermediate states with an a_1 resonance. The second largest contribution, about 25%, comes from $\rho^0\rho^0$ intermediate final states. The goodness of fit is estimated with a χ^2 technique. A low probability of about 10^{-17} is obtained. FOCUS tried adding additional resonances, but did not find any significant improvements in the fit probability.

Another use of four-body decays of D mesons is the search by FOCUS (Link *et al.*, 2005d) for CP violation using triple-product correlations. FOCUS studied the time reversal odd product $\mathbf{p_1} \cdot (\mathbf{p_2} \times \mathbf{p_3})$ by forming the asymmetry

$$A_T \equiv \frac{\Gamma(\mathbf{p_1} \cdot (\mathbf{p_2} \times \mathbf{p_3}) > 0) - \Gamma(\mathbf{p_1} \cdot (\mathbf{p_2} \times \mathbf{p_3}) < 0)}{\Gamma(\mathbf{p_1} \cdot (\mathbf{p_2} \times \mathbf{p_3}) > 0) + \Gamma(\mathbf{p_1} \cdot (\mathbf{p_2} \times \mathbf{p_3}) < 0)}. \tag{122}$$

However, strong phases can cause a nonzero value of A_T without the presence of CP violation. A true T-violating signal can be established by measuring a nonzero value of

$$A_{T_{\rm viol}} \equiv \tfrac{1}{2}(A_T - \bar{A}_T), \tag{123}$$

where $\bar{A}_T$ is the T-odd asymmetry measured for the CP-conjugate process. FOCUS considered three different four-body decays in this analysis and measured the following asymmetries:

$$A_{T_{\rm viol}}(D^0 \to K^-K^+\pi^-\pi^+) = 0.010 \pm 0.057 \pm 0.037, \tag{124}$$

$$A_{T_{\rm viol}}(D^+ \to K_S^0K^+\pi^-\pi^+) = 0.023 \pm 0.062 \pm 0.022, \tag{125}$$

$$A_{T_{\rm viol}}(D_s^+ \to K_S^0K^+\pi^-\pi^+) = -0.036 \pm 0.067 \pm 0.023, \tag{126}$$

all consistent with no T violation.

X. CONCLUSIONS

Charm decays remain an exciting field for both theoretical and experimental investigations. In fact, most discoveries in heavy flavor physics in the last 5 years involved charm quarks in one way or another. These include $D^0\bar{D}^0$ mixing, new open-charm D_{sJ} states, charmonium states X, Y, Z, states with ordinary and exotic quantum numbers, etc.

TABLE XXXV. Dalitz-plot parameters from *BABAR* analysis of $D_s^+ \to \pi^+\pi^-\pi^+$. From Aubert *et al.* (2009).

Resonance	Amplitude	Phase (rad)	Fit fraction (%)
$f_2(1270)\pi^+$	1 (fixed)	0 (fixed)	$10.1 \pm 1.5 \pm 1.1$
$\rho(770)^0\pi^+$	$0.19 \pm 0.02 \pm 0.12$	$1.1 \pm 0.1 \pm 0.2$	$1.8 \pm 0.5 \pm 1.0$
$\rho(1450)^0\pi^+$	$1.2 \pm 0.3 \pm 1.0$	$4.1 \pm 0.2 \pm 0.5$	$2.3 \pm 0.8 \pm 1.7$
S wave	See Aubert *et al.* (2009)		$83.0 \pm 0.9 \pm 1.9$

TABLE XXXVI. Fit fractions and phases from the MARK-III analysis of the decay $D^0 \to K^-\pi^+\pi^-\pi^+$. From Adler *et al.* (1990a).

Resonance	Fit fraction (%)	Phase (rad)
$\bar{K}^{*0}\rho^0$ transverse (S wave)	$0.142 \pm 0.016 \pm 0.05$	-1.39 ± 0.09
$K^-a_1(1260)^+$	$0.492 \pm 0.024 \pm 0.08$	0
$K_1(1270)^-\pi^+$	$0.066 \pm 0.019 \pm 0.03$	0.71 ± 0.25
$\bar{K}^{*0}\pi^+\pi^-$	$0.140 \pm 0.018 \pm 0.04$	3.07 ± 0.09
$K^-\rho^0\pi^+$	$0.084 \pm 0.022 \pm 0.04$	-0.30 ± 0.13
Four-body nonresonant	$0.242 \pm 0.025 \pm 0.06$	-1.07 ± 0.08

TABLE XXXVII. Fit fractions and phases from the FOCUS analysis of the decay $D^0 \to K^-K^+\pi^-\pi^+$. From Link *et al.* (2005e).

Mode	Magnitude	Phase (deg)	Fraction (%)
$K_1(1270)^+K^-$, $K_1 \to \rho(770)^0K^+$	1 (fixed)	0 (fixed)	$18 \pm 6 \pm 3$
$K_1(1270)^+K^-$, $K_1 \to K_0^*(1430)^0\pi^+$	$0.27 \pm 0.08 \pm 0.06$	$354 \pm 19 \pm 19$	$2 \pm 1 \pm 0$
$K_1(1270)^+K^-$, $K_1 \to K^*(892)^0\pi^+$	$0.94 \pm 0.16 \pm 0.13$	$12 \pm 12 \pm 15$	$16 \pm 4 \pm 5$
$K_1(1270)^+K^-$	⋯	⋯	$33 \pm 6 \pm 4$
$K_1(1400)^+K^-$	$1.18 \pm 0.19 \pm 0.09$	$259 \pm 11 \pm 13$	$22 \pm 3 \pm 4$
$K^*(892)^0\bar{K}^*(892)^0$	$0.39 \pm 0.09 \pm 0.11$	$28 \pm 13 \pm 10$	$3 \pm 2 \pm 1$
$\phi(1020)\rho(770)^0$	$1.30 \pm 0.11 \pm 0.07$	$49 \pm 11 \pm 12$	$29 \pm 2 \pm 1$
$\rho(770)^0K^+K^-$	$0.33 \pm 0.12 \pm 0.16$	$278 \pm 26 \pm 20$	$2 \pm 2 \pm 2$
$\phi(1020)\pi^+\pi^-$	$0.30 \pm 0.06 \pm 0.06$	$163 \pm 16 \pm 15$	$1 \pm 1 \pm 0$
$K^*(892)^0K^+\pi^-$	$0.83 \pm 0.09 \pm 0.10$	$234 \pm 10 \pm 11$	$11 \pm 2 \pm 1$
$f_0(980)\pi^+\pi^-$	$0.91 \pm 0.13 \pm 0.05$	$240 \pm 11 \pm 17$	$15 \pm 3 \pm 2$

TABLE XXXVIII. Amplitudes, phases, and fit fractions from the FOCUS analysis of the decay $D^0 \to \pi^-\pi^+\pi^-\pi^+$. From Link *et al.* (2007).

Mode	Magnitude	Phase (deg)	Fraction (%)
$a_1^+\pi^-$, $a_1^+ \to \rho^0\pi^+$ (S wave)	1 (fixed)	0 (fixed)	$43.3 \pm 2.5 \pm 1.9$
$a_1^+\pi^-$, $a_1^+ \to \rho^0\pi^+$ (D wave)	$0.241 \pm 0.033 \pm 0.024$	$82 \pm 5 \pm 4$	$2.5 \pm 0.5 \pm 0.4$
$a_1^+\pi^-$, $a_1^+ \to \sigma\pi^+$	$0.439 \pm 0.026 \pm 0.021$	$193 \pm 4 \pm 4$	$8.3 \pm 0.7 \pm 0.6$
$a_1^+\pi^-$ (all)	⋯	⋯	$60.0 \pm 3.0 \pm 2.4$
$\rho^0\rho^0$ (parallel)	$0.157 \pm 0.027 \pm 0.020$	$120 \pm 7 \pm 8$	$1.1 \pm 0.3 \pm 0.3$
$\rho^0\rho^0$ (perpendicular)	$0.384 \pm 0.020 \pm 0.015$	$163 \pm 3 \pm 3$	$6.4 \pm 0.6 \pm 0.5$
$\rho^0\rho^0$ (longitudinal)	$0.624 \pm 0.023 \pm 0.015$	$357 \pm 3 \pm 3$	$16.8 \pm 1.0 \pm 0.8$
$\rho^0\rho^0$ (all)	⋯	⋯	$24.5 \pm 1.3 \pm 1.0$
$f_0(980)\pi^+\pi^-$	$0.233 \pm 0.019 \pm 0.015$	$261 \pm 7 \pm 4$	$2.4 \pm 0.5 \pm 0.4$
$f_2(1270)\pi^+\pi^-$	$0.338 \pm 0.021 \pm 0.016$	$317 \pm 4 \pm 4$	$4.9 \pm 0.6 \pm 0.5$
$\sigma\pi^+\pi^-$	$0.432 \pm 0.027 \pm 0.022$	$254 \pm 4 \pm 5$	$8.2 \pm 0.9 \pm 0.7$
$R\pi^+\pi^-$ (all)	⋯	⋯	$20.0 \pm 1.2 \pm 1.0$

In this review, we touched only a part of a vast field of charm physics, the hadronic transitions of charmed mesons. We did not review many other exciting developments in charm physics. For example, a set of hadronic resonant states with new and exciting properties was discovered in both open- and hidden-charm quark systems [see, e.g., Swanson (2006) and Voloshin (2008) for recent reviews], many exciting results were obtained in theoretical (lattice) computations and experimental measurements of leptonic and semileptonic decays of charmed mesons (Bianco *et al.*, 2003; Artuso, Meadows, and Petrov, 2008), $D^0\bar{D}^0$ mixing was discovered and used to constrain new physics at the scales of several TeV (Golowich *et al.*, 2007), etc. Also, experimental searches for CP violation in charm transitions remains one of the primary ways of probing new physics in low-energy interactions (Grossman, Kagan, and Nir, 2007). Finally, we did not discuss inclusive charm decays, lifetimes of charmed states (Bianco *et al.*, 2003; Gabbiani, Onishchenko, and Petrov, 2004) [for older references, see Bigi (1995) and Bigi, Uraltsev, and Vainshtein (1992)], as well as charmed spectroscopy and decays of charmed baryons (Voloshin, 1999).

Our knowledge of hadronic charm decays has improved significantly over the last few years. The B-factory experiments, *BABAR* and Belle, have large charm data samples that have allowed them to do precise studies, including the absolute hadronic branching fractions for both D^0 and D_s^+ mesons. In addition, the unique CLEO-c data samples allow detailed studies of D^0, D^+, and D_s^+ decays. In this review we covered the status of the determination of the absolute branching fractions first for D^0 and D^+ mesons. These measurements are dominated by results from CLEO-c and *BABAR* and have statistical uncertainties now below $\pm 1\%$ and systematic uncertainties of about $\pm 1.8\%$. The determination of D_s^+ branching fractions is dominated by CLEO-c. The previously commonly used normalization mode $D_s^+ \to \phi\pi^+$ is not used by CLEO-c anymore as it is ambiguous at the level of precision now obtained by CLEO-c. CLEO-c instead quotes partial branching fractions for different K^+K^- mass ranges around the ϕ resonance. These partial branching fractions do not try to disentangle the contributions from the ϕ or other resonance contributing to the rate. The CLEO-c measurement obtained a statistical precision of about 4.2% and systematic uncertainties of about 3% in the $D_s^+ \to K^+K^-\pi^+$ mode. This result should improve when CLEO-c includes their full data sample. The large charm samples now available allowed more detailed studies of Cabibbo-suppressed D and D_s decays. Decays with smaller branching fractions have been explored as well as final states with π^0 and η mesons that traditionally have been harder to reconstruct, but thanks to the excellent electromagnetic calorimeters of the *BABAR*, Belle, and CLEO-c are now accessible. Finally, a summary of Dalitz decay studies of D mesons is given. Many of the three-body final states have now been

analyzed for their resonant substructure, and also a few final states with more than three particles in the final state have been studied. These studies show that most of the D decays proceed via pseudo-two-body decays.

The study of charm will continue with new experiments. The upgraded BES III experiment started to take data at the $\psi(3770)$ in 2010. In their first run they recorded about 900 pb^{-1} of comparable size to the CLEO-c data sample at this energy. BES III will carry on a similar physics program as CLEO-c with increased statistics. Running at design luminosity for 1 year, e.g., at the $\psi(3770)$ resonance, would provide a data sample a factor of 6 times larger than the CLEO-c data sample. Analyses that are statistics limited will be improved with the larger data samples. However, analyses that are limited by systematic uncertainties will see smaller gains. LHCb started taking data in 2010 at the LHC. LHCb has a sophisticated trigger designed for B physics, but will also select a large charm sample. Future e^+e^- Super B factories will produce large charm samples. The goal of the Super B factories is to produce data samples at least an order of magnitude larger than the current B factories. In particular, this will provide tight constraints on CP-violating observables. All of these experiments will continue to provide new data on charm physics. New measurements will play a big role in the development of the theoretical understanding of hadronic D meson decays. For example, they will allow tuning of the models of hadronic decays. Experiments with quantum-coherent initial states will produce measurements of the phases of decay amplitudes, i.e., the quantities that QCD-based calculations can predict. Finally, measurements of the new hadronic modes will allow complete fits of the flavor-flow amplitudes, and thus better predictions of new decay rates, especially for the PV, VV, AV, and other final states. While lattice QCD had enormous influence on the studies of leptonic and semileptonic transitions, the internal limitations of the lattice approach, i.e., the fact that the calculations are done in the Euclidean space-time, means that lattice QCD will have only a limited impact on the studies of hadronic D decays. These experimental and theoretical developments will allow us to understand in more detail the charm decays reviewed in this article and hopefully allow us to explore new physics beyond the standard model.

ACKNOWLEDGMENTS

We thank David Cinabro and Rob Harr for carefully reading the manuscript and insightful comments. A. R. was supported in part by the U.S. National Science Foundation under Grant No. PHY-0757894 and CAREER Award No. PHY-0846388. A. R. also thanks the Alfred P. Sloan foundation for their support. A. A. P. was supported in part by the U.S. National Science Foundation under CAREER Award No. PHY-0547794, and by the U.S. Department of Energy under Contract No. DE-FG02-96ER41005.

REFERENCES

Aaltonen, T., *et al.* (CDF Collaboration), 2008, Phys. Rev. Lett. **100**, 121802.
Abachi, S., *et al.* (HRS Collaboration), 1988, Phys. Lett. B **205**, 411.
Abe, K., *et al.* (Belle Collaboration), 2007, hep-ex/0701053.
Abe, K., *et al.* (Belle Collaboration), 2008, 0803.3375v1.
Ablikim, M., *et al.* (BES Collaboration), 2005, Phys. Lett. B **622**, 6.
Ablikim, M., *et al.* (BES Collaboration), 2006a, Phys. Rev. Lett. **97**, 121801.
Ablikim, M., *et al.* (BES Collaboration), 2006b, Phys. Lett. B **641**, 145.
Ablikim, M., *et al.* (BES Collaboration), 2007, Phys. Rev. D **76**, 122002.
Ablikim, M., *et al.* (BES Collaboration), 2008, Phys. Lett. B **659**, 74.
Abrams, G. S., *et al.*, 1979a, Phys. Rev. Lett. **43**, 477.
Abrams, G. S., *et al.*, 1979b, Phys. Rev. Lett. **43**, 481.
Acosta, D. E., *et al.* (CDF Collaboration), 2005, Phys. Rev. Lett. **94**, 122001.
Adam, N. E., *et al.* (CLEO Collaboration), 2005, Phys. Rev. Lett. **94**, 232002.
Adams, G. S., *et al.* (CLEO Collaboration), 2007, Phys. Rev. Lett. **99**, 191805.
Adler, J., *et al.* (MARK-III Collaboration), 1987, Phys. Lett. B **196**, 107.
Adler, J., *et al.* (MARK-III Collaboration), 1988, Phys. Rev. Lett. **60**, 89.
Adler, J., *et al.* (MARK-III Collaboration), 1990a, Phys. Rev. Lett. **64**, 2615.
Adler, J., *et al.* (MARK-III Collaboration), 1990b, Phys. Rev. Lett. **64**, 169.
Aitala, E. M., *et al.* (E791 Collaboration), 1997, Phys. Lett. B **404**, 187.
Aitala, E. M., *et al.* (E791 Collaboration), 1998a, Phys. Lett. B **421**, 405.
Aitala, E. M., *et al.* (E791 Collaboration), 1998b, Phys. Lett. B **423**, 185.
Aitala, E. M., *et al.* (E791 Collaboration), 2001a, Phys. Rev. Lett. **86**, 770.
Aitala, E. M., *et al.* (E791 Collaboration), 2001b, Phys. Rev. Lett. **86**, 765.
Aitala, E. M., *et al.* (E791 Collaboration), 2002, Phys. Rev. Lett. **89**, 121801.
Aitala, E. M., *et al.* (E791 Collaboration), 2006, Phys. Rev. D **73**, 032004.
Akerib, D. S., *et al.* (CLEO Collaboration), 1993, Phys. Rev. Lett. **71**, 3070.
Albrecht, H., *et al.* (ARGUS Collaboration), 1990, Phys. Lett. B **241**, 278.
Albrecht, H., *et al.* (ARGUS Collaboration), 1991, Phys. Lett. B **255**, 634.
Albrecht, H., *et al.* (ARGUS Collaboration), 1993, Phys. Lett. B **308**, 435.
Albrecht, H., *et al.* (ARGUS Collaboration), 1994a, Phys. Lett. B **324**, 249.
Albrecht, H., *et al.* (ARGUS Collaboration), 1994b, Phys. Lett. B **340**, 125.
Alexander, J. P., *et al.* (CLEO Collaboration), 1990a, Phys. Rev. Lett. **65**, 1531.
Alexander, J. P., *et al.* (CLEO Collaboration), 1990b, Phys. Rev. Lett. **65**, 1184.
Alexander, J. P., *et al.* (CLEO Collaboration), 2008, Phys. Rev. Lett. **100**, 161804.
Alvarez, M. P., *et al.* (NA14/2 Collaboration), 1990, Phys. Lett. B **246**, 261.
Alvarez, M. P., *et al.* (NA14/2 Collaboration), 1991, Z. Phys. C **50**, 11.
Amsler, C., *et al.* (Particle Data Group), 2008, Phys. Lett. B **667**, 1.

Anisovich, V. V., and A. V. Sarantsev, 2003, Eur. Phys. J. A **16**, 229.
Anjos, J. C., *et al.*, 1989, Phys. Rev. Lett. **62**, 125.
Anjos, J. C., *et al.*, 1990, Phys. Rev. D **41**, 2705.
Anjos, J. C., *et al.*, 1991, Phys. Rev. D **44**, R3371.
Anjos, J. C., *et al.* (E691 Collaboration), 1993, Phys. Rev. D **48**, 56.
Artuso, M., B. Meadows, and A. A. Petrov, 2008, Annu. Rev. Nucl. Part. Sci. **58**, 249.
Artuso, M., *et al.*, 2003, Nucl. Instrum. Methods Phys. Res., Sect. A **502**, 91.
Artuso, M., *et al.* (CLEO Collaboration), 1996, Phys. Lett. B **378**, 364.
Artuso, M., *et al.* (CLEO Collaboration), 1998, Phys. Rev. Lett. **80**, 3193.
Artuso, M., *et al.* (CLEO Collaboration), 2008, Phys. Rev. D **77**, 092003.
Ashmanskas, B., *et al.* (CDF-II Collaboration), 2004, Nucl. Instrum. Methods Phys. Res., Sect. A **518**, 532.
Asner, D. M., and W. M. Sun, 2006, Phys. Rev. D **73**, 034024; **77**, 019901(E) (2008).
Asner, D. M., *et al.*, 2008, 0809.1869.
Asner, D. M., *et al.* (CLEO Collaboration), 1996, Phys. Rev. D **54**, 4211.
Aston, D., *et al.*, 1988, Nucl. Phys. B **296**, 493.
Athar, S. B., *et al.* (CLEO Collaboration), 2008, Phys. Rev. Lett. **100**, 181802.
Atwood, D., I. Dunietz, and A. Soni, 2001, Phys. Rev. D **63**, 036005.
Atwood, D., and A. A. Petrov, 2005, Phys. Rev. D **71**, 054032.
Atwood, D., and A. Soni, 2002, Phys. Lett. B **533**, 37.
Aubert, B., *et al.* (*BABAR* Collaboration), 2005a, Phys. Rev. D **72**, 052008.
Aubert, B., *et al.* (*BABAR* Collaboration), 2005b, Phys. Rev. Lett. **95**, 121802.
Aubert, B., *et al.* (*BABAR* Collaboration), 2005c, Phys. Rev. D **71**, 091104.
Aubert, B., *et al.* (*BABAR* Collaboration), 2005d, Phys. Rev. D **72**, 091101.
Aubert, B., *et al.* (*BABAR* Collaboration), 2006a, Phys. Rev. D **74**, 011107.
Aubert, B., *et al.* (*BABAR* Collaboration), 2006b, Phys. Rev. Lett. **97**, 221803.
Aubert, B., *et al.* (*BABAR* Collaboration), 2006c, Phys. Rev. D **74**, 031103.
Aubert, B., *et al.* (*BABAR* Collaboration), 2007a, Phys. Rev. D **76**, 011102.
Aubert, B., *et al.* (*BABAR* Collaboration), 2007b, Phys. Rev. Lett. **98**, 211802.
Aubert, B., *et al.* (*BABAR* Collaboration), 2007c, Phys. Rev. Lett. **99**, 251801.
Aubert, B., *et al.* (*BABAR* Collaboration), 2008a, Phys. Rev. D **78**, 034023.
Aubert, B., *et al.* (*BABAR* Collaboration), 2008b, Phys. Rev. Lett. **100**, 051802.
Aubert, B., *et al.* (*BABAR* Collaboration), 2009, Phys. Rev. D **79**, 032003.
Aubert, J. J., *et al.* (E598 Collaboration), 1974, Phys. Rev. Lett. **33**, 1404.
Augustin, J. E., *et al.*, 1974, Phys. Rev. Lett. **33**, 1406.
Augustin, J. E., *et al.*, 1975, Phys. Rev. Lett. **34**, 233.
Bai, J. Z., *et al.* (BES Collaboration), 1994, Nucl. Instrum. Methods Phys. Res., Sect. A **344**, 319.
Bai, J. Z., *et al.* (BES Collaboration), 1995, Phys. Rev. D **52**, 3781.
Bai, J. Z., *et al.* (BES Collaboration), 2001, Nucl. Instrum. Methods Phys. Res., Sect. A **458**, 627.
Bai, J. Z., *et al.* (BES Collaboration), 2005, Phys. Lett. B **605**, 63.
Balest, R., *et al.* (CLEO Collaboration), 1994, Phys. Rev. Lett. **72**, 2328.
Baltrusaitis, R. M., *et al.* (MARK-III Collaboration), 1986, Phys. Rev. Lett. **56**, 2140.
Barate, R., *et al.* (ALEPH Collaboration), 1997, Phys. Lett. B **403**, 367.
Barberio, E., and Z. Was, 1994, Comput. Phys. Commun. **79**, 291.
Bartelt, J. E., *et al.* (CLEO Collaboration), 1998, Phys. Rev. Lett. **80**, 3919.
Bauer, M., B. Stech, and M. Wirbel, 1987, Z. Phys. C **34**, 103.
Beane, S. R., P. F. Bedaque, K. Orginos, and M. J. Savage, 2007, Phys. Rev. D **75**, 094501.
Beneke, M., G. Buchalla, M. Neubert, and C. T. Sachrajda, 1999, Phys. Rev. Lett. **83**, 1914.
Benvenuti, A. C., *et al.*, 1975a, Phys. Rev. Lett. **35**, 1199.
Benvenuti, A. C., *et al.*, 1975b, Phys. Rev. Lett. **34**, 419.
Bergmann, S., Y. Grossman, Z. Ligeti, Y. Nir, and A. A. Petrov, 2000, Phys. Lett. B **486**, 418.
Bergmann, S., and Y. Nir, 1999, J. High Energy Phys. 09, 031.
Bernabeu, J., F. J. Botella, and J. Roldan, 1988, Phys. Lett. B **211**, 226.
Bernstein, D., *et al.*, 1984, Nucl. Instrum. Methods Phys. Res., Sect. A **226**, 301.
Besson, D., *et al.* (CLEO Collaboration), 2006, Phys. Rev. Lett. **96**, 092002.
Besson, D., *et al.* (CLEO Collaboration), 2009, Phys. Rev. D **80**, 032005.
Bhattacharya, B., and J. L. Rosner, 2008, Phys. Rev. D **77**, 114020.
Bhattacharya, B., and J. L. Rosner, 2009, Phys. Rev. D **79**, 034016; **79**, 034016(E) (2009).
Bianco, S., F. L. Fabbri, D. Benson, and I. Bigi, 2003, Riv. Nuovo Cimento Soc. Ital. Fis. **26**, 1.
Bigi, I. I. Y., 1995, hep-ph/9508408.
Bigi, I. I. Y., N. G. Uraltsev, and A. I. Vainshtein, 1992, Phys. Lett. B **293**, 430.
Bigi, I. I. Y., and H. Yamamoto, 1995, Phys. Lett. B **349**, 363.
Björken, B. J., and S. L. Glashow, 1964, Phys. Lett. **11**, 255.
Bloch, F., and A. Nordsieck, 1937, Phys. Rev. **52**, 54.
Blok, B., and M. A. Shifman, 1993, Nucl. Phys. B **399**, 441.
Bonvicini, G., *et al.* (CLEO Collaboration), 2007, Phys. Rev. D **76**, 012001.
Bonvicini, G., *et al.* (CLEO Collaboration), 2008a, Phys. Rev. D **77**, 091106.
Bonvicini, G., *et al.* (CLEO Collaboration), 2008b, Phys. Rev. D **78**, 052001.
Brandenburg, G., *et al.* (CLEO Collaboration), 2001, Phys. Rev. Lett. **87**, 071802.
Briere, R. A., *et al.* (CLEO Collaboration), 2009, Phys. Rev. D **80**, 032002.
Briere, R. A., *et al.* (CLEO Collaboration), 2001, Cornell Report, No. CLNS 01/1742.
Buccella, F., M. Lusignoli, G. Miele, A. Pugliese, and P. Santorelli, 1995, Phys. Rev. D **51**, 3478.
Buccella, F., M. Lusignoli, and A. Pugliese, 1996, Phys. Lett. B **379**, 249.
Buccella, F., *et al.*, 1993, Phys. Lett. B **302**, 319.
Buras, A. J., J. M. Gerard, and R. Ruckl, 1986, Nucl. Phys. B **268**, 16.
Butler, F., *et al.* (CLEO Collaboration), 1992, Phys. Rev. Lett. **69**, 2041.
Butler, F., *et al.* (CLEO Collaboration), 1994, Phys. Lett. B **324**, 255.

Cawlfield, C., *et al.* (CLEO Collaboration), 2007, Phys. Rev. Lett. **98**, 092002.
Chau, L. L., and H. Y. Cheng, 1986, Phys. Rev. Lett. **56**, 1655.
Chau, L.-L., and H.-Y. Cheng, 1989, Phys. Lett. B **222**, 285.
Chau, L.-L., and H.-Y. Cheng, 1992, Phys. Lett. B **280**, 281.
Chen, A., *et al.* (CLEO Collaboration), 1983, Phys. Rev. Lett. **51**, 634.
Chen, C.-H., H.-Y. Cheng, and Y.-K. Hsiao, 2008, Phys. Lett. B **663**, 326.
Chen, W. Y., *et al.* (CLEO Collaboration), 1989, Phys. Lett. B **226**, 192.
Cheng, H.-Y., 2003, Eur. Phys. J. C **26**, 551.
Chiang, C.-W., Z. Luo, and J. L. Rosner, 2003, Phys. Rev. D **67**, 014001.
Chung, S. U., *et al.*, 1995, Ann. Phys. (N.Y.) **507**, 404.
Cinabro, D., *et al.* (CLEO Collaboration), 1994, Phys. Rev. Lett. **72**, 1406.
Coan, T. E., *et al.* (CLEO Collaboration), 1998, Phys. Rev. Lett. **80**, 1150.
BES III Collaboration, 2009, Nucl. Instrum. Methods Phys. Res., Sect. A **598**, 7.
Cronin-Hennessy, D., *et al.* (CLEO Collaboration), 2009, Phys. Rev. D **80**, 072001.
Csorna, S. E., *et al.* (CLEO Collaboration), 2002, Phys. Rev. D **65**, 092001.
Dai, Y.-S., D.-S. Du, X.-Q. Li, Z.-T. Wei, and B.-S. Zou, 1999, Phys. Rev. D **60**, 014014.
Dalitz, R. H., 1953, Philos. Mag. **44**, 1068.
Decamp, D., *et al.* (ALEPH Collaboration), 1991, Phys. Lett. B **266**, 218.
Dobbs, S., *et al.* (CLEO Collaboration), 2007, Phys. Rev. D **76**, 112001.
Donoghue, J. F., 1986, Phys. Rev. D **33**, 1516.
Donoghue, J. F., and B. R. Holstein, 1980, Phys. Rev. D **21**, 1334.
Dunietz, I., J. Hauser, and J. L. Rosner, 1987, Phys. Rev. D **35**, 2166.
Dytman, S. A., *et al.* (CLEO Collaboration), 2001, Phys. Rev. D **64**, 111101.
Dytman, S. A., *et al.* (CLEO Collaboration), 2006, Phys. Rev. D **74**, 071102; **74**, 079904(E) (2006).
Edera, L. (FOCUS Collaboration), 2004, in *Proceedings of DAFNE 2004: Physics at Meson Factories*, edited by F. Anulli, M. Bertani, G. Capon, C. Curceanu-Petrascu, F. L. Fabbri, and S. Miscetti, Frascati Physics Series Vol. 36 (Istituto Naz. Fis. Nucl., Frascati, Italy), p. 532.
Eeg, J. O., S. Fajfer, and J. Zupan, 2001, Phys. Rev. D **64**, 034010.
Fajfer, S., A. Prapotnik, P. Singer, and J. Zupan, 2003, Phys. Rev. D **68**, 094012.
Falk, A. F., Y. Nir, and A. A. Petrov, 1999, J. High Energy Phys. 12, 019.
Falk, A. F., and A. A. Petrov, 2000, Phys. Rev. Lett. **85**, 252.
Frabetti, P. L., *et al.* (E687 Collaboration), 1992, Phys. Lett. B **286**, 195.
Frabetti, P. L., *et al.* (E687 Collaboration), 1993, Phys. Lett. B **313**, 253.
Frabetti, P. L., *et al.* (E687 Collaboration), 1994a, Phys. Lett. B **321**, 295.
Frabetti, P. L., *et al.* (E687 Collaboration), 1994b, Phys. Lett. B **331**, 217.
Frabetti, P. L., *et al.* (E687 Collaboration), 1994c, Phys. Lett. B **340**, 254.
Frabetti, P. L., *et al.* (E687 Collaboration), 1995a, Phys. Lett. B **351**, 591.
Frabetti, P. L., *et al.* (E687 Collaboration), 1995b, Phys. Lett. B **359**, 403.
Frabetti, P. L., *et al.* (E687 Collaboration), 1995c, Phys. Lett. B **354**, 486.
Frabetti, P. L., *et al.* (E687 Collaboration), 1997, Phys. Lett. B **407**, 79.
Gabbiani, F., A. I. Onishchenko, and A. A. Petrov, 2004, Phys. Rev. D **70**, 094031.
Gaillard, M. K., and B. W. Lee, 1974, Phys. Rev. D **10**, 897.
Gaillard, M. K., B. W. Lee, and J. L. Rosner, 1975, Rev. Mod. Phys. **47**, 277.
Gao, D.-N., 2007, Phys. Lett. B **645**, 59.
Ge, J. Y., *et al.* (CLEO Collaboration), 2009a, Phys. Rev. D **80**, 051102.
Ge, J. Y., *et al.* (CLEO Collaboration), 2009b, Phys. Rev. D **79**, 052010.
Gedalia, O., and G. Perez, 2010, 1005.3106.
Gell-Mann, M., 1964, Phys. Lett. **8**, 214.
Glashow, S. L., J. Iliopoulos, and L. Maiani, 1970, Phys. Rev. D **2**, 1285.
Goldhaber, G., *et al.*, 1976, Phys. Rev. Lett. **37**, 255.
Golowich, E., J. Hewett, S. Pakvasa, and A. A. Petrov, 2007, Phys. Rev. D **76**, 095009.
Golowich, E., and A. A. Petrov, 1998, Phys. Lett. B **427**, 172.
Gronau, M., Y. Grossman, and J. L. Rosner, 2001, Phys. Lett. B **508**, 37.
Gronau, M., O. F. Hernandez, D. London, and J. L. Rosner, 1994, Phys. Rev. D **50**, 4529.
Gronau, M., and J. L. Rosner, 2009, Phys. Rev. D **79**, 074006.
Grossman, Y., A. L. Kagan, and Y. Nir, 2007, Phys. Rev. D **75**, 036008.
Harrison, P. F., and R. H. Quinn (*BABAR* Collaboration), 1998, Eds., papers from *Workshop on Physics at an Asymmetric B Factory (BABAR Collaboration Meeting)*, Rome, Italy, 1996, Princeton, NJ, 1997, Orsay, France, 1997, and Pasadena, CA, 1997.
He, Q., *et al.* (CLEO Collaboration), 2008, Phys. Rev. Lett. **100**, 091801.
He, Q., *et al.* (CLEO Collaboration), 2005, Phys. Rev. Lett. **95**, 121801; **96**, 199903(E) (2006).
Hinchliffe, I., and T. A. Kaeding, 1996, Phys. Rev. D **54**, 914.
Hoshino, K., *et al.*, 1975, Prog. Theor. Phys. **53**, 1859.
Iizuka, J., 1966, Prog. Theor. Phys. Suppl. **37**, 21.
Kamal, A. N., and R. C. Verma, 1987, Phys. Rev. D **35**, 3515.
Kölbig, K. S., and H. Lipps, 1990, CERN Program Library E211.
Kopp, S., *et al.* (CLEO Collaboration), 2001, Phys. Rev. D **63**, 092001.
Kubota, Y., *et al.* (CLEO Collaboration), 1992, Nucl. Instrum. Methods Phys. Res., Sect. A **320**, 66.
Lange, D. J., 2001, Nucl. Instrum. Methods Phys. Res., Sect. A **462**, 152.
Link, J. M., *et al.* (FOCUS Collaboration), 2002a, Nucl. Instrum. Methods Phys. Res., Sect. A **484**, 270.
Link, J. M., *et al.* (FOCUS Collaboration), 2002b, Phys. Lett. B **541**, 227.
Link, J. M., *et al.* (FOCUS Collaboration), 2002c, Phys. Lett. B **537**, 192.
Link, J. M., *et al.* (FOCUS Collaboration), 2002d, Nucl. Instrum. Methods Phys. Res., Sect. A **484**, 174.
Link, J. M., *et al.* (FOCUS Collaboration), 2003, Phys. Lett. B **555**, 167.
Link, J. M., *et al.* (FOCUS Collaboration), 2004a, Phys. Lett. B **585**, 200.
Link, J. M., *et al.* (FOCUS Collaboration), 2004b, Phys. Lett. B **601**, 10.

Link, J. M., *et al.* (FOCUS Collaboration), 2004c, Nucl. Instrum. Methods Phys. Res., Sect. A **516**, 364.
Link, J. M., *et al.* (FOCUS Collaboration), 2005a, Phys. Rev. Lett. **95**, 052003.
Link, J. M., *et al.* (FOCUS Collaboration), 2005b, Phys. Lett. B **607**, 59.
Link, J. M., *et al.* (FOCUS Collaboration), 2005c, Phys. Lett. B **624**, 166.
Link, J. M., *et al.* (FOCUS Collaboration), 2005d, Phys. Lett. B **622**, 239.
Link, J. M., *et al.* (FOCUS Collaboration), 2005e, Phys. Lett. B **610**, 225.
Link, J. M., *et al.* (FOCUS Collaboration), 2007, Phys. Rev. D **75**, 052003.
Link, J. M., *et al.* (FOCUS Collaboration), 2008, Phys. Lett. B **660**, 147.
Link, J. M., *et al.* (FOCUS Collaboration), 2009, Phys. Lett. B **681**, 14.
Lipkin, H. J., 1968, Phys. Rev. **176**, 1715.
Lipkin, H. J., 1980, Phys. Rev. Lett. **44**, 710.
Lipkin, H. J., 1987, Nucl. Phys. B **291**, 720.
Malvezzi, S., 2000, AIP Conf. Proc. **549**, 569.
Mitchell, R. E., *et al.* (CLEO Collaboration), 2009, Phys. Rev. D **79**, 072008.
Muramatsu, H., *et al.* (CLEO Collaboration), 2002, Phys. Rev. Lett. **89**, 251802; , **90**, 059901(E) (2003).
Niu, K., E. Mikumo, and Y. Maeda, 1971, Prog. Theor. Phys. **46**, 1644.
Okubo, S., 1977, Phys. Rev. D **16**, 2336.
Peruzzi, I., *et al.*, 1976, Phys. Rev. Lett. **37**, 569.
Peruzzi, I., *et al.*, 1977, Phys. Rev. Lett. **39**, 1301.
Peterson, D., *et al.*, 2002, Nucl. Instrum. Methods Phys. Res., Sect. A **478**, 142.
Petrov, A. A., 2004, Phys. Rev. D **69**, 111901.
Pham, X. Y., 1980a, Phys. Rev. Lett. **45**, 1663.
Pham, X.-Y., 1980b, Phys. Lett. B **94**, 231.
Pham, X.-Y., 1987, Phys. Lett. B **193**, 331.
Poluektov, A., *et al.* (Belle Collaboration), 2006, Phys. Rev. D **73**, 112009.
Richman, J. D., and P. R. Burchat, 1995, Rev. Mod. Phys. **67**, 893.
Richter-Was, E., 1993, Phys. Lett. B **303**, 163.
Rosner, J. L., 1999, Phys. Rev. D **60**, 114026.
Rubin, P., *et al.* (CLEO Collaboration), 2004, Phys. Rev. Lett. **93**, 111801.
Rubin, P., *et al.* (CLEO Collaboration), 2006, Phys. Rev. Lett. **96**, 081802.
Rubin, P., *et al.* (CLEO Collaboration), 2008, Phys. Rev. D **78**, 072003.
Sanda, A. I., 1980, Phys. Rev. D **22**, 2814.
Savage, M. J., 1991, Phys. Lett. B **257**, 414.
Schindler, R. H., *et al.*, 1981, Phys. Rev. D **24**, 78.
Selen, M., *et al.* (CLEO Collaboration), 1993, Phys. Rev. Lett. **71**, 1973.
Summers, D. J., *et al.*, 1984, Phys. Rev. Lett. **52**, 410.
Sun, W. M., 2006, Nucl. Instrum. Methods Phys. Res., Sect. A **556**, 325.
Swanson, E. S., 2006, Phys. Rep. **429**, 243.
Tian, X. C., *et al.* (Belle Collaboration), 2005, Phys. Rev. Lett. **95**, 231801.
Voloshin, M. B., 1999, Phys. Rep. **320**, 275.
Voloshin, M. B., 2008, Prog. Part. Nucl. Phys. **61**, 455.
Zemach, C., 1965, Phys. Rev. **140**, B109.
Zhang, L. M., *et al.* (Belle Collaboration), 2006, Phys. Rev. Lett. **96**, 151801.
Zweig, G., 1964, CERN-TH-412.